EXPERIMENTAL AND NUMERICAL MODELLING OF CLIMATE-CHANGE ADAPTIVE VERTICAL SEAWALL STRUCTURES

Stefano Kerr

Submitted under the supervision of

Dr. Ioan Nistor

A thesis submitted to the University of Ottawa in partial fulfillment of the requirements for the degree of

Master of Applied Science in Civil Engineering

Department of Civil Engineering

Faculty of Engineering

University of Ottawa

uOttawa

Abstract

The performance of coastal structures will be affected as climate change drives sea level rise and increasing storminess. When re-designs are not possible, engineers may need to retrofit existing coastal structures to account for harsher design conditions. Previous research at the National Research Council of Canada (NRC) investigated how adaptations to traditional coastal revetments reduced wave overtopping, forming the basis of the current investigation.

A literature review revealed that, while design guidance exists for retrofits like parapets and toe berms, an otherwise limited amount of guidance exists regarding retrofitting vertical structures. However, all relevant studies used physical modelling to some degree, stressing the importance of physical experimentation in this regard.

This study investigated how retrofits to vertical structures (bulkhead, caissons, seawalls, etc.) improves their wave overtopping resistance under rising sea levels. Experimental modelling was conducted at the Coastal, Ocean, and River Engineering (OCRE) Laboratory of the National Research Council (NRC) in Ottawa to investigate several conventional and novel adaptation concepts: crest extensions, low-crested eco-friendly breakwater, revetments, perched sandy beach, perched cobble beach, landward drainage swales, and secondary wall/stilling wave basins. To the candidate's knowledge, the research presents a novel application of ECOncrete Coastalock armour units. Also, the implementation of a perched beach, and drainage swales as retrofit structures are also novel. Test results revealed that crest extensions are powerful retrofit solutions. Existing wave overtopping design equations were also modified to account for the addition of key adaptations.

In addition, a two-dimensional numerical model (IH2VOF) was assessed for its ability to replicate key experimental test cases. The numerical modelling results had acceptable accuracy compared to the experimental results when both were individually scrutinized against EurOtop (2018) prediction equations. The study aimed to contribute to the knowledge base of vertical structure retrofits, and to design guidance.

Acknowledgements

Thank you to my supervisors, Dr. Ioan Nistor and Scott Baker, for their consistent guidance, support, and patience. I remember how quickly and thoroughly Dr. Nistor responded to my very first email to him – in the last two and a half years, his determination to support his students has never waivered. Scott's knowledge of modelling and experimentation was invaluable; I am very grateful for how much I have learned about coastal engineering research and design.

Ioan and Scott provided me with the opportunity to conduct research at the National Research Council of Canada, a unique and fulfilling experience. At the NRC, I met many researchers and technical officers and learned invaluable engineering skills. I feel extremely privileged, and I would not trade my time at the University of Ottawa and the NRC for anything! I am also thankful for the guidance of Dogac Sayar, a PhD student who on many occasions gave his time and support of my research. Finally, thank you to my friends and family who supported me continuously during my time in Ottawa. I could not have done it without any of you!

Table of Contents

List of Tables

List of Figures

List of Acronyms

2D	Two-Dimensional
AWA	Active Wave Absorption
CC	Climate Change
FS	Full Scale
HYF	100-Year Flood
LD	Long Domain
LWCF	Large Wave-Current Flume
LWD	Large Woody Debris
MNR	Ministry of Natural Resources
MS	Model Scale
MWL	Mean Water Level
NBS	Nature Based Solution(s)
NRC-OCRE	National Research Council of Canada's Ocean, Coastal, and River Engineering Research Centre
OT	Overtopping
RANS	Reynolds Averaged Navier-Stokes
RD	Relative Difference
SD	Short Domain
SLR	Sea Level Rise
SWB	Stilling Wave Basin
TS	Test Series
USACE	United States Army Corps of Engineers
VARANS	Volume-Averaged Reynolds Averaged Navier-Stokes

VOF	Volume of Fluid
W/L	Water Level
WLR	Water Level Rise
WM	Wave Machine
WP	Wave Probe

List of Symbols

A_h	Total area of drainage holes (m^2)
A_w	Total area of the seaward face of the vertical structure (m^2)
b, r_0	Calibration constants for Eqn. 5
C_b	Blocking coefficient ratio (Kisacik et al. 2019; Kisacik et al. 2022)
d_1	Distance from structure toe of vertical structure to center of drainage hole (m)
d_b	Depth of breakwater structure to crest (at lengthwise midpoint) (m)
d_w	Depth of water over crest of breakwater (at lengthwise midpoint) (m)
F	EurOtop Eqn. 7.7 or 7.8, depending on relative freeboard (EurOtop 2018)
f_q	"Reduction factor for scale and model effects" (EurOtop 2018, pp. 306)
h	Water depth at toe of structure (EurOtop 2018, pp. 306) (m)
H	Wave height (m)
H_{m0}	Spectral analysis approximation of wave height (EurOtop 2018, pp.306) (m)
$H_{m0,deep}$	H_{m0} in deep water (EurOtop 2018, pp. 306) (m)
h_t	Water depth at the toe of the structure (EurOtop 2018, pp. 306). For TSCC, the value was taken to be equal to the value for TSAA/TSBB. (m)
IQR	interquartile range
k	ratio of OT at structure with adaptation to OT at structure without adaptation = $q_{adaptation}/q_{baseline}$ (Pearson et al. 2005, pp.4)
k_{AB}	for TSAA and TSBB data
k_C	for TSCC data
k_G	for TSGG data
k_J	for TSJJ data
k_K	for TSKK data

L	wavelength (m)
L_a	length of armoured portion of drainage swale (m)
L_c	length of horizontal portion of revetment crest (m)
$L_{m-1,0}$	"spectral wavelength in deep water" (EurOtop 2018, pp. 307) (m)
L_s	length of sloping portion of the revetment (m)
L_t	length of either drainage swale (TSJJ) or length of secondary wall setback (TSKK) (m)
q	"mean overtopping discharge per meter structure width" (EurOtop 2018, pp. 308) ($m^3/s/m$)
q_{east}	for the east OT tray ($m^3/s/m$)
q_o	observed value of overtopping ($m^3/s/m$)
q_{west}	for the west OT tray ($m^3/s/m$)
$q/(gH_{m0}^3)^{0.5}$	dimensionless overtopping rate
$[q/(gH_{m0}^3)^{0.5}]_o$	observed dimensionless overtopping rate
$[q/(gH_{m0}^3)^{0.5}]_p$	predicted dimensionless overtopping rate using EurOtop equations
$Q3$	third quartile
R_c	"crest freeboard of structure" (EurOtop 2018, pp.308) (m)
R_c/H_{m0}	relative freeboard
r_i	calibration coefficient for Eqn. 5
RMSE	Root Mean Squared Error
$RMSE_{east}$	for east OT Tray
$RMSE_{west}$	for west OT Tray
R_s	crest height to secondary wall (m)
$s_{m-1,0}$	wave steepness = $H_{m0}/L_{m-1,0}$ (EurOtop 2018, pp. 308)
T_p	"spectral peak wave period" (EurOtop 2018, pp.309) (s)
y_i	dimensionless parameter for Eqn. 5

γ_f	"Influence factor for permeability and roughness of or on the slope" (EurOtop 2018, pp.310)
$\Delta x/\Delta y$	x-direction cell length/y-direction cell length = aspect ratio in numerical model
σ	standard deviation

1 Introduction

1.1 Background

Climate change is already impacting large storms. Strauss et al. (2021) determined that for hurricane Sandy, climate change induced sea level rise caused approximately $8.1B of the $50B-$60B (PlaNYC 2013; Strauss et al. 2021) in damages. Moreover, that climate change caused an additional 71 thousand people to fall within Hurricane Sandy's floodplain (Strauss et al. 2021). Additionally, Smiley et al. (2022) predicted that, without climate change effects, 30 to 50 percent fewer properties would have flooded during Hurricane Harvey in Harris County, Texas.

Climate change effects are expected to worsen. Sweet et al. (2022) presents a comprehensive document *Global and Regional Sea Level Rise Scenarios for the United States*, noting that average sea level rise (SLR) for the contiguous U.S. coastline over the next 30 years (2020-2050) is expected to be equal to the last 100 years' rise (1920-2020) (0.25 – 0.3m). Moreover, the gulf coasts are expected to have 0.1 – 0.15 m relative SLR higher than the U.S. average – this may exacerbate hurricane and storms along the east coast. Often destructive high tide flooding events, where flooding is ~1.2 m above mean higher high water (MHHW), are expected to increase 400 percent from 0.04 to 0.2 events per year.

Consequently, coastal engineers will need to account for increased storminess and more severe coastal hazards. For example, on the Great Lakes, regional consultant reports have included 100-year flood levels, with various global warming levels (Stantec 2022). However, Gittman et al. (2015) determined that 14 percent of the continental U.S. (22,842 km) coastline is hardened. Many of those structures may not be designed for climate change impacts; upgrading existing structures may be necessary (Foti et al. 2020).

Previous research at the National Research Council of Canada's Ocean, Coastal, and River Engineering Research Centre (NRC-OCRE) by Baker et al. (2023) investigated through physical modelling how adaptations to a traditional coastal revetment reduced the wave overtopping when subjected to harsher sea states. The current study builds on this preliminary work by completing a study of similar scope but instead considering traditional vertical seawalls.

1.2 Objectives

The objectives of this study were determined as a function of the background (section *1.1*) and the literature review (Section *2*):

1) Understand how vertical seawalls can be adapted to resist rising sea levels
2) Contribute to design guidelines for the retrofit of vertical seawalls
3) Assess the performance of numerical models at replicating experimental tests for vertical seawalls

1.3 Novelty

A limited number of studies exist which review adaptations to vertical seawalls. To the author's knowledge, the use of perched beaches and landward drainage swales as adaptations for vertical seawalls are also novel. In addition, limited work exists on the influence of drainage holes on the face of the vertical wall, which is a more realistic assumption than a smooth face. The study novelly applies ECOncrete Coastalock armour units, an eco-friendly amour unit, by implementing them in the retrofit of existing vertical seawalls. To the author's knowledge, limited studies exist which review IH2VOF's ability to replicate overtopping discharge over a traditional vertical seawall.

1.4 Scope

The objectives are achieved through a well-defined project scope:

1) ***Understand how vertical seawalls can be adapted to rising sea levels.***
    a. Two-dimensional experimental modelling was conducted at NRC-OCRE in the Large Wave-Current Flume (LWCF).
    b. The tests considered wave overtopping as the main performance indicator. Structure stability is not considered.
    c. Input wave conditions for the experimental model included climate change-representative conditions and was based on conditions on the Great Lakes.
    d. Eco-friendly armour units were implemented in the physical model tests to better understand the units' hydraulic performance.
    e. Field work was not used in this study.
2) ***Contribute to design guidelines for the retrofit of vertical seawalls.***
    a. The wave overtopping discharge for a traditional vertical seawall was compared to the discharge for a retrofitted vertical seawall.
        i. Existing EurOtop (2018) prediction equations were modified to account for several retrofits.
    b. A simple bathymetry was selected to improve applicability of results.
    c. Tested retrofits were selected with reference to *i)* relevant literature, and *ii)* possible construction restrictions – a distribution of adaptations on the crest, and on the seaward and landward sides were implemented.
3) ***Assess the performance of numerical models at replicating experimental tests for vertical seawalls.***
    a. A state-of-the-art two-dimensional numerical model, IH2VOF (see section 2.2.2) was used (Lara et al. 2007; Losada et al. 2011).
    b. Only geometries with non-porous make-ups were used.
    c. non-uniform meshes were optimized for performance and computation time through a sensitivity analysis.

d. To assess the model's overtopping discharge predictions, results from numerical simulations were scrutinized against existing prediction formulae and the experimental results.

1.5 Publications

The following is a list of publications affiliated with the work presented in the thesis, for which the author is the primary contributor.

Journal Publications

1) **Kerr, S.**, Nistor, I., Baker, S. "Adapting Vertical Coastal Structures to Sea Level Rise." **[In submission]**.
2) **Kerr, S.**, Baker, S., Nistor, I. "Experimental and Numerical Modelling of Adaptive Vertical Coastal Structures." **[In submission]**.

Conference Presentations

1) **Kerr, S.**, Baker, S., Nistor, I. (2025). "Experimental and Numerical Modeling of Climate Change-Adaptive Coastal Structures, Phase II: Vertical Seawalls." Oral Presentation. Coastal Zone Canada, Charlottetown, PEI.

1.6 Outline of the Thesis

The outline of the remaining sections of the thesis are as follows:

- ***Section 2.0*** reviews relevant background information regarding coastal structures and IH2VOF, as well as the state of the art for retrofitting vertical structures and implementing IH2VOF for overtopping discharge measurements.
- ***Section 3.0*** presents a pre-print of a submitted article, entitled *Adapting Vertical Coastal Structures to Sea Level Rise*. The study details the methodology of the experimental test program, information about the tested retrofitted structures, raw and processed results, and the modification of overtopping prediction equations for the retrofits.
- ***Section 4.0*** presents a pre-print of a submitted article, entitled *Experimental and Numerical Modelling of Adaptive Vertical Coastal Structures*. The study details the sensitivity analysis, as well as the primary tests and the performance of the numerical model.
- ***Section 5.0*** discusses the applications of this study and limitations.
- ***Section 6.0*** presents conclusions of the study and recommendations for future work.

2 Literature Review

2.1 Introduction

Kamphuis (2020) argues in *Introduction to Coastal Engineering and Management* that coastal management success depends on integrating physical and numerical modelling, and prototype measurements (i.e., field work). In this sense, where physical modelling is the primary undertaking of a project, like this study, it is still critical to understand how numerical modelling may be used in lieu; moreover, to review how other researchers have completed work to this effect. Given that this study aims to have practical deliverables, it is crucial to consider the use of both mediums. Note that field work was not completed for this study.

This literature review first provides context regarding alternatives to coastal protection, from hard structures to nature-based solutions (NBS). Then, a state-of-the-art review is conducted for *i)* physical modelling of retrofitted vertical structures, and *ii)* IH2VOF implementation for overtopping discharge measurement.

2.2 Background

2.2.1 Coastal Protection Structures

2.2.1.1. Traditional Structures

One traditional coastal structure is a revetment. Revetments are foremost designed to protect shorelines from eroding (USACE 1995), as is the purpose of many coastal structures. Revetments are particularly used for embankments or slopes (USACE 1995). A typical revetment may either be described as flexible or rigid, depending on the armouring material (USACE 2002). Stone-based armour tends to be more flexible, accommodating some armour layer movement without failure. Rigid armour is the opposite, and can take the form of slabs on grade, either asphalt or concrete (USACE 2002). Typical examples of revetments are shown in *Fig. 2.1*:

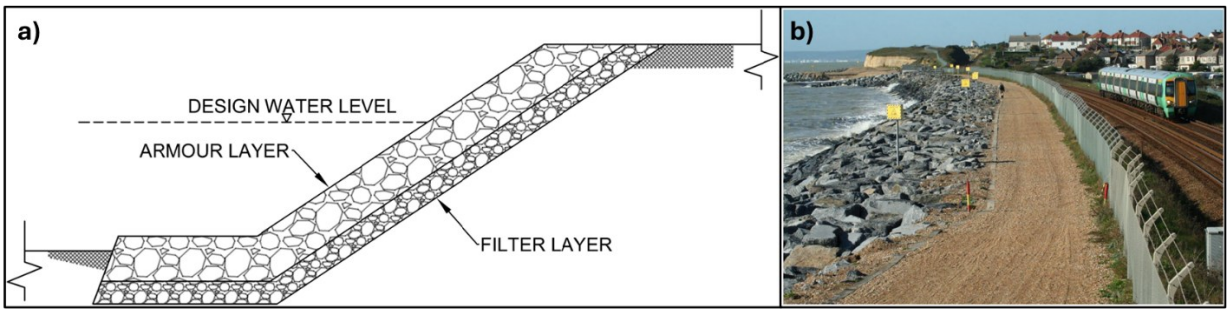

Fig 2.1 (*a*) Cross section of typical revetment (adapted from USACE, 1995), (*b*) Real revetment (EurOtop 2018)

Other key revetment features include a toe designed to resist scour and to support the upper structure, and a filter layer which supports the primary layer and allows percolation through the

structure (USACE 2002). Revetment design is well understood – design manuals give guidance for structural considerations (USACE 2002) and overtopping (EurOtop 2018).

Seawalls are noted to be massive structures (USACE 1995; USACE 2002) and are supported either by piles or gravity (USACE 1995). *Seawall* is a general description, encompassing vertical walls, curved walls, sloping structures, and even rubble mound walls and breakwaters, as shown in *Fig. 2.2*.

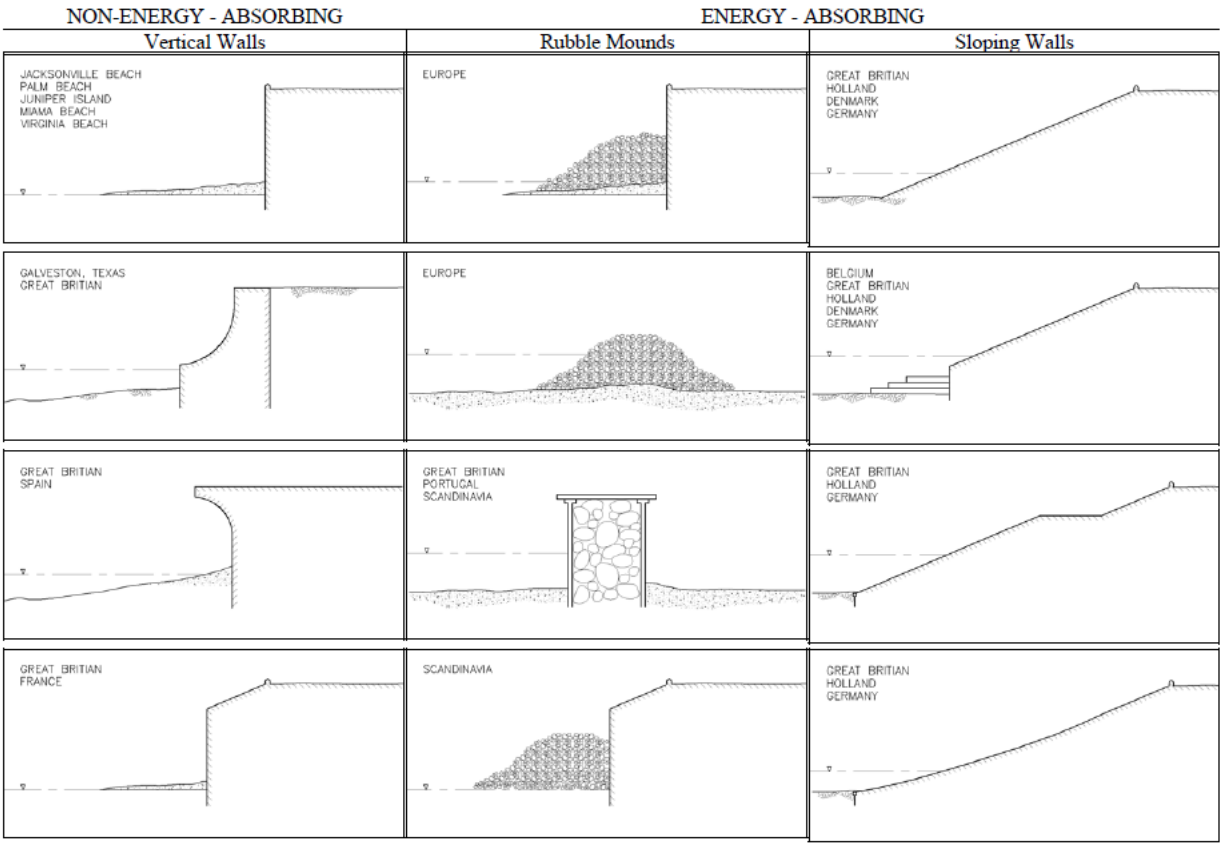

Fig 2.2. Examples of seawalls (USACE 2002)

However, structure classifications often overlap. For example, in the above figure, sloping seawalls are classified similarly to dikes – sloping flood defense structures with roughness elements (EurOtop 2018), and rubble mound seawalls are designed similarly to classical breakwaters (USACE 1995).

Vertical seawalls, particularly the top left cross section in *Fig. 2.2*, are like traditional bulkheads but defined differently: bulkheads are retaining structures first, and coastal protection structures second (USACE 1995; USACE 2002). However, in terms of wave overtopping design, these structures are identical; as are vertical breakwaters (also called caissons) (EurOtop 2018). Examples of a vertical structure and bulkhead are shown in *Fig. 2.3*.

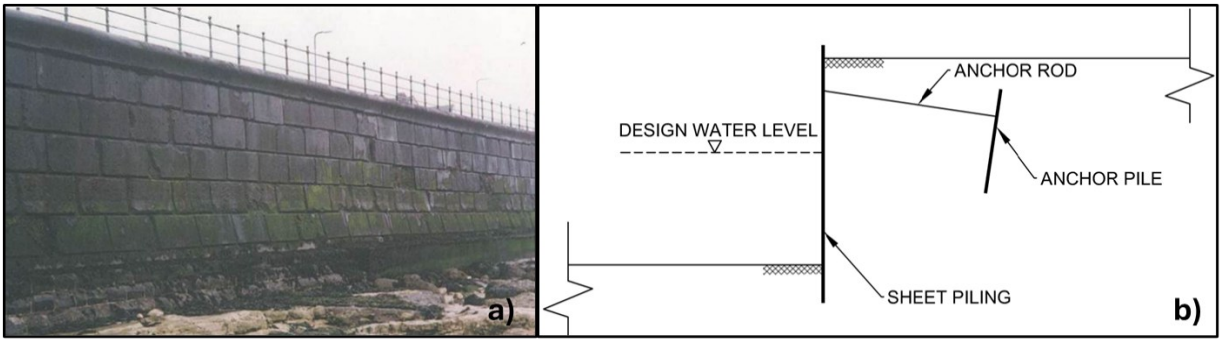

Fig 2.3. (*a*) Example of a vertical seawall (EurOtop 2018), (*b*) Cross section of a typical bulkhead (adapted from USACE 2002)

Breakwaters are different from other types of coastal structures because they are sometimes detached from the shoreline for the purpose of, for example, protecting harbours and marinas (EurOtop 2018). Detached breakwaters also reduce energy in their lee, depositing sediment between the shoreline and the breakwater and forming beach structures similar to pocket beaches (USACE 2002). Structurally, detached breakwaters are typically built as rubble-mound structures (USACE 2002). Moreover, standard breakwater design is well understood and is available in both manuals (USACE 2002) and books (Takahashi 2002; Kamphuis 2020). Typical breakwaters are shown in *Fig 2.4*.

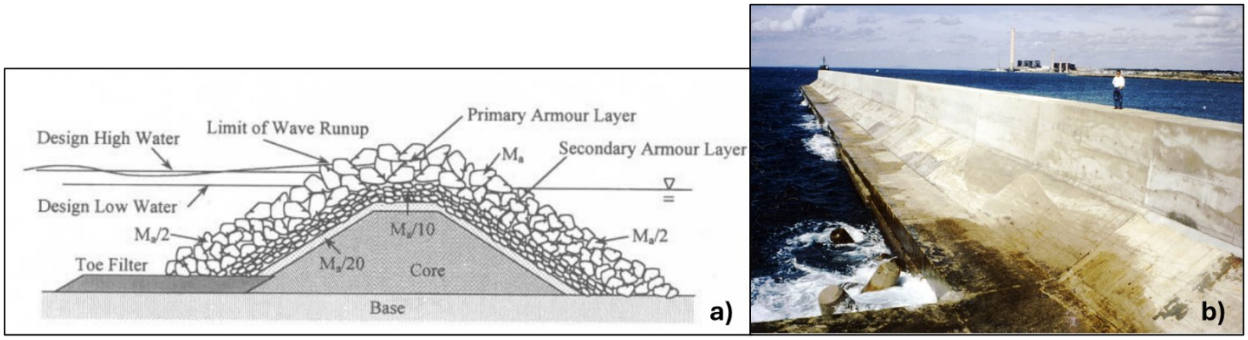

Fig 2.4. (*a*) cross section of a rubble mound breakwater (Kamphuis 2000), (*b*) vertical breakwater (EurOtop 2018)

USACE (2002) also outlines several other types of coastal structures. Some structures, like groynes and beach sills, reduce erosion without the use of armouring; they slow longshore and cross-shore sediment transport, respectively. Related processes like beach nourishment strategically add sediment to account for erosion. Other structures serve different purposes entirely. For example, structures like jetties protect navigation channels at inlets, while piles support decks or mooring (USACE 2002).

2.2.1.2. Non-Conventional Structures

Non-conventional structures may entail a unique shape or design of an already understood structure, such as a non-conventional rubble mound breakwater (Stagnitti et al. 2023), or a non-conventional vertical caisson which contains a system to convert overtopped water to mechanical energy (Di Lauro et al. 2020). However, non-conventional structures may not be directly designed to protect coastlines. For example, Berrio et al. (2023) used numerical models (XBeach and Delft3D) to investigate how offshore wave energy converters affected the morphological beach response under various orientations. They found maximum wave height reductions of 35 percent on average, and erosion reductions of approximately 20 percent.

Other structures such as dynamic revetments are also non-conventional. Dynamic revetments, also called rock slopes or gravel beaches (Van der Meer 1988), are structures where movement of the armour material is acceptable. The armour layer re-shapes, eventually reaching an equilibrium where net transport is zero (Van der Meer 1988). Some fundamental work has made efforts to predict equilibrium profiles (Van der Meer 1988; Ahrens 1989). More recent work has focussed on the effects of stone size and grading (Foss et al. 2023) or tracking individual cobbles using radio frequency identification (RFID) surveys (Bayle et al. 2021).

2.2.1.3 Nature Based Solutions

Nature based solutions (NBS) use site-specific natural elements and processes (van der Meulen et al. 2022). NBS are also an avenue for the adaptation of coastlines to climate change effects (van der Meulen et al. 2022). NBS can take many forms. For example, previous authors have considered the implementation of large woody debris (LWD). LWD is driftwood on the coastline; in terms of coastal protection, it can either be naturally occurring, or artificially placed (Wilson 2020). Focussing on its use as designed protection, novel work by Wilson (2020) investigated various orientations of anchored LWD, producing preliminary design guidance. Other work by Falkenrich et al. (2021) completed physical modelling to compare a traditional vertical seawall to various configurations of LWD, including stacked logs which imitated a vertical structure.

Another approach to NBS includes the use of vegetation. Odériz et al. (2020) studied how a combination of vegetation (*Ipomea pes-caprae* or bayhops) and a rock core affected the wave energy dissipation and a dune profile's morphodynamical response. The use of mangroves has also been investigated. Weaver et al. (2024) completed physical modelling on live mangroves to validate a representative dowel model. Using their dowel model, they were able to predict wave attenuation and changes in erosion. The effect of salt marshes on wave attenuation for dikes was studied by Marin-Diaz et al. (2023), finding that the marshes reduced wave loading on the dikes. However, the marshes were not developing in critical locations, meaning engineered works were necessary to either promote salt marsh growth or account for their shortcomings. Baker et al. (2022) completed physical modelling, using birch dowels as representative marsh vegetation, to determine how the marsh vegetation reduced wave overtopping and dissipated energy. The authors

discovered that narrow, densely vegetated marshes attenuated waves similarly to wide, sparsely vegetated marshes.

Some solutions promote the development of biological assemblages. One example are eco-friendly armour units. For example, Rosenberg (2023) investigated ECOncrete, a type of ecologically friendly concrete, finding that the biodiversity on the ECOncrete was five to seven times more abundant than over the control blocks. Moreover, Sayar et al. (2024) used ECOncrete Coastalock armour units in hydraulic stability tests of both low-crested and emergent breakwaters, under different wave conditions and breakwater characteristics.

Some authors investigated coastal management practices involving maintaining or re-instating natural shoreline functions, as opposed to engineered works. Toft et al. (2023) studied sites undergoing ecological restoration, finding that efforts to remove or avoid armoured protection and restore natural processes are increasing. Moreover, the authors found that wrack and logs were quick to recover, but other processes like biological richness took longer. Moreover, from a coastal management perspective, Cooper and Pile (2013) discuss options like migration, stating that in some cases it may be the only means to avoid climate change risks.

2.2.2. IH2VOF Fundamentals

Numerical modelling was completed as part of this study. To this effect, IH2VOF, a two-dimensional numerical model was used (Losada et al. 2007; Lara et al. 2011). Both Losada et al. (2007) and Lara et al. (2011) provide complete descriptions of the model. However, key information about the model is described herein.

IH2VOF solves the two-dimensional Reynolds Averaged Navier-Stokes (RANS) equations over cells which are rectangularly discretized. However, the model employs a cutting cell method which treats an obstacle as an object with infinite density. Therefore, a coefficient, θ, which describes the volume fraction of each cell that is open, is applied to the RANS equations to correct for obstacles. For reference, the vector form of the Navier-Stokes equations is shown below (Shaughnessy 2005):

$$\rho \frac{D\boldsymbol{u}}{Dt} = \rho \boldsymbol{f} - \nabla p + \mu \nabla^2 \boldsymbol{u} \tag{2.1}$$

In IH2VOF, the RANS equations are then re-defined as (IHCantabria 2026):

$$\frac{\partial(\theta u_i)}{\partial x_i} = 0 \tag{2.2}$$

and

$$\frac{\partial(\theta u_i)}{\partial t} + \theta u_j \frac{\partial(\theta u_i)}{\partial x_j} = -\frac{\theta}{\rho}\frac{\partial p}{\partial x_i} + \rho g_i + \frac{\theta}{\rho}\frac{\partial \tau_{ij}}{\partial x_j} + f_b \tag{2.3}$$

Where ρ is the fluid density, g_i is the ith component of gravitational acceleration, τ_{ij} represents the sum of the viscous and Reynold's stresses, and u_i is the velocity. Also, i represents the horizontal

cells and *j* represents the vertical cells (IHCantabria 2012). In the implementation of θ, coefficients between 0 (completely solid) and 1 (completely fluid) need to be defined at all four edges of the cell, i.e., θ_{right}, θ_{left}, θ_{bottom}, and θ_{top}.

The wave maker mechanism is also represented in the model through the openness coefficients. In a simple case: one-dimensional flow and piston-type wave generation, the wave board is represented as in *Fig. 2.5,* where the cell with the paddle is a partial cell, the left-adjacent cell is a solid cell, and the right-adjacent cell is a fluid cell. The movement of the wave maker is discretized using the two-step projection method and then included in the momentum equation as a source term.

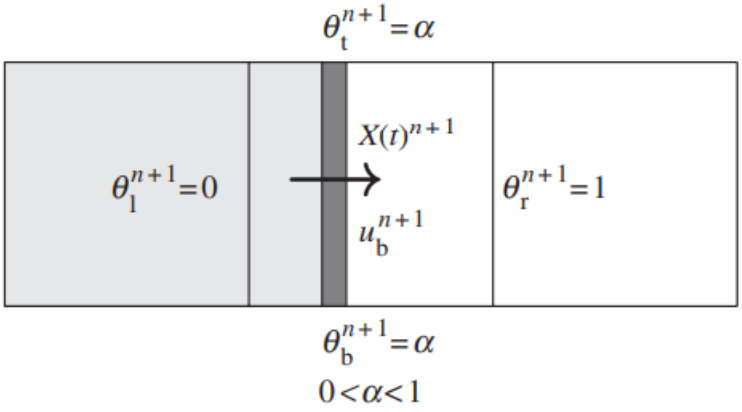

Fig. 2.5. Wave-board representation for piston-type generation (Lara et al. 2011)

For flow through porous media, IH2VOF employs the Volume-Averaged Reynolds Averaged Navier Stokes (VARANS) equations (IHCantabria 2012). The full VARANS equations are shown below (IHCantabria 2026):

$$\frac{\partial \bar{u}_i}{\partial x_i} = 0 \tag{2.4}$$

$$\frac{1+c_A}{n}\frac{\partial \bar{u}_i}{\partial t} + \frac{\bar{u}_j}{n^2}\frac{\partial \bar{u}_i}{\partial x_j} = -\frac{1}{\rho}\frac{\partial \bar{p}}{\partial x_i} + \rho g_i + \frac{\nu}{n}\frac{\partial^2 \bar{u}_i}{\partial x_j \partial x_j} - \frac{1}{n^2}\frac{\partial \overline{u_i' u_j'}}{\partial x_j} - \frac{\alpha v (1-n)^2}{n^3 D_{50}^2}\bar{u}_i - \frac{\beta(1-n)}{n^3 D_{50}}\bar{u}_i \overline{|u|} \tag{2.5}$$

Where additionally, α and β are empirical linear and non-linear drag force coefficients, c_A is an added mass coefficient, n is porosity, and D_{50} is the nominal diameter (IHCantabria 2026).

2.3 State of the Art

2.3.1 Physical Modelling

The state of the art in the adaptation of vertical structures to climate change is intertwined with design guidance. Therefore, this section will first review the state of the art of accepted design manuals, which is the basis of modern wave overtopping design for vertical structures and their adaptations. Then, recent studies which investigate how wave overtopping of vertical structures is affected by structural adaptations are reviewed. Those studies present both the state of the art in adaptation design, as well as some of the newest development in design guidance.

2.3.1.1 Design Manuals and Fundamental Studies

Wave overtopping design of traditional vertical walls is well understood, and guidance exists in several design manuals. Firstly, the *Manual on wave overtopping of sea defences and related structures* (EurOtop 2018) contains wave overtopping guidance for various structures, including dikes and embankment seawalls, armored rubble slopes and mounds, and vertical and steep walls. For vertical walls, several prediction equations and curves are provided for various configurations, shown in *Table 2.1*.

Table 2.1. Vertical wall calculation table (EurOtop 2018)

	Mean value approach	Design approach
Discrimination – mound influence?	Eq. 7.3	Eq. 7.3
Discrimination – impulsive / non-impulsive regime		
Plain vertical walls	Eq. 7.4	Eq. 7.4
Composite vertical walls	Eq. 7.13	Eq. 7.13
Plain vertical walls; overtopping discharge		
No influencing foreshore	Eq. 7.1 (= Eq. 5.17)	Eq. 7.2
Foreshore; non-impulsive conditions	Eq. 7.5	Eq. 7.6
Foreshore; impulsive conditions	Eqs. 7.7, 7.8	Eqs. 7.9, 7.10
Broken wave conditions (emergent toe)	Figure 7.10	
Steeply-battered walls	Eq. 7.11	
Composite vertical walls		
No influencing foreshore	Eq. 7.1	Eq. 7.2
Foreshore; non-impulsive conditions	Eq. 7.5	Eq. 7.6
Foreshore; impulsive conditions	Eqs. 7.14, 7.15	
Oblique wave attack	Figure 7.17	
Influence of short- vs long-crestedness	Eqs. 7.16, 7.17	
Non-impulsive conditions	Eqs. 7.18, 7.19	
Impulsive conditions		(Eq. 7.20)
Vertical walls with wave return wall / bullnose	Eqs. 7.21 - 7.23; Figure 7.22, Figure 7.23	
Perforated walls	Section 7.3.7 (commentary)	
Proportion of overtopping waves		
Normal wave attack	Eqs. 7.24, 7.25	
Oblique waves, non-impulsive conditions	Eqs. 7.29, 7.30	
Oblique waves, impulsive conditions	Eqs. 7.31 - 7.33	
Individual overtopping volumes	Eqs. 7.26, 7.28; impulsive b = 0.85	
with oblique waves	Eqs. 7.26, 7.28; impulsive b = 0.85 and Table 7.2, with Eqs. 7.31-7.33	
Overtopping velocities	Eq. 7.34	

In many design cases, the foreshore will have an influence if $h_t/H_{m0,deep} \leq 4$ (EurOtop 2018), where h_t is the water depth at the toe of the structure. For example, for the case of a plain vertical wall, no mound influence, and impulsive overtopping conditions, then the following mean value equations apply, depending on the relative freeboard (EurOtop 2018):

$$\frac{q}{\sqrt{gH_{m0}^3}} = 0.011\left(\frac{H_{m0}}{hs_{m-1,0}}\right)^{0.5}\exp\left(-2.2\frac{R_c}{H_{m0}}\right), \qquad 0 < \frac{R_c}{H_{m0}} < 1.35 \tag{2.6}$$

$$\frac{q}{\sqrt{gH_{m0}^3}} = 0.0014\left(\frac{H_{m0}}{hs_{m-1,0}}\right)^{0.5}\left(\frac{R_c}{H_{m0}}\right)^{-3}, \qquad \frac{R_c}{H_{m0}} \geq 1.35 \tag{2.7}$$

where q is the mean overtopping discharge per unit width, H_{m0} is the significant wave height, R_c is the crest freeboard, h is the depth at the structure toe, and $s_{m-1,0}$ is the wave steepness. As referenced in *Table 2.1*, EurOtop distinguishes two forms of equations: a mean value approach, and a design and assessment approach whereby the prediction is increased one standard deviation by increasing the value of the leading coefficient.

EurOtop also provides guidance for vertical walls with additions. A toe berm (*Fig. 2.6* (*a*)) and wave return wall (*Fig 2.6*. (*b*)) are two examples presented in the manual. The detailed design procedures are available in (EurOtop 2018).

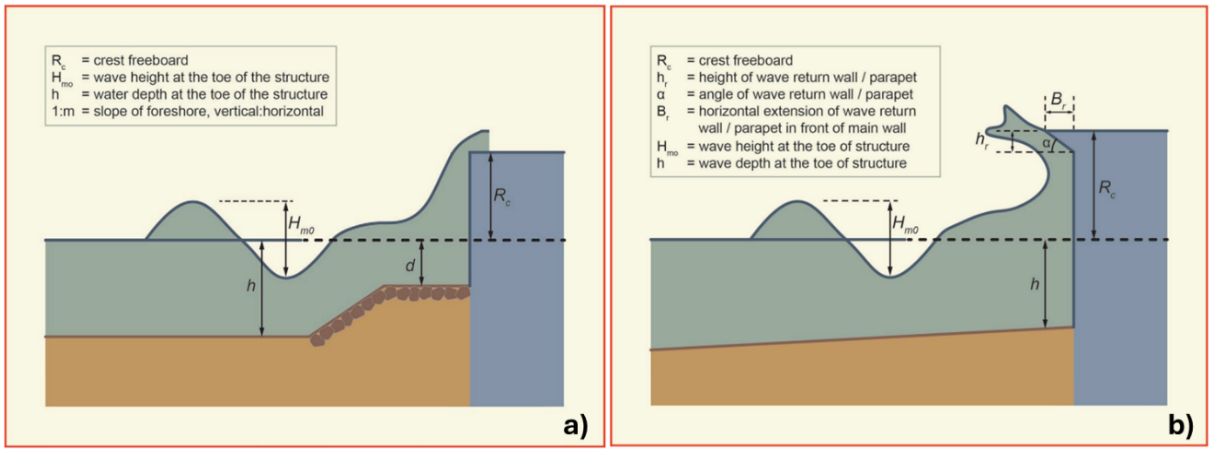

Fig 2.6. EurOtop (2018) schematics for vertical walls with various additions: (*a*) toe berm, and (*b*) wave return wall/bullnose

The United States Army Corps of Engineers (USACE) has developed multiple guidelines for vertical walls. *Design of Coastal Revetments, Seawalls, and Bulkheads* contains guidance for seawalls and bulkheads (USACE 1995). The manual presents many forms of seawalls, including sheet pile, treated timber, and even used concrete pipes and used tires. The document provides one overtopping design equation from Ward and Ahrens (1992), used for bulkheads and simple vertical seawalls with small parapets:

$$Q' = C_0\exp\left[C_1F' + C_2\left(\frac{F}{d_s}\right)\right] \tag{2.8}$$

and,

$$F' = \frac{F}{(H_{m0}^2 L_o)^{\frac{1}{3}}} \tag{2.9}$$

where F is the crest freeboard, d_s is the depth at the structure toe, and C_0, C_1, and C_2 are regression coefficients equal to 0.338, -7.385, and -2.178 respectively. However, the manual does not provide equations for more complicated vertical wall cases and suggests either referring to Ward and Ahrens (1992) or conducting physical modelling (USACE 1995).

Ward and Ahrens (1992) tested many different configurations. However, the case which yielded *Eqn. 2.5* and *2.6* was from a vertical wall with a recurved parapet, not a traditional vertical wall (see *Fig 2.7*).

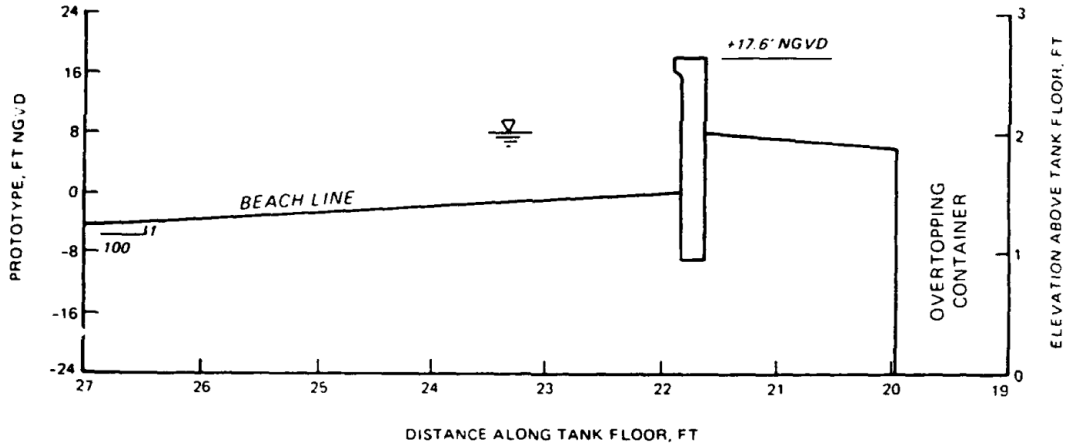

Fig 2.7. Vertical wall with recurved parapet, tested in Ward and Ahrens (1992)

The study also reviewed many adapted seawalls, including various fronting revetments, revetment with/without a toe berm and with/without caps on the parapet, recurved seawalls with revetments, plain vertical walls with revetments, and stepped seawalls with a recurved parapet and revetments. The plain vertical wall case is relevant to the EurOtop vertical wall discussions, and is shown in *Fig 2.8*, with the associated prediction equation presented in *Eqn. 2.10* (Ward and Ahrens 1992).

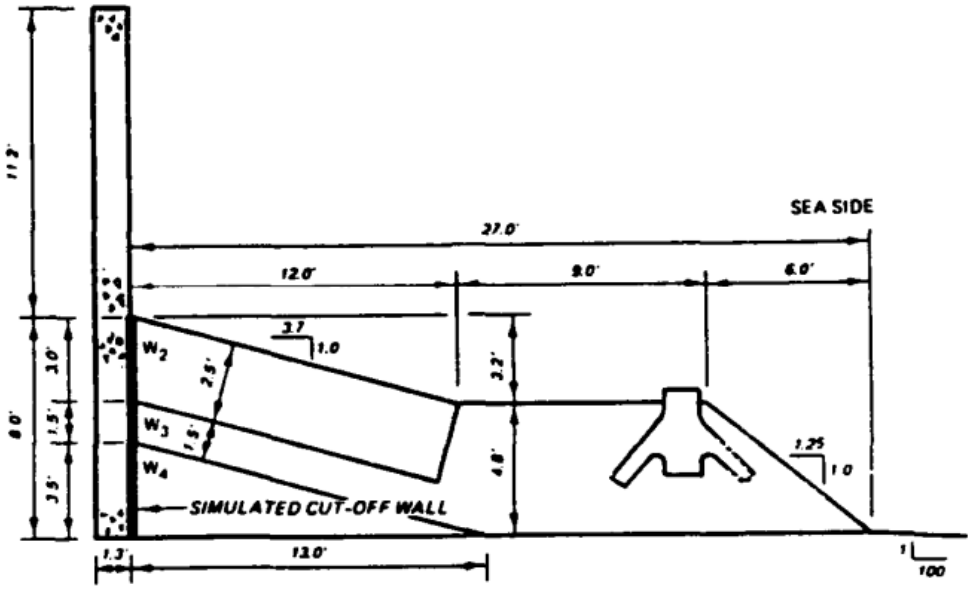

Fig. 2.8. Vertical wall with fronting revetment, tested in Ward and Ahrens (1992)

$$Q' = C_0 \exp\left[C_1 F' + C_2 \left(\frac{H_{m0}}{L_o}\right)^{1/2}\right] \tag{2.10}$$

where $C_0 = 0.541$, $C_1 = -11.702$, and $C_2 = -5.771$. USACE also developed the *Coastal Engineering Manual* (USACE 2002). In part six (chapter five) the manual reviews overtopping guidance for many types of structures. For vertical structures, the manual references work by Franco and Franco (1999). Franco and Franco studied several vertical wall setups, under non-breaking waves, as well as oblique, and long and short crested conditions. The study also considered the effects of several additions to the vertical wall, such as recurved walls, and perforated walls both with and without an open deck. The authors noted that the open deck acted as an air intake which promoted energy absorption. USACE (2002) presented the following equation:

$$\frac{q}{\sqrt{gH_s^3}} = 0.082 \exp\left(-3.0 \frac{R_c}{H_s} \frac{1}{\gamma_\beta \gamma_s}\right) \tag{2.11}$$

Note the addition of the γ terms. γ_β acts as a correction factor for oblique waves and was calculated separately depending on whether the waves were long or short crested, and γ_s acted as a correction factor for the different additions to the vertical wall, shown in *Table 2.2*.

Table 2.2. γ_s for *Eqn. 2.8* (USACE 2002; Franco and Franco 1999)

Front Geometry	γ_s
Plain impermeable wall	1.00
Plain impermeable wall with recurved nose	0.78
Perforated front (20% hole area) and deck	0.72-0.79
Perforated front (20% hole area) and open deck	0.58

While not specified as vertical wall studies, USACE (2002) provides overtopping guidance for other structures, including for rock armoured slopes with a berm in front of a crown wall (Bradbury and Allsop 1988), various straight armour slopes with a berm in front of a crown wall (Aminti and Franco 1988), and permeable rock armoured slopes with a berm in front of a crown wall (Pedersen and Burcharth 1992; Pedersen 1996). This author's opinion is those structures are like a vertical wall with a fronting armoured slope.

The use of correction factors (*Table 2.2*, Franco and Franco 1999) to account for vertical wall additions was considered later by other authors. One foundational study by Kortenhaus et al. (2003) provided guidance for parapet additions. The study used data from previous sources and authors, deriving a reduction factor for the parapet effect. The study used identical conditions, with and without the parapet. When an equivalent plain vertical wall case was not available, a validated formula for vertical wall prediction was used to predict the overtopping. The authors developed a *k*-factor, in the following form (Kortenhaus et al. 2003):

$$k = \frac{q_{parapet}}{q_{no\ parapet}} \tag{2.12}$$

k was a function of wave conditions and parapet characteristics: relative freeboard, parapet width, and parapet angle parameters. The authors corrected the points in the overarching dataset for the parapet and re-plotted the results for comparison. The authors noted that if both overtopping rates are low, calculation of the *k*-factor may cause additional data scattering (Kortenhaus et al. 2003).

Pearson et al. (2005) also focused on design guidance for recurved walls and furthered Kortenhaus et al.'s work. Pearson et al. considered the higher values of reduction, developing a more detailed approach for higher relative freeboards, where scatter was large and a lot of data was subsequently overpredicted by accepted curves. The authors provided a new design methodology, whereby predictions at higher relative freeboard were further separated depending on R_c/h_s, which helped improve scatter (h_s is the water depth at the structure toe). Otherwise, the approach was identical to Kortenhaus et al. (2003).

2.3.1.2. Recent Design Guidance

Correcting design equations for adaptations beyond parapet walls was investigated more recently and constitutes design guidance. Specifically for vertical walls, Dong et al. (2020) investigated how multiple adaptations to a traditional vertical wall (recurve wall, reef breakwater, vegetation, and diffraction pillars) affected the overtopping discharge. Schematics of the four adaptation cases are shown in *Fig 2.9*. The traditional vertical wall may also be isolated.

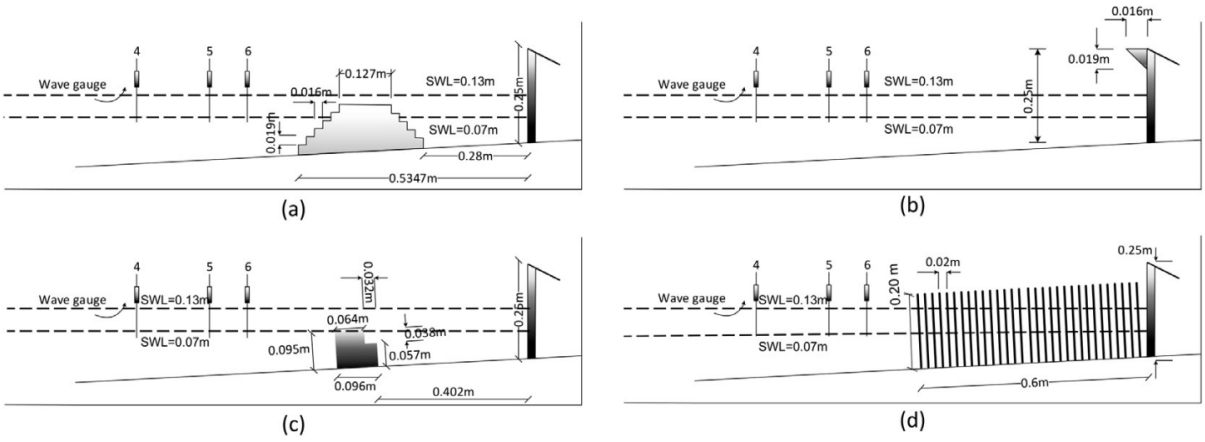

Fig. 2.9. Four tested vertical wall adaptation cases, (*a*) reef breakwater, (*b*) re-curve wall, (*c*) diffraction pillars, and (*d*) vegetation (Dong et al. 2020)

For these tests, the vertical wall was 12.21 m from the wave board. The authors calibrated the *a*, *b*, *c*, and *d* coefficients on the following EurOtop equations for each of the retrofits, shown in *Eqn. 2.13* and *2.14* (Dong et al. 2020). For convenience, the coefficients are summarized in *Table 2.3*.

$$\frac{q}{\sqrt{gH_{m0}^3}} = \boldsymbol{a}\left(\frac{H_{m0}}{hs_{m-1,0}}\right)^{0.5} \exp\left(\boldsymbol{b}\frac{R_c}{H_{m0}}\right), \qquad 0 < \frac{R_c}{H_{m0}} < 1.35 \tag{2.13}$$

$$\frac{q}{\sqrt{gH_{m0}^3}} = \boldsymbol{c}\left(\frac{H_{m0}}{hs_{m-1,0}}\right)^{0.5} \left(\frac{R_c}{H_{m0}}\right)^{\boldsymbol{d}}, \qquad \frac{R_c}{H_{m0}} \geq 1.35 \tag{2.14}$$

Table 2.3. Calibration parameters for the four retrofits (Dong et al. 2020)

Retrofit	a	b	c	d	Total RMSE
Reef breakwater	0.0055	-3.15	0.0002	-3.1	0.527
Diffraction Pillars	0.01	-3	0.00046	-3.23	0.190
Recurve wall	0.0016	-4.5	0.00011	-3.5	0.500
Vegetation	0.0053	-3.5	0.00011	-2.78	0.248

Dong et al. (2024) completed a study of a similar scope but calibrated their retrofit equations more consistently with (Kortenhaus et al. 2003; Pearson et al. 2005). The study focused solely on recurve wall adaptations and aimed to improve the prediction methods by Kortenhaus et al. (2003) and Pearson et al. (2005) by incorporating the incident wave conditions into the prediction, via R_c/H_{m0}, and $s_{m-1,0}$. The study used the same flume as Dong et al. (2020). They reviewed four different recurve geometries. Based on the results, the authors proposed a correction factor to the equations developed by Kortenhaus et al. (2003), by applying the α factor in *Eqn. 2.15*. The corrected Kortenhaus et al. (2003) equation is shown in *Eqn 2.16* (Dong et al. 2024):

$$\alpha = 0.056 + 0.00035\left(\frac{R_c}{H_{m0}}\right)^{-4.8} s_{m-1,0}^{-2.1} \tag{2.15}$$

$$k = \begin{cases} \alpha & \frac{R_c}{H_s} \leq R_0^* \\ \alpha\left[1 - \frac{1}{m}\left(\frac{R_c}{H_s} - R_0^*\right)\right] & R_0^* < \frac{R_c}{H_s} \leq R_0^* + m^* \\ \alpha\left[k_{23} - 0.01\left(\frac{R_c}{H_s} - R_0^* - m^*\right)\right] & \frac{R_c}{H_s} \geq R_0^* + m^* \end{cases} \tag{2.16}$$

where R_0^* and m^* are terms based on the recurve wall geometry. Dong et al. (2024) found that the proposed method had better RMSE accuracy for discharge reduction (in the form of the *k*-factor) and overtopping discharge.

Kisacik et al. (2022) placed their study in the context of sea level rise. They investigated adaptations which, from a design perspective, accommodate recreational functionality. Adaptations such as a promenade, storm walls, and parapets were considered. Additionally, they considered several stilling wave basins. *Fig. 2.10* (*a*) shows the promenade-based adaptations general form, and *Fig. 2.10* (*b*) shows the stilling wave basin-based adaptations general form.

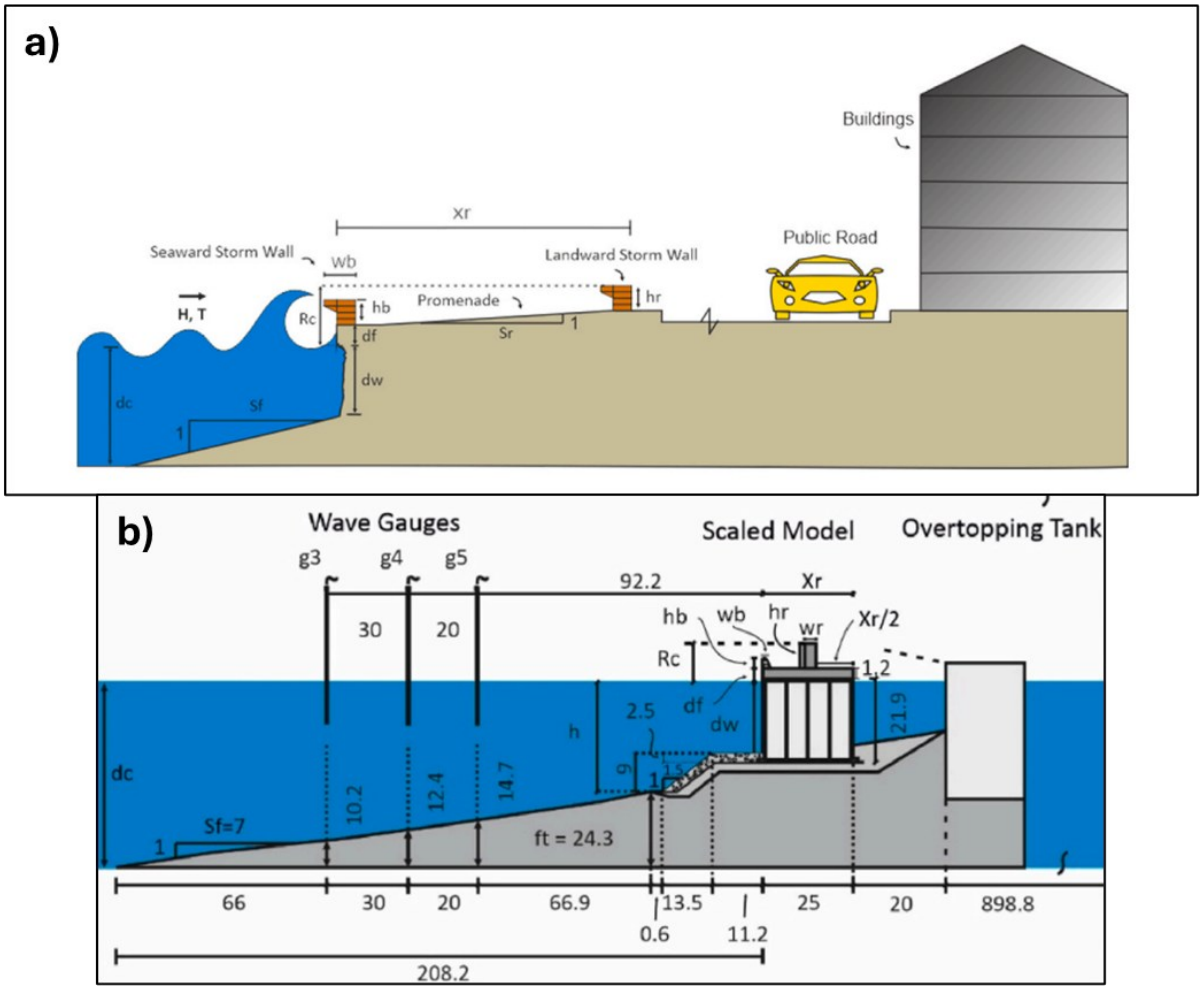

Fig 2.10. (*a*) Promenade and (*b*) stilling wave basin-based adaptations schematic (Kisacik et al. 2022)

The study incorporated two different experimental programs, hence the different geometries. The promenade alone was not very effective, but the storm wall and parapet combinations, as well as the stilling wave basin cases reduced overtopping considerably, especially at higher relative freeboard. Reduction coefficients were determined to correct R_c/H_{m0} in the EurOtop (2018) equations (Kisacik et al. 2022):

$$\frac{R_c}{H_{m0}}\frac{1}{\gamma} \tag{2.17}$$

where,

$$\gamma = k + l\frac{R_c}{H_{m0}} \tag{2.18}$$

k and l are regression coefficients based on the geometry. k and l were only calibrated once for all sea states tested, entailing the equation is only valid within the conditions tested (Kisacik et al.

2022). For promenade cases only, the effect of dimensionless promenade width, $X_r/L_{m-1,0}$, was considered instead of relative freeboard to remain consistent with EurOtop guidance for dikes.

Kisacik et al. (2022) also investigated the accuracy of combining reduction parameters. They multiplied the coefficients for a stilling wave basin with landside storm wall, γ_1, and for a stilling wave basin with seaside storm wall, γ_2, and assessed how well it compared to the experimentally determined coefficient for a stilling wave basin with seaside and landside storm walls. The results were promising, specifically for low-crested structures. The authors recognized that combining coefficients simply combines individual effects and does not account for how the overtopping mechanism changes due to the altered geometry.

2.3.2 Numerical Modelling

2.3.2.1 Relevant Work

Di Lauro et al. (2020) compared the hydraulic performance of a unique vertical breakwater design to a traditional structure. The unique breakwater incorporated a wave energy conversion system. It included a crown wall with a parapet, and a reservoir on the sea side of the crown wall. Using IH2VOF, ten overtopping simulations for nine different geometries were completed. The overtopping of the traditional vertical breakwater and the novel design were compared to relevant EurOtop equations. The numerical simulations generally fell within the equation's 90 percent confidence intervals. However, to account for the novel breakwater's geometry, an influence factor, γ_{OBREC}, was introduced to correct the relative freeboard on the EurOtop equation (similar to the method of Kisacik et al. (2022)). The coefficient was defined as follows (Di Lauro et al. 2020):

$$\gamma_{OBREC} = 1.163 \cdot exp\left(-1.737 \frac{B_{wall}}{L_{m-1,0}}\right) \tag{2.19}$$

where B_{wall} was the distance from the primary face of the caisson to the primary face of the crown wall. The modified formula had good performance. The results were corrected and plotted against the applicable EurOtop equation, shown in *Fig. 2.11*.

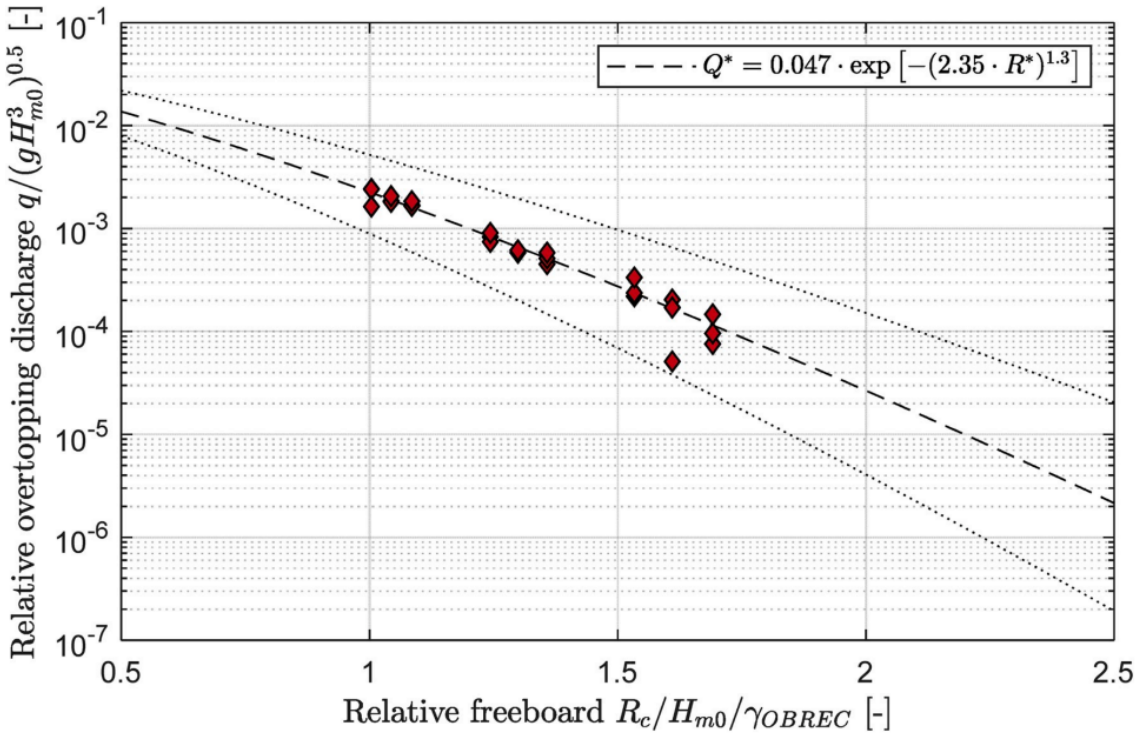

Fig. 2.11. Corrected numerical overtopping data using γ_{OBREC} (Di Lauro et al. 2020)

Pilechi et al. (2018) compared IH2VOF wave overtopping and free surface results to two-dimensional physical modelling tests for a rubble mound revetment. IH2VOF's built-in turbulence model created less than a 5 percent difference in results compared to the laminar turbulence model. The discrepancies in wave overtopping were correlated to discrepancies in free-surface elevations. For example, for one of the test cases they noted that the overprediction of overtopping values over a specific time was related to the overprediction of wave period for some wave modes. The study's key results are shown in *Table 2.4*. The average overtopping discharges were reproduced with an accuracy of approximately 20 percent.

Table 2.4. Results from Pilechi et al. (2018)

Test Case	**Experiment**				**IH2VOF**			
	H_{m0} (m)	$H_{1/3}$ (m)	T_p (s)	Q_{avg} (m^3/m/s)	H_{m0} (m)	$H_{1/3}$ (m)	T_p (s)	Q_{avg} (m^3/m/s)
1	2.53	2.73	14.5	0.037	2.42	2.34	14.7	0.046
2	2.64	2.84	14.6	0.075	2.36	2.83	27.9	0.062

Oliveira et al. (2020) compared XBeach and IH2VOF performance to empirical formulas at predicting wave overtopping over a sloped structure with a crest berm. Two cases were tested. In the first case, no overtopping occurred, allowing free-surface elevation and wave runup comparisons. For free-surface elevations, the correlation between XBeach and IH2VOF was better for wave gauges that were less affected by the profile bottom. For the second case, overtopping

occurred. For a duration of 50 waves, results differed for all three prediction methods. *Table 2.5* shows that IH2VOF underpredicted the empirical formulas.

Table 2.5. Results from the second test from Oliveira et al. (2020)

Method	Q_{av} ($m^3/s/m$)	V_{tot} (m^3/m)
IH2VOF	0.18	107.57
XBeach	0.03	16.88
Empirical formulas	0.46	276.48

Neves et al. (2021) compared three numerical models, namely IH2VOF, DualSPHysics, and FLUENT, with various physical modelling results for a dike with a promenade. Comparatively, the structure was similar to Oliveira et al. (2020). For two total tests, IH2VOF underpredicted the Ru_{max}, the maximum runup, compared to the physical model tests. However, IH2VOF comparatively overpredicted the mean overtopping discharge, shown in *Table 2.6*. Wave breaking and overtopping were both sensitive to the use of the turbulence model in all three numerical models. All results were compared after simulations involving 25 waves.

Table 2.6. Mean overtopping discharge results from Neves et al. (2021)

Test no.	h (m)	T (s)	H (m)	Q (L/s/m)			
				Physical Model	IH2VOF	DualSPHysics	FLUENT
1	0.50	2.04	0.116	0.00	0.00	0.00	0.00
2		2.04	0.230	0.00	0.01	0.01	0.13
3		1.50	0.230	0.00	0.00	0.00	0.00
4	0.58	2.04	0.116	0.02	0.00	0.00	0.20
5		2.04	0.230	0.35	1.80	0.87	2.26
6		1.50	0.230	0.05	0.05	0.02	0.14
7	0.62	2.04	0.116	0.35	0.51	0.45	0.98
8		2.04	0.230	2.84	3.95	2.41	5.30
9		1.50	0.230	0.98	1.58	0.70	1.55

Dang et al. (2021) used IH2VOF, EurOtop (2018) equations, and neural network predictions to compare the mean overtopping discharge for a novel seawall structure which included stepped sections and a recurve near the crest. A calibration series with physical and theoretical data was completed. Then, eight tests (four with regular waves and four with irregular waves) were conducted. At lower levels of relative freeboard (R_c/H_s in this study), significant discrepancies arose between IH2VOF and the other methods (Dang et al. 2021), shown in *Table 2.7*.

Table 2.7. Mean overtopping discharges for all tests and approaches from Dang et al. (2021)

Test Case	H_s (m)	T_s (m)	Empirical equation ($m^3/s/m$)	IH2VOF ($m^3/s/m$)
Regular Waves	1.35	8.67	0.00321	0.00849
	1.50	7.64	0.00562	0.01021
	1.90	9.20	0.03034	0.03307
	2.10	9.24	0.04950	0.07706
Irregular Waves	1.68	8.99	0.01436	0.01796
	1.78	9.31	0.02044	0.02895
	2.07	9.32	0.04631	0.05080
	2.36	9.24	0.08494	0.05799

2.3.2.2 Design Guidelines

Stagnitti et al. (2023) used IH2VOF, aiming to build wave overtopping design guidance for existing and upgraded rubble mound structures, shown in *Fig. 2.12*:

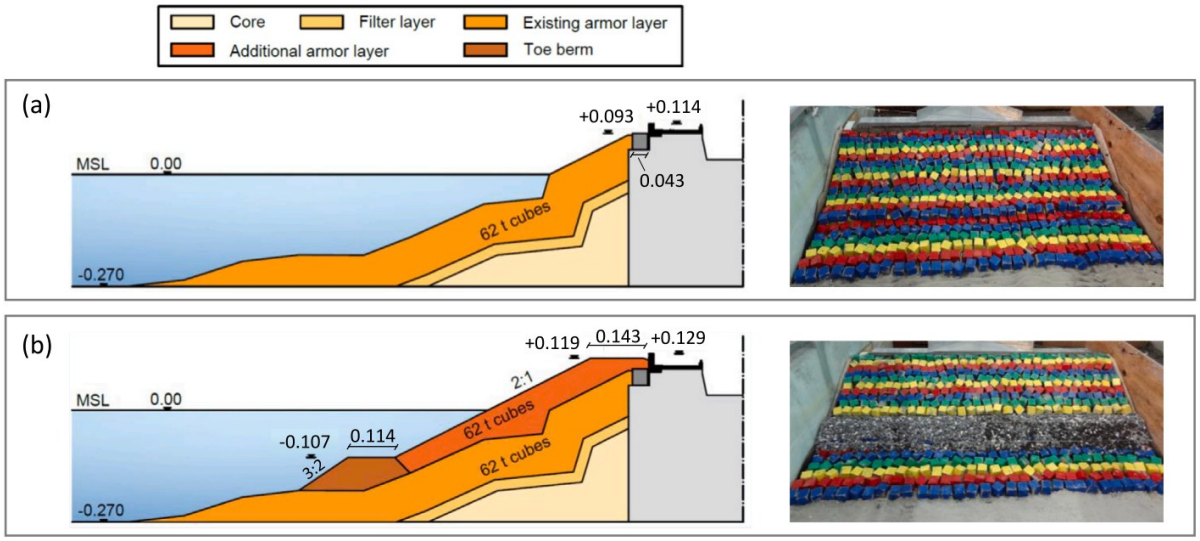

Fig 2.12. Investigated structures by Stagnitti et al. (2023), both (*a*) existing, and (*b*) upgraded geometries

The authors placed the study in the context of augmented design conditions due to climate change. The numerical model was first calibrated using experimental data, then validated by adjusting the wave seedings of the chosen irregular parameters. Using the validated model, 300 total numerical simulations were compared to several existing design equations, including EurOtop (2018) equations. However, the data did not fit the equations sufficiently. So, the authors built their own in the following form (Stagnitti et al. 2023):

$$\frac{q}{\sqrt{gH_s^3}} = \boldsymbol{a_q} \cdot \exp\left[-\left(\boldsymbol{b_q} \cdot \frac{R_c}{H_s \xi_{m-1,0}}\right)^{\boldsymbol{c_q}}\right] \tag{2.20}$$

where c_q was determined for the entire dataset (both existing and upgraded structures) and a_q and b_q were regression coefficients. The authors found good correlation to numerical predictions for the existing ($R^2 = 0.94$) and upgraded ($R^2 = 0.78$) structures. A similar analysis was completed for both overtopping probability, P_o, and overtopping volume statistics, through $P_{Vi}(V)$.

The authors noted that design guidance in this realm is very limited and that, while experimental data is needed to calibrate numerical models, the calibrated numerical model can be used to reduce the uncertainty in the assessment of the damaged and upgraded structures. Moreover, derived prediction formulas from the numerical dataset can be aptly used during the design phase for such structures.

2.5 Discussion and Research Needs

The review revealed how best to contribute to adaptation design. To this effect, several vertical wall design equations were presented. Various corrected equations were also presented, showing how researchers accounted for additions to vertical structures. Of the presented equations, the most useful approaches were also the most intuitive. For example, Kortenhaus et al.'s *k* approach is an intuitive representation of an adaptation's influence. Moreover, developing *k* as a function of both incident wave conditions and geometrical parameters aids design, better capturing the causation of an adaptation's hydrodynamic influence on the overtopping (as shown in Dong et al. 2024). For engineers, it is also useful to present corrected data relative to existing design equations, as in (Di Lauro et al. 2020) (refer to *Fig 2.11*).

Section 2.3.2 reviewed several studies that compared IH2VOF (and in two instances, other numerical models) to either experimental modelling or empirical formulae. Referencing *Table 2.6*, when only the bottom four rows of *Table 2.6* were considered, the *RMSE* between the physical modelling data and IH2VOF (0.150) was lower than DualSPHysics (0.222) and FLUENT (0.358). And, although for only one test, IH2VOF comparatively outperformed XBeach at replicating both wave overtopping discharges and volumes.

Using the presented raw data from those studies, the average absolute percent differences and the *RMSE* was calculated for each study, and cumulatively for all four studies for IH2VOF only, shown in *Table 2.8*. See Sections *3.0* and *4.0* for details regarding the *RMSE* calculation.

Table 2.8. IH2VOF performance for several studies

Study	Compared to	Structure type	Average absolute percent differences	*RMSE*
Pilechi et al. (2018)	Physical modelling	Rubble mound revetment	20.8	0.089
Neves et al. (2021)		Dike with promenade	60.9	0.345
Oliviera et al. (2020)	Empirical equations	Slope with crest berm	110.1	-
Dang et al. (2021)		Stepped seawall	52.4	0.208
	Cumulative		*69.5*	*0.265*

The model is 69.5 percent different on average from either experimental results or empirical formulae. Moreover, while not captured by absolute value calculations, IH2VOF typically overpredicted results, with only 4 of 17 tests being underpredicted. Notably, however, none of the listed studies were for a vertical wall. Especially since the model's performance fluctuated significantly between the structures in *Table 2.8*, IH2VOF's overtopping representation is uncertain for vertical structures, and needs further investigation.

The literature review admittedly lacks detailed descriptions regarding the state of the art of numerical models other than IH2VOF and is therefore limited. There have certainly been published works presenting the capabilities of, for example, OpenFOAM for similar scopes as the reviewed IH2VOF studies. Recently, Jonker et al. (2024) used OpenFOAM to numerically investigate how a homogeneous low crested structure (HLCS) affected the wave overtopping over a vertical wall, considering both geometrical parameters and incident wave heights. Also, Wang et al. (2025) used OpenFOAM in part to understand how wind speed affected the cumulative wave overtopping volume at a vertical wall on a flat reef. Alternatively, Tuozzo et al. (2024) investigated how attached and detached breakwaters affected the wave overtopping and then compared the results to FLOW-3D simulations. In this work, however, IH2VOF was found to be a user-friendly, easy to learn model for a first-time numerical modeller. Moreover, because using IH2VOF for this work seemed to address a gap in the literature (see Section 2.5), other models were not specifically considered.

A small number of physical modelling studies exist which reviewed adaptations to vertical walls. Of those studies, investigations mostly focused on crest adaptations, with few (Dong et al. 2020; Kisacik et al. 2022) reviewing landward or seaward adaptations. Those solutions will also be important for engineers, who may face construction restrictions for one or more locations relative to the seawall. Subsequently, data and prediction equations should exist to aid engineers in adaptation design. There is a need to investigate more adaptations, whether at the crest, or seaward, or landward of it. There is also a need to incorporate numerical modelling for vertical structure adaptation design, for the development of numerically generated prediction equations in design (Stagnitti et al. 2023).

While some investigations considered a vertical wall alternative made of LWD (Falkenrich et al. 2021), few studies have reviewed how NBS, eco-friendly, or less gray solutions can be incorporated into adaptation design, especially for vertical structures. All the solutions presented in Section 2.2.1.3 are possible as retrofit structures. For example, LWD could be installed as an independent anchored system (see Wilson 2020) just lakeward of the wall, akin to a breakwater. Vegetation has already been investigated as a retrofit structure by Dong et al. (2020), and its potential as a retrofit certainly deserves further investigation. Possibly, like in Odériz et al. (2020), the dissipative effects of vegetation and rock cores/slopes could be combined as a retrofit option. Armour units which promote biological growth, like ECOncrete units, are promising alternatives to traditional armour units. Even structures like dynamic revetments are intriguing retrofit options.

Moreover, the reviewed works investigate adaptation to climate change effects; mitigation of effects should also be considered.

The review presented several experimental cross sections. Of those presented, few cross sections were standard vertical walls with simple bathymetries, akin to the vertical wall representation for EurOtop equations. Therefore, testing with a simple bathymetry would be a valuable contribution.

Engineers need adaptation guidance to be valid under regionally relevant wave conditions. In Ontario, coastal engineers may find applicability if guidance is developed using Great Lakes-representative conditions. Of course, using regional wave conditions does not nullify the study's relevance to other coastal areas – the results may still be useful globally.

3 Experimental Modelling of Climate Change-Adaptive Vertical Seawalls

Preprint of an article in preparation for submission, entitled "Adapting Vertical Seawalls to Water Level Rise"

3.1 Introduction

Storms like Hurricane Sandy significantly impact coastal communities: of the US$50 billion in damages recorded across the United States due to Hurricane Sandy, US$19 billion occurred in New York City alone (PlaNYC 2013). However, climate change may further impact coastal communities. In one study, Garner et al. (2017) noted that the 500-year flood level in New York City in 2080-2100 could be between 4.0 and 5.1 m (relative to preindustrial baseline levels) due to climate change – a significant impact. Furthermore, sea level rise and storm surges will harm community well-being and damage infrastructure (Sinay and Carter 2020). Clearly, climate change may significantly affect coastal communities via intensified coastal hazards. On the Great Lakes, consultants and coastal zone managers are addressing climate change's impact on flood hazards. For example, Stantec produced the *Municipality of Lakeshore Shoreline Management Plan* in 2022, including predictions of the 100-year flood level on Lake St. Clair under various global warming levels (Stantec 2022).

Future coastal structure designs need to account for increases in design water levels due to climate change. However, the necessity of upgrading the many existing coastal structures is apparent (Foti et al. 2020). In 2023, Baker et al. conducted an experimental study in the Large Wave-Current Flume (LWCF) at the National Research Council of Canada's Ocean, Coastal, and River Engineering Research Centre (NRC-OCRE). The study reviewed various adaptations to a traditional coastal revetment with the goal of understanding how each adaptation reduced the wave overtopping (OT) (Baker et al. 2023). To the authors' knowledge, literature regarding adapting vertical structures to water level rise (WLR) and climate change is limited, representing a significant knowledge gap.

3.2 Literature Review

3.2.1 Provisions of specific manuals and design guidelines

The *Design of Coastal Seawalls, Revetments, and Bulkheads* (USACE 1995) provides one design equation for vertical walls and emphasises quantifying and accounting for overtopping in design. The *Coastal Engineering Manual* (USACE 2002) provides more detail about wave overtopping for various structures. For vertical walls, this manual references Franco and Franco (1999), who present dimensionless OT equations for standard vertical walls, and factors for oblique waves and various adaptations: bullnose, perforated front face, and perforated deck on the crest of the structure. The EurOtop manual (EurOtop 2018) provides prediction equations for standard vertical

walls, and guidance or information for select deviations: battered (near vertical) walls, composite vertical walls, wave return walls, and perforated walls (EurOtop 2018). However, provisions are not available for seaward perched beaches or breakwaters, nor landward drainage swales.

Regarding regional guidelines, the Ministry of Natural Resources (MNR) in the Province of Ontario, Canada authored the *Technical Guide for Great Lakes – St. Lawrence River System* (MNR 2001). Section seven of this guideline discusses OT of vertical seawalls but only directs readers to other relevant studies. For larger scale studies, the guidelines recommend physical modelling (MNR 2001). Another document, *Wave Uprush and Overtopping: Methodologies and Applications – Great Lakes – St. Lawrence River Shorelines* (Atria 1997) reviews in depth guidance for vertical walls, but only for simple cases. The lack of recent regional guidance in the Province of Ontario, Canada is further evidence that more in-depth, design-focused information should be readily available.

3.2.2 Studies on vertical walls

A limited number of studies exist which investigate adapting or upgrading vertical seawalls to climate change. Rambabu & Srineash (2022) discuss several options for adaptations: recurve walls, reef breakwaters, vegetation, and diffraction pillars. However, few of their reviewed studies involved determining through physical modelling how the adaptations reduced wave overtopping at vertical structures.

Recurve walls are well-studied, and the EurOtop (2018) manual contains design provisions. Regarding physical modelling, Kortenhaus et al. (2003) and Pearson et al. (2005) developed early design guidance for recurve walls via a k factor: the overtopping reduction factor from a vertical wall without a parapet to a vertical wall with a parapet. They incorporated parameters related to the geometry of the recurve wall to construct the k coefficients. Developing prediction equations or correcting existing OT equations for adaptations, like Kortenhaus et al. (2003) and Pearson et al. (2005) is useful because sometimes no formulae exist (Foti et al. 2020). Recently, Dong et al. (2024) completed physical modelling on vertical wall structures and devised a new methodology (with greater statistical accuracy than Pearson et al. (2005) and Kortenhaus et al. (2003)) by considering wave steepness and freeboard in their correction of the Kortenhaus et al. (2003) equations.

Other authors used similar approaches for other adaptations. Dong et al. (2020) investigated through physical modelling how four adaptations (recurve wall, reef breakwater, vegetation, and diffraction pillars) improved a baseline vertical structure's wave overtopping resistance. They discovered that adaptations performed better at higher relative freeboards (R_c/H_{m0}) and also noted the importance of overtopping rate. The authors re-calibrated the EurOtop equations for the retrofitted vertical wall, based primarily on wave impulsivity and relative freeboard. Kisacik et al. (2022) completed physical modelling and presented reduction factors for a variety of adaptations: parapets, stilling wave basins (single and double row seaside configurations), and promenades, to

correct R_c/H_{m0} in the standard EurOtop equations as a function of relative freeboard. For one of their cross sections, the authors incorporated drainage holes on the primary vertical face.

3.2.3 Studies on adaptations to other types of structures, and Nature-Based Solutions (NBS)

Nature Based Solutions (NBS) are alternatives to typical engineered coastal protection works and involve the restoration of habitats either in a soft (non-engineered works) or hybrid approach (Rupasinghe et al. 2023). There are many promising options: Large Woody Debris (LWD) as a standalone solution (Kennedy & Woods 2012; Johannessen et al. 2014; Wilson 2020; Falkenrich et al. 2021); improving the sustainability of materials such as concrete (Rupasinghe et al. 2023); or using vegetation (Carus et al. 2016; Schoonees et al. 2019; Odériz et al. 2020); or using Geobags (Yuanita et al. 2021; Jebakumar et al. 2022). There are even some studies which discuss allowing natural processes to occur and dealing with the consequences (Cooper & Pile 2014; Sinay & Carter 2020; Toft et al. 2023).

A particularly interesting option is the integration of biodiversity into coastal structures. Several authors have considered this or provided analysis (Li et al. 2005; Loke & Todd 2015; Lv et al. 2021a; Lv et al. 2021b; Natanzi et al. 2020; Suedel et al. 2022), while others have voiced reservations about current practices (Chapman & Underwood 2011). One way to enhance biological growth is through ecologically friendly armour units. Sayar et al. (2025) completed a novel collaborative study between the University of Ottawa, Canada, and NRC-OCRE regarding the hydraulic performance of ECOncrete breakwater units (an ecologically friendly armour unit). The ecological performance of ECOncrete units was previously studied by others (Perkol-Finkel et al. 2017; Sella et al. 2021; Rosenberg 2023).

In addition to Baker et al.'s research, some other studies discuss adaptations for coastal structures. However, they do not specifically address vertical walls (Soerensen et al. 2011; van Gent 2019; Foti et al. 2020).

3.2.4 Research Needs and Objectives

Limited knowledge appears to exist regarding vertical wall WLR adaptations' effects on OT. Moreover, no data exists regarding adapting vertical walls using options like perched beaches or landward drainage swales. There is also limited consideration of drainage holes on the vertical face, which is a more realistic condition than assuming a smooth face. More understanding is needed about how NBS, such as eco-friendly armour units, can be incorporated into adaptations. Testing of a diverse array of design options, and quantification of adaptations' performance relative to well known EurOtop equations is necessary. The objectives of this study are to understand how WLR adaptations to a traditional vertical seawall affect the OT discharge. This is the first time that ECOncrete armour units were used to this effect.

3.3 Experimental Program

3.2.1 Testing Setup

This comprehensive experimental test program was completed at NRC-OCRE, in Ottawa, Canada in collaboration with the University of Ottawa. Tests were completed in the 97m long, 2m wide, and 2.9m deep LWCF, shown in *Fig. 3.1*.

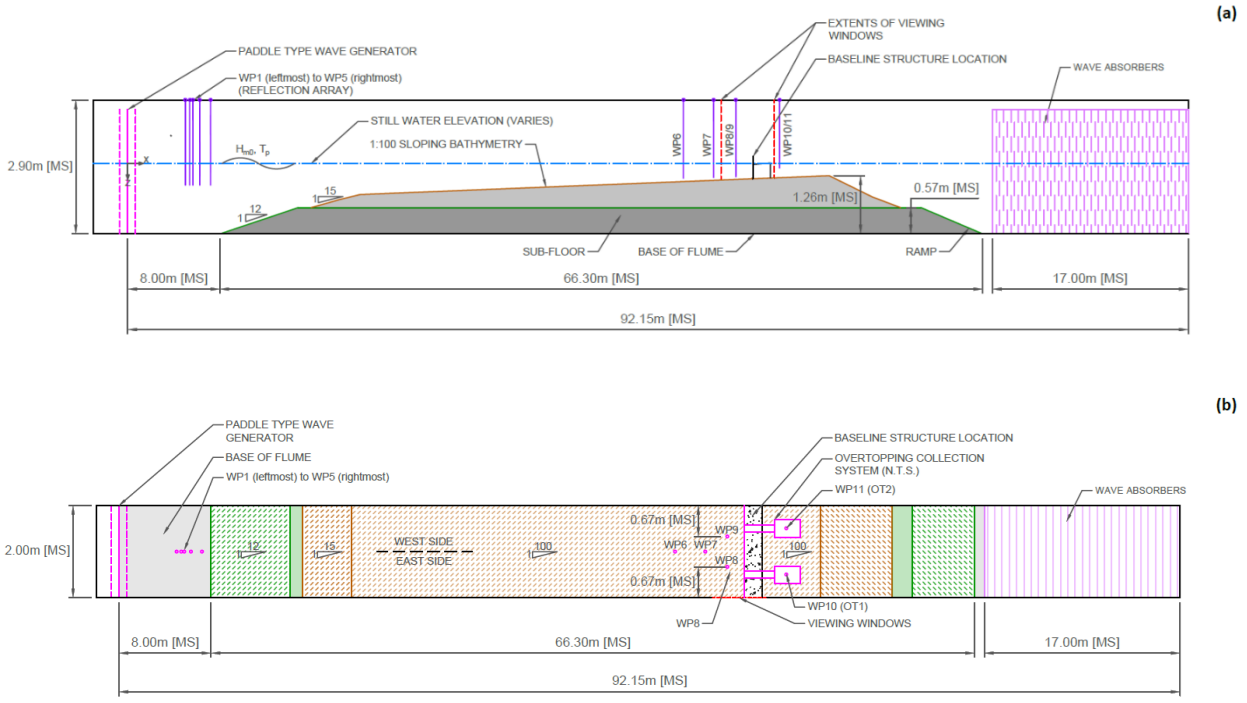

Fig. 3.1. (a) Profile, and (b) Plan view of the large wave flume at NRC-OCRE (Not to Scale)

The bathymetry had sections of different slopes. The key section inducing wave breaking was a 34.10 m (model scale, MS) long section of 1V:100H slope. The baseline structure's (Test Series AA's, TSAA's) toe was placed approximately 54.29 m (MS) from the wave machine. Eleven capacitance wave probes (WPs) were used. Five probes (WP1 to WP5) formed an offshore reflection array to determine incident wave conditions, and to evaluate coefficients of reflection. The wave machine used active wave absorption to minimize reflected waves. Four probes (WP6 to WP9) measured nearshore wave and water level conditions. Two probes (WP10 and WP11) were for OT measurements. Portable wave absorbers were installed at the down wave section of the flume.

Table 3.1 shows the wave test matrix. The conditions were based on representative hydrodynamic conditions on Lake Ontario near the Greater Toronto Area. 75.0 m represents mean water level, while 76.2 m is a 1:100-year flood level, and 76.5 m is an augmented 1:100-year flood level accounting for WLR due to climate change. The first stage was a wave verification series, which was completed using no structure. To ensure repeatability, one test for each water level was re-run.

The primary test series followed the verification series – the primary test matrix is below in *Table 3.2*.

Table 3.1. Wave test matrix

Test no.	Ref. Name	Water Level at toe (m, MS)	Water Level at WM (m, MS)	Wave Height, H_{m0} (m, FS)	Wave Height, H_{m0} (m, MS)	Peak Period, T_p (s, FS)	Peak Period, T_p (s, MS)
1	M1			1.90	0.127	6.9	1.8
2	M2			2.57	0.171	8.1	2.1
3	M3	0.251	1.450	3.24	0.216	9.0	2.3
4	M4			3.91	0.261	9.7	2.5
5	M5			5.00	0.333	10.8	2.8
6	F1			1.90	0.127	6.9	1.8
7	F2			2.57	0.171	8.1	2.1
8	F3	0.331	1.530	3.24	0.216	9.0	2.3
9	F4			3.91	0.261	9.7	2.5
10	F5			5.00	0.333	10.8	2.8
11	C1			1.90	0.127	6.9	1.8
12	C2			2.57	0.171	8.1	2.1
13	C3	0.351	1.550	3.24	0.216	9.0	2.3
14	C4			3.91	0.261	9.7	2.5
15	C5			5.00	0.333	10.8	2.8

Note: FS = Full Scale; MS = Model Scale; WM = Wave Machine

Table 3.2. Experimental test series matrix

Test series ref. name	Description	Wave conditions tested
TSAA	Baseline vertical wall	M1-M5, F1-F5, C1-C5,
TSBB	Vertical extension	M1,M3,M5, F1,F3,F4, C1,C3-C5,
TSCC	Eco-friendly submerged breakwater	M1,M3,M5, F1,F3-F5, C1,C3,C5
TSDD	Perched beach	M1,M3-M5
TSEE	Modified perch beach	M1,M3,M4
TSFF	Cobble beach	M1,M3,M4, F1,F3,F4, C1,C3,C4
TSGG	Revetment	Same as TSFF
TSHH	Drainage swale	M1,M3
TSII	Modified drainage swale	M3,M4
TSJJ	Further modified drainage swale	M3,M4, F1,F3,F4, C1,C3,C4
TSKK	Secondary wall	Same as TSFF

Only TSAA was investigated under the full range of sea states (M1 – M5, F1 – F5, and C1 – C5), to maximize the number of investigated retrofits. Some test series (DD, EE, HH, II) were further truncated based on preliminary observations. To confirm repeatability of results, tests were re-run consistently.

3.3.2 Baseline Structure and Retrofits

The adaptation geometries considered real-world construction restrictions. If waterfront property or usage is directly landward of an existing vertical wall, landward construction may not be possible. If environmental, access, or legislative restrictions prohibit construction in the water, landward construction may be the only option. Moreover, the best solution may be adaptation on the crest (i.e., vertical extension, recurve wall, etc.) in the most restrictive cases. *Fig. 3.2.* shows the baseline vertical seawall case (TSAA).

Fig. 3.2. Baseline vertical seawall case (TSAA)

To minimize the construction time and effort between sections (with specific consideration of TSHH to TSKK), and to permit the common incorporation of overtopping collection trays and bins (Cecioni et al. 2024; Pearson et al. 2003), the vertical face had a concrete (lower) and plywood (upper) composite face. The baseline crest elevation was 78.5m to remain consistent with Baker

et al. (2023). Two overtopping measurement systems were used. Each collection tray was placed approximately 0.5 m from the flume sidewalls. Drainage holes were included to better mimic a real-world design; considering guidance documents (MNR 2001), the design drained the maximum predicted overtopping (via EurOtop equations) through the holes when the TSHH/II/JJ swale was full. *Fig. 3.3*. presents the baseline structure in (a), and the retrofit designs in (b) to (l). All proceeding drawings present the as-built profile views. Moreover, elevations are in full-scale [FS], while measurements and dimensions are in model scale [MS]. Since this study is a companion to Baker et al. (2023), using the same elevation system was convenient.

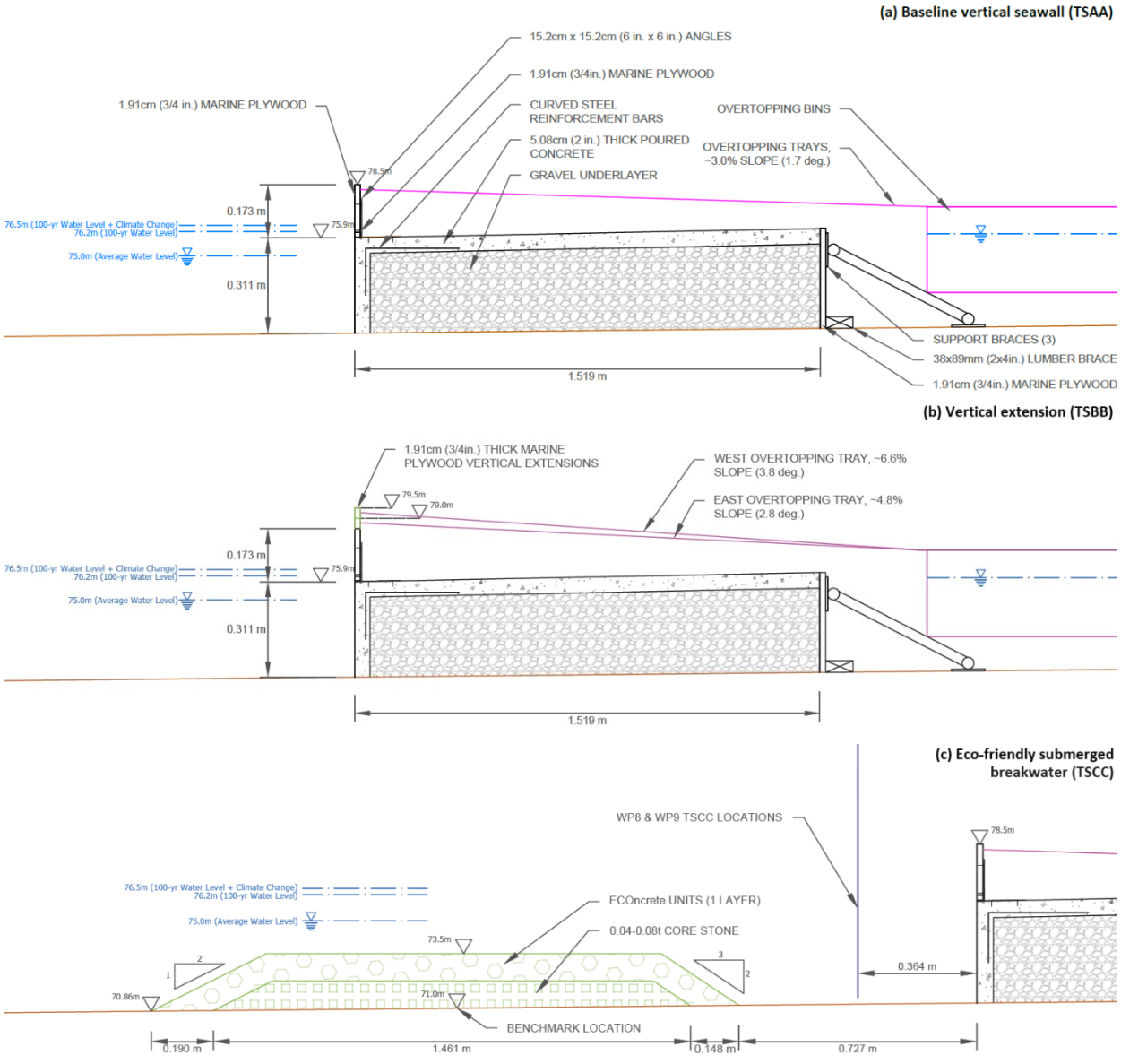

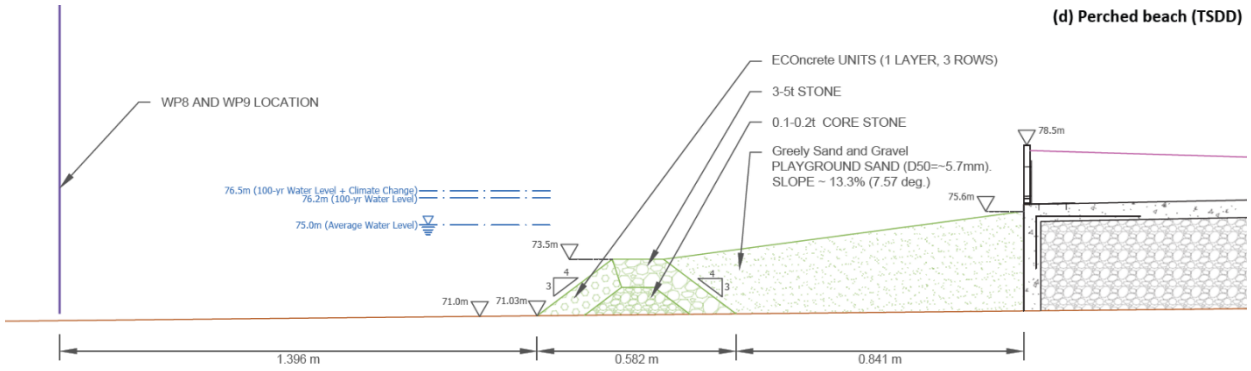
(d) Perched beach (TSDD)
WP8 AND WP9 LOCATION
ECOncrete UNITS (1 LAYER, 3 ROWS)
3-5t STONE
0.1-0.2t CORE STONE
Greely Sand and Gravel
PLAYGROUND SAND (D50=~5.7mm).
SLOPE ~ 13.3% (7.57 deg.)
76.5m (100-yr Water Level + Climate Change)
76.2m (100-yr Water Level)
75.0m (Average Water Level)
78.5m
75.6m
73.5m
71.0m
71.03m
1.396 m
0.582 m
0.841 m

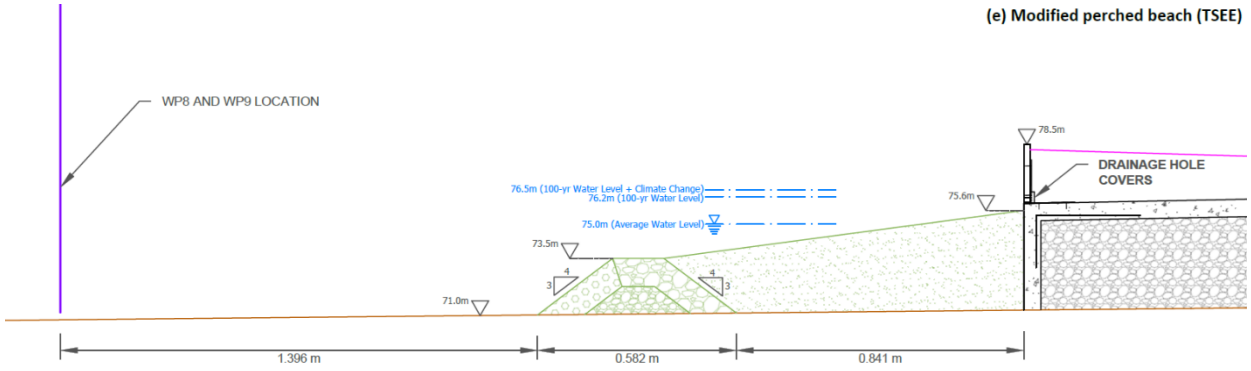
(e) Modified perched beach (TSEE)
WP8 AND WP9 LOCATION
DRAINAGE HOLE COVERS
76.5m (100-yr Water Level + Climate Change)
76.2m (100-yr Water Level)
75.0m (Average Water Level)
78.5m
75.6m
73.5m
71.0m
1.396 m
0.582 m
0.841 m

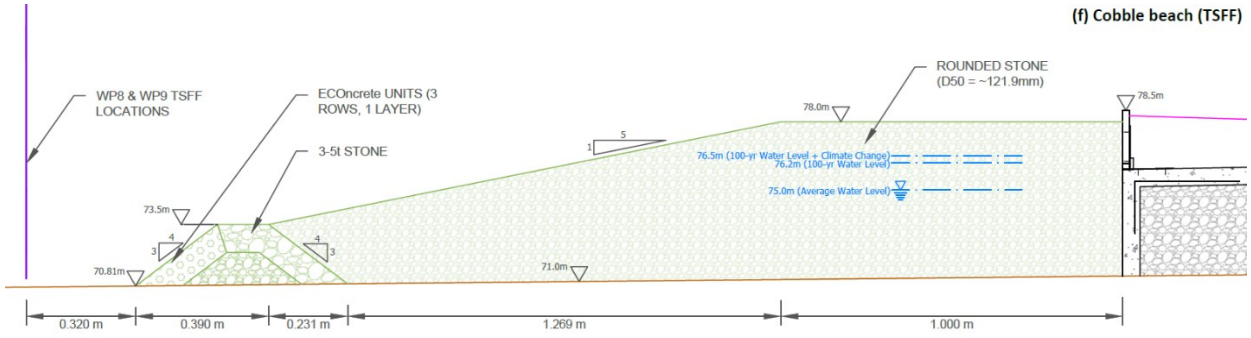
(f) Cobble beach (TSFF)
WP8 & WP9 TSFF LOCATIONS
ECOncrete UNITS (3 ROWS, 1 LAYER)
3-5t STONE
ROUNDED STONE (D50 = ~121.9mm)
76.5m (100-yr Water Level + Climate Change)
76.2m (100-yr Water Level)
75.0m (Average Water Level)
78.0m
78.5m
73.5m
70.81m
71.0m
0.320 m
0.390 m
0.231 m
1.269 m
1.000 m

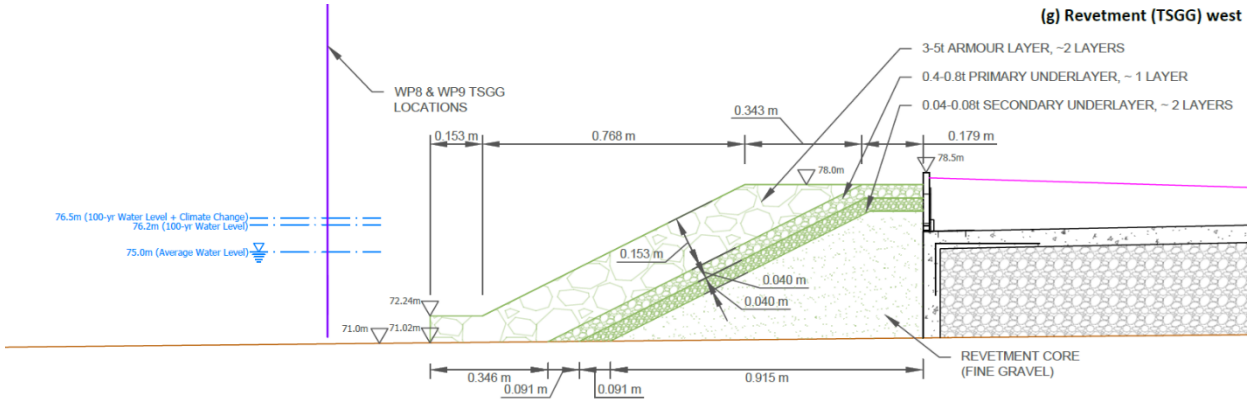
(g) Revetment (TSGG) west
WP8 & WP9 TSGG LOCATIONS
3-5t ARMOUR LAYER, ~2 LAYERS
0.4-0.8t PRIMARY UNDERLAYER, ~ 1 LAYER
0.04-0.08t SECONDARY UNDERLAYER, ~ 2 LAYERS
76.5m (100-yr Water Level + Climate Change)
76.2m (100-yr Water Level)
75.0m (Average Water Level)
0.153 m
0.768 m
0.343 m
0.179 m
78.0m
78.5m
0.153 m
0.040 m
0.040 m
72.24m
71.0m
71.02m
REVETMENT CORE (FINE GRAVEL)
0.346 m
0.091 m
0.091 m
0.915 m

(h) Revetment (TSGG) east

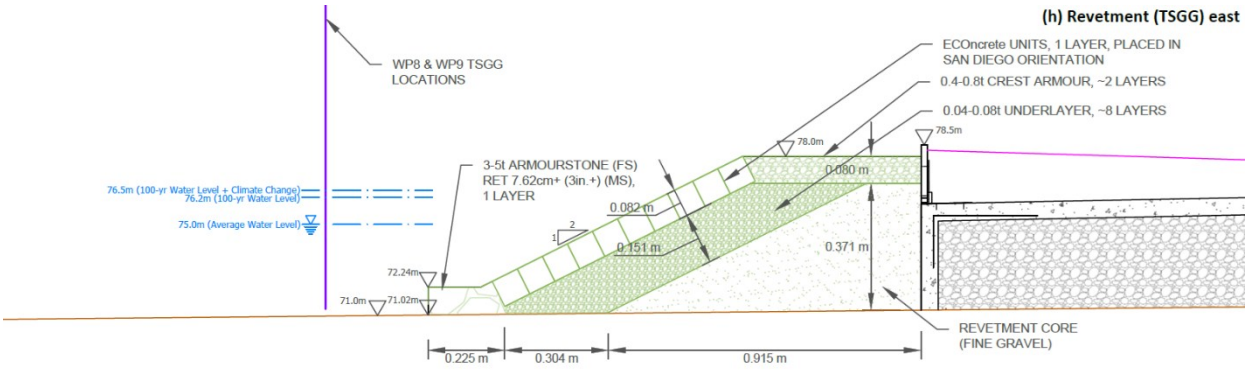

(i) Drainage swale (TSHH)

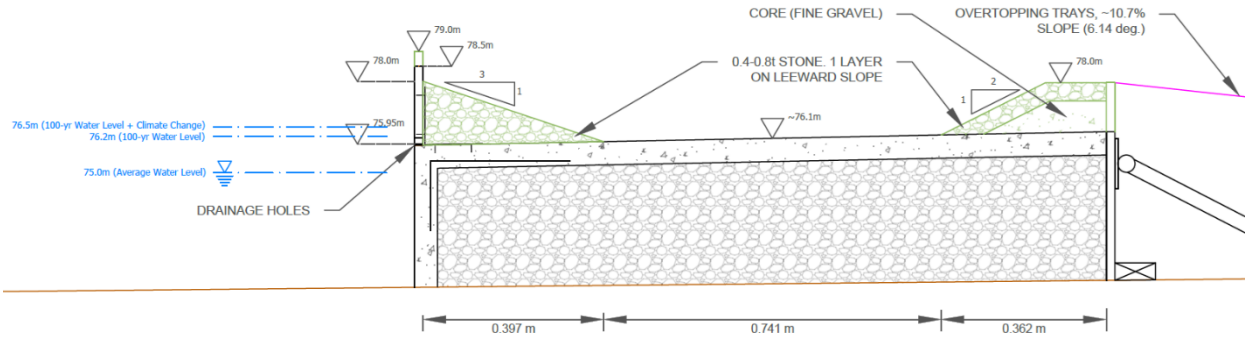

(j) Modified drainage swale (TSII)

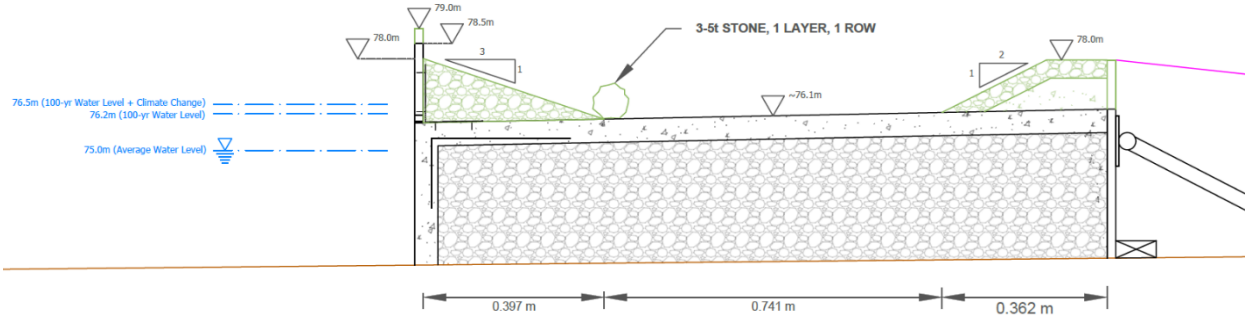

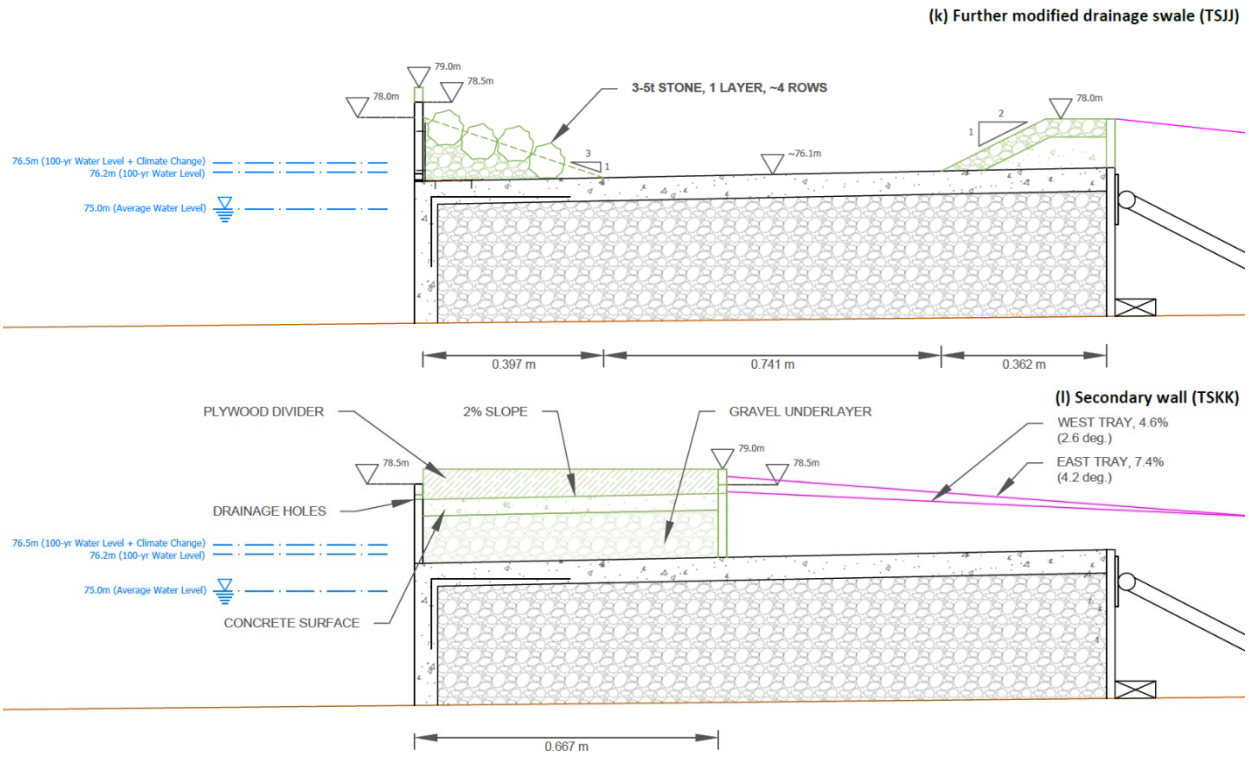

Fig. 3.3. Section sketches of tested structures

TSBB (*Fig. 3.3b*). added a vertical extension. There were two different crest heights, each 1 m in width [MS]. The west side (left side of *Fig. 3.2.*, for reference) had a 1 m [FS] extension (crest elevation of 79.5m), whereas the east side had a 0.5 m [FS] extension (crest elevation of 79.0 m). To install the extensions, strips of plywood were affixed on top of the original wall. One overtopping collection system was used for each side of the flume.

TSCC (*Fig. 3.3c.*) was investigated with reference to Sayar et al. (2025) and Baker et al. This study used 1:15 scale models of ECOncrete® Coastalock® armour units. The total length of the breakwater in the current study was approximately 1.8 m (27 m in FS). The west side used cavity upwards orientation, while the east side used cavity sideways.

TSDD (*Fig. 3.3d.*) introduced a perched beach, designed with reference to (MNR 2001; Moreno et al. 2020). A submerged sill structure contained the beach: ECOncrete units were placed on the seaward slope, while 3 to 5 tonne [FS] armour stone was used on the crest and leeward slope. The ECOncrete units were placed in the forward orientation, at two different spacings. The sediment represents mostly gravel, with some sand and cobble (USGS 2003; Albert 2007). Moreover, the material reasonably represented a typical Great Lakes sediment perched beach (MNR 2001; USGS 2003; US EPA 2005; Albert 2007). TSEE (*Fig. 3.3e.*) covered the drainage holes to mitigate sand losses. TSFF (*Fig. 3.3f.*) implemented a cobble beach contained by a submerged sill structure to further mitigated sediment losses. The sediment represents cobble in full scale (USGS 2003) and

is applicable to large sections of cobble beaches on the Great Lakes (US EPA 2005). Additionally, the drainage holes remained covered using the same backings as in TSEE.

TSGG (*Fig. 3.3g.* and *h.*) installed revetments. A traditional armour stone revetment was used on the west side. On the east side, ECOncrete units armoured the slope, while armour stone was used at the toe and on the crest. Both sides had the same crest and toe elevations and locations, and total widths. The layer compositions were different, however. The ECOncrete units were only placed in a single layer, which increased the required size of the underlayers. Moreover, the ECOncrete units were better placed on a finer filter stone (see Sayar et al. 2025), entailing only one underlayer for the east side. The ECOncrete units were placed in the San Diego configuration (see Sayar et al. 2025).

TSHH (*Fig. 3.3i.*) was a drainage swale and was based on previous investigations by Baker et al. (2023). The west side's crest height was 78.5 m [FS], while the east side's crest height was 79.0m [FS] (0.5 m extension). The OT trays were located behind the secondary wall. A plywood divider separated the two sides and eliminated error from oblique secondary waves. The drainage holes were open to drain water that overtopped the primary wall. TSII (*Fig. 3.3j.*) incorporated a single row of 3-5t [FS] armour stone at the toe of the lakeward slope because toe stones failed almost immediately during TSHH testing, leading to the slope's collapse. The leeward slope incurred negligible damage and therefore remained unchanged. TSJJ (*Fig. 3.3k*) made further modifications. The 0.4-0.8t stone remained the core material, while 3-4 rows of 3 to 5 t stone [FS] were introduced as an armour layer so that the entire slope was covered. As in TSII, the leeward slope incurred negligible damage and remained unchanged.

TSKK (*Fig. 3.3l.*) was a stilling wave basin, or a secondary wall. The secondary crest's setback (10 m, [FS]) accommodated a two-lane urban roadway in FS, if placed just landward of the original seawall's crest (City of Toronto 2017). The secondary crest heights were 78.5 m and 79.0 m on the east and west sides, respectively. Relative to previous literature, the section had a blocking coefficient of $C_b \approx 90.9$ %, slightly lower than $C_b = 95.1$ % in Kisacik et al. (2022).

Photographs of TSBB to TSKK, the location of WPs for each test series, and section drawings for each geometry are available in the supplementary materials (*Fig. A1* to *Fig. A11*, *Fig. A12* to *Fig. A16*, and *Fig. A17* to *Fig. A25*, respectively).

3.4 Test Results and Analysis

3.4.1 Uncertainty Analysis

Regarding preliminary data processing, comprehensive time- and frequency-domain analysis algorithms computed individual and statistical wave heights and periods, reflection data, and raw overtopping rates and volumes. Relevant outputs were exported to a spreadsheet for secondary analysis.

Because several adaptations were split across the flume, the wave height differences between WP8 and WP9 for the wave verification series were reviewed to address the flume's east to west variability. An *RMSE* of 0.028 m [FS] was determined, revealing minor differences in wave heights across the flume. However, the average deviation (0.0035 m) and the standard deviation (0.028 m) indicate there is not a clear east to west bias. Comparing the east and west overtopping results of WP10 (east, corresponding to WP8) and WP11 (west, corresponding to WP9) for TSAA yielded similar results. The *RMSE* between OT measurements at WP8 and WP9 was 0.014 m^3/s [FS], whereas the average deviation was 0.0031 m^3/s – roughly a magnitude less. The standard deviation of the differences was 0.014 m^3/s. A second approach calculated the relative differences, *RD*s, using Eqn. *3.1*:

$$RD\ (\%) = \left(\frac{\left| q_1 - \frac{1}{2}(q_1 + q_2) \right|}{\frac{1}{2}(q_1 + q_2)} \right) \cdot 100\% \tag{3.1}$$

which references the magnitude of the east tray's deviation relative to the average overtopping for a given test. $q_1 = q_{east}$ and $q_2 = q_{west}$ are the mean overtopping rates for the east and west trays, respectively. The average *RD* value for TSAA was approximately 4.2%, with a σ of 2.9%. Therefore, OT results were analyzed separately for the east and west sides.

Comparing the two OT trays separately entails assessing the uncertainty for each tray. To this effect, the *RD*s between repeat tests (i.e. tests for the same geometry and hydrodynamic conditions) were computed. Dynamic structures (i.e., TSDD to TSFF) were omitted because deviations were not solely a result of uncertainty. For every set of repeat tests, and separately for the east and west trays, *RD* was computed using equation *3.1*. For tests with three or more results, the average between all repeat tests in that set was used instead of $(q_1 + q_2)/2$. The average *RD* was 3.2% (σ = 2.4%) for the east side, and 3.7% (σ = 3.8%) for the west side. And, with 95 percent confidence, the *RD* is 8.05% for the west and 11.33% for the east.

3.4.2 Data Processing

TSAA and TSBB results were compared to existing prediction equations. EurOtop (2018) provides dimensionless prediction equations for vertical walls depending on: whether there is an influencing foreshore, the degree of impulsiveness, and the relative freeboard. Equations 7.7 and 7.8 (Eqn. *3.2* and 3.3 below) in the EurOtop manual were applicable (EurOtop 2018):

$$\frac{q}{\sqrt{gH_{m0}^3}} = 0.011 \left(\frac{H_{m0}}{hs_{m-1,0}} \right)^{0.5} \exp\left(-2.2 \frac{R_c}{H_{m0}} \right), \qquad 0 < \frac{R_c}{H_{m0}} < 1.35 \tag{3.2}$$

$$\frac{q}{\sqrt{gH_{m0}^3}} = 0.0014 \left(\frac{H_{m0}}{hs_{m-1,0}} \right)^{0.5} \left(\frac{R_c}{H_{m0}} \right)^{-3}, \qquad \frac{R_c}{H_{m0}} \geq 1.35 \tag{3.3}$$

where H_{m0} is the significant wave height, h is the depth of water at the structure toe, $s_{m-1,0}$ is the wave steepness, and R_c is the crest freeboard. *Fig. 3.4.* shows TSAA and TSBB data plotted alongside EurOtop equations 7.7 and 7.8. All OT values are in FS. Equation *3.4* calculated the *RMSE*.

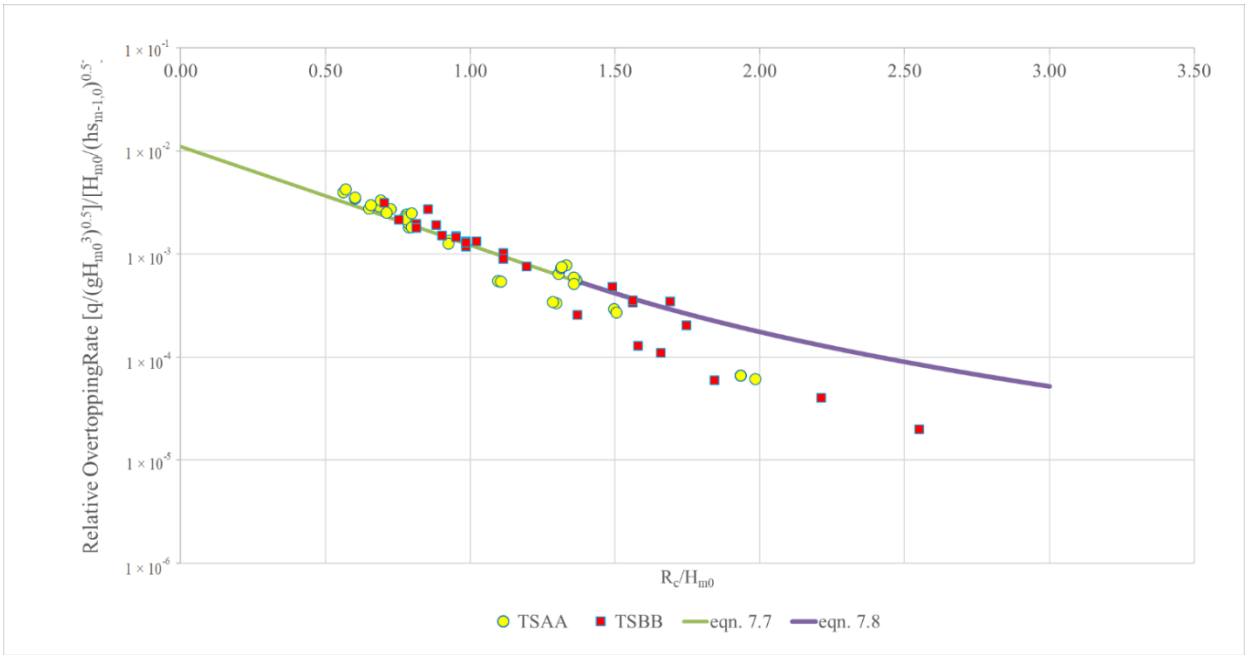

Fig. 3.4. Baseline vertical wall case (TSAA) and vertical extension case (TSBB) data with respect to EurOtop equations

$$RMSE = \sqrt{\frac{1}{n}\sum_{i=1}^{n}\left(\log\left(\frac{q}{\sqrt{gH_{m0}^3}}\right)_o - \log\left(\frac{q}{\sqrt{gH_{m0}^3}}\right)_p\right)^2} \tag{3.4}$$

where n is the number of data points, $(q/(gH_{m0}^3)^{0.5})_o$ is the observed relative overtopping, and $(q/(gH_{m0}^3)^{0.5})_p$ is the predicted relative overtopping (via EurOtop equations). The *RMSE* was 0.2050, shown on *Fig. 3.4.* The *log* of the relative OT values was taken (Salauddin and Pearson 2019; Dong et al. 2020; Dong et al. 2024). Other EurOtop equations were considered; however, plotting against 7.7/7.8 produced the most accurate results. The deepwater $s_{m-1,0}$ was used, which may slightly deviate from EurOtop guidance.

Eqn. 6.5 in EurOtop (2018) applies to TSGG if the crest height of the vertical wall is taken as R_c. *Fig. 3.5.* shows the west OT TSGG data alongside EurOtop Eqn. 6.5, using a γ_f of 0.55 (as per EurOtop guidance, two rock layers and an impermeable core) (EurOtop 2018). The EurOtop f_q factor (EurOtop 2018, eqn. 6.13) was used during data processing for TSGG to correct for model scale effects for rubble mound slopes (EurOtop 2018).

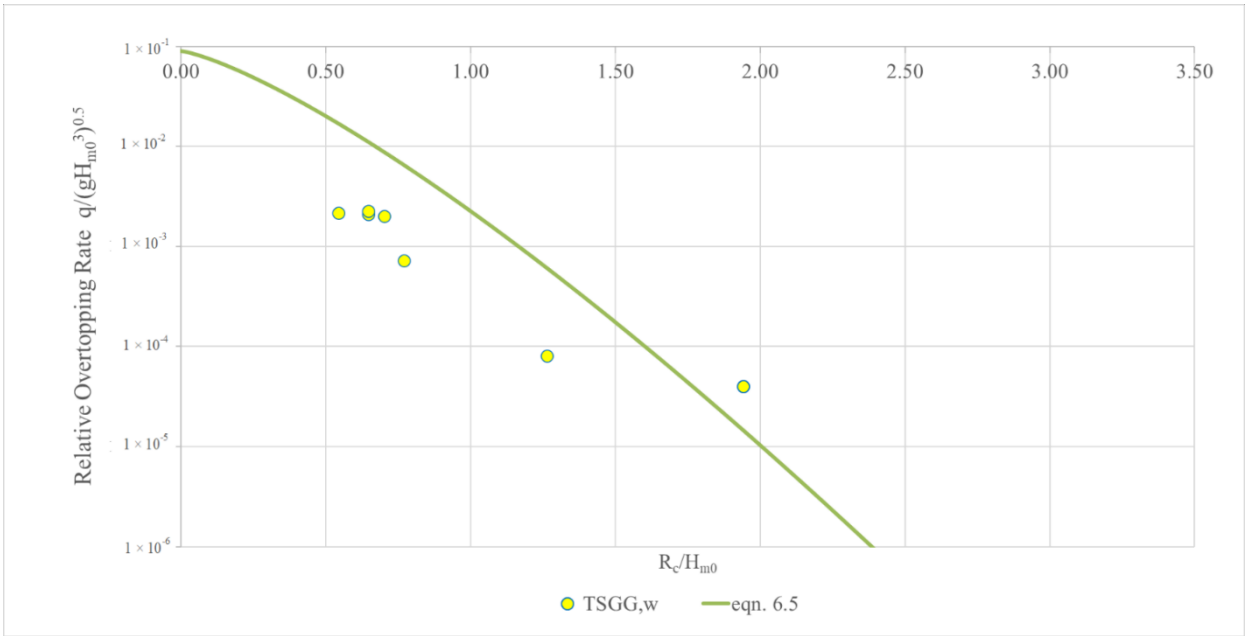

Fig. 3.5. Comparison between revetment case (TSGG) and EurOtop Eqn. 6.5. $\gamma_f = 0.55$

Fig. 3.6 compares FS dimensionless OT between all test series with respect to relative freeboard, and separately for the east and west sides of the flume. EurOtop equations 7.7 and 7.8 were also included. Note the use of EurOtop eqn. 6.13/6.15 was considered for TSFF. However, the roughness value was uncertain; therefore, the OT results herein are uncorrected.

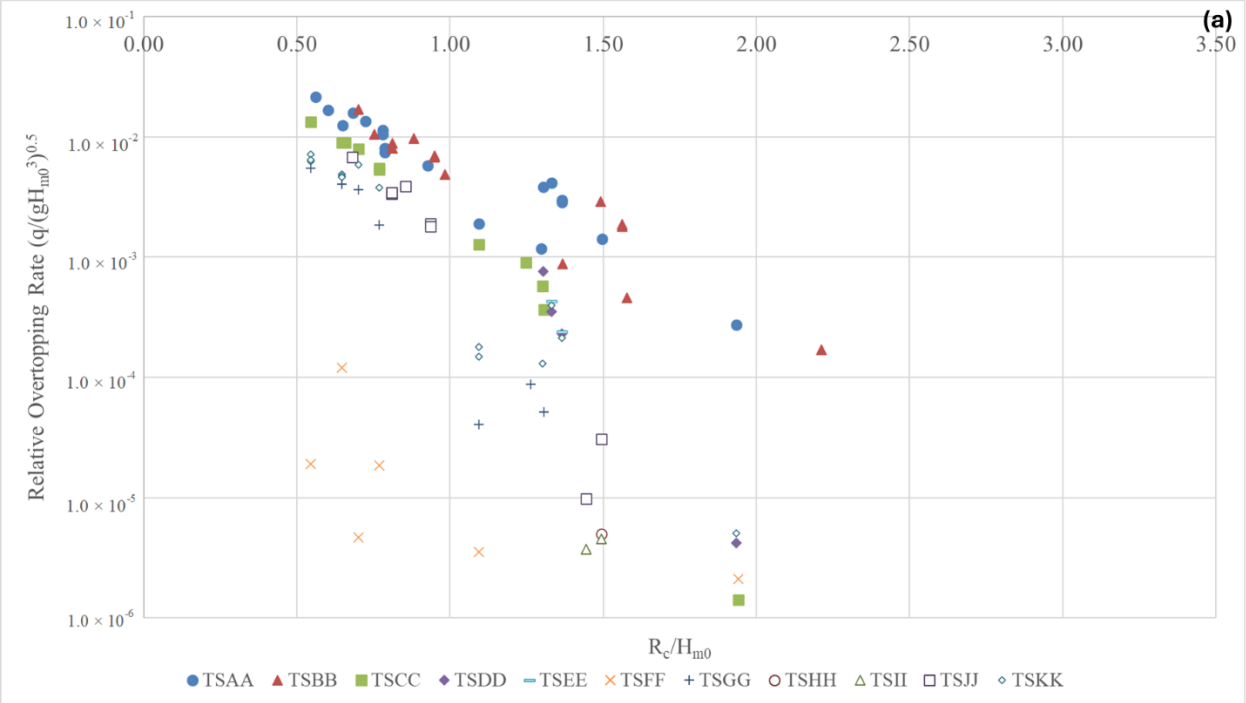

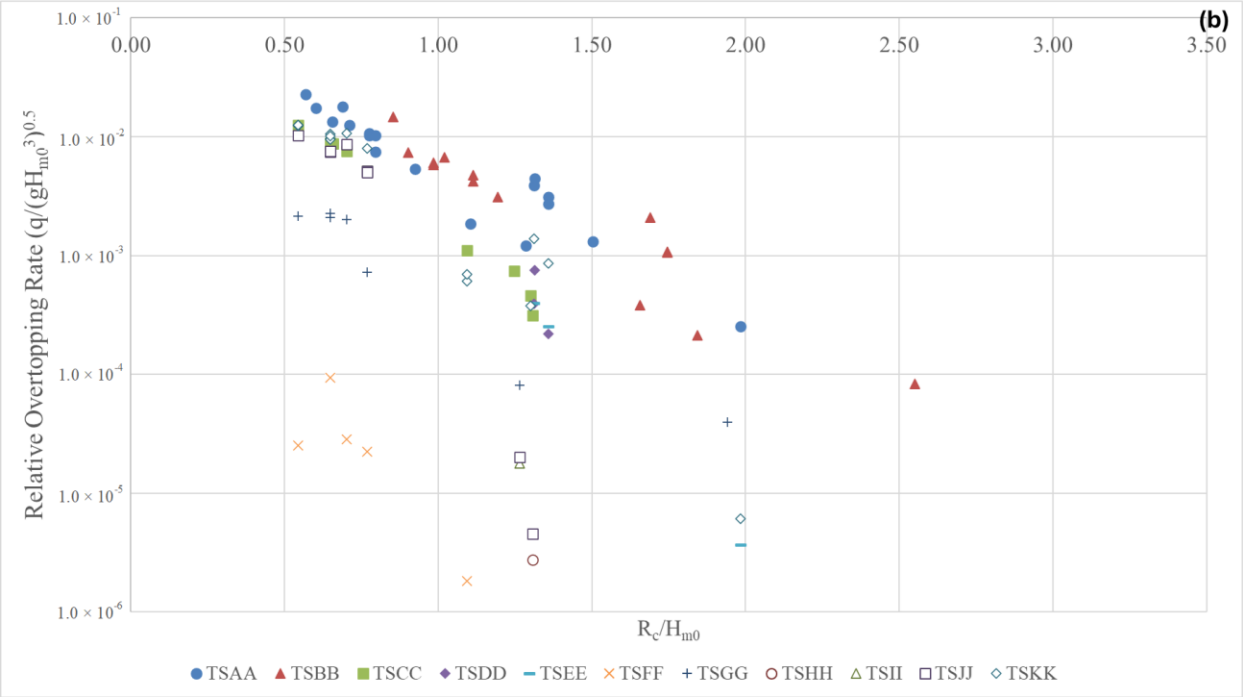

Fig. 3.6. (*a*) East and (*b*) west OT tray comparison

Verification series wave heights were used because the vertical structure caused significant wave reflections and WP6 to WP9 could not separate incident and reflected waves. While WP1 to WP5 computed reflections, using the verification data was considered more accurate. Moreover, TSCC and TSFF used WP7 H_{m0} values for the east and west sides, and all other test series used WP8 and WP9 values. Using the WP8 and WP9 data was preferred – however, TSCC's and TSFF's toe geometries were seaward of the verification series WP8 and WP9 locations.

Table 3.3. provides average percent differences in dimensionless overtopping for each water level. Potentially, deviations are also functions of wave height, but a lack of data prevented more complex calculations.

Table 3.3. Percent differences in dimensionless OT relative to baseline vertical wall case (TSAA)

Test Case	Percent Difference in Dimensionless Overtopping, $q/(gH_{m0}^3)^{0.5}$, relative to Baseline Case (TSAA)					
	75.0m (MWL)		76.2m (100-year flood)		76.5m (100-year flood + CC)	
	East	West	East	West	East	West
TSAA	-	-	-	-	-	-
TSBB	-34.3	-61.9	-41.0	-60.9	-36.8	-60.0
TSCC	-87.8	-90.9	-47.4	-51.2	-54.5	-58.9
TSDD	-90.6	-91.4	-	-	-	-
TSEE	-95.9	-95.4	-	-	-	-
TSFF	-99.7	-100.0	-99.9	-99.9	-99.8	-99.9
TSGG	-98.9	-94.1	-85.4	-92.4	-86.0	-91.8
TSHH	-99.9	-100.0	-	-	-	-
TSII	-99.9	-99.8	-	-	-	-
TSJJ	-99.5	-99.7	-84.4	-58.6	-85.0	-67.7
TSKK	-93.6	-75.0	-70.5	-35.9	-75.5	-47.7

Note: MWL = mean water level; CC = Climate Change

3.4.3 Prediction Equations

The *k*-factor approach is used for this study (Kortenhaus et al. 2003; Pearson et al. 2005; Dong et al. 2024). If $k = q_i/q_{known} = q_i/F$, where q_i is the OT for an experimental test, and $q_{known} = F$ is the corresponding EurOtop OT prediction for a traditional vertical seawall (in this study, Eqn. 7.7 and 7.8), then $q_i = kq_{TSAA} = kF$ and $F = q_i/k$.

To determine *k*, dimensionless relationships for six adaptations (TSAA and TSBB, TSCC, TSGG, TSJJ, and TSKK) were derived. TSGG already has a defining equation, shown in *Fig. 3.5.* However, the vertical wall equation was corrected for the addition of the revetment to determine if a better fit exists. Equation 5 was fit to each of the test series:

$$\frac{q}{\sqrt{gH_{m0}^3}} = r_0\left(\sum_{i=1}^{m} y_i^{r_i} + b\right)F = kF \tag{3.5}$$

where $q/(gH_{m0}^3)^{0.5}$ is the dimensionless overtopping, y_i is a dimensionless parameter, m is the number of dimensionless parameters used for the k factor, b and r_0 are calibration constants, and r_i is the calibration coefficient for y_i. Iterative calculations determined the constants and coefficients.

The relative freeboard and other parameters likely to reduce overtopping were separated, referencing (Kortenhaus et al. 2003). Iterative calculations minimised *RMSE* between *F* and the

experimental relative overtopping by changing the calibration parameters. Parameters were manually removed or altered until satisfactory results were obtained. Using *log* in the *RMSE* calculations meant omitting all $q_o \approx 0$, which improved correlations. Also, a separate r_0 for each y_i value was ideal; however, limited data prevented this. Equation 6 is for TSAA – it corrects the bias, assumed to be a function of the drainage holes, observed at high relative freeboards – the EurOtop (2018) equations were formulated for a smooth vertical surface:

$$k_{AB} = 14.7527\left[\left(\frac{d_1}{R_c}\right)^{-0.0840} + \left(\frac{A_h}{A_w}\right)^{0.1937} + \left(\frac{R_c}{H_{m0}}\right)^{-0.0912} - 2.2398\right];\ for:$$

$$1.0697 \leq \frac{d_1}{R_c} \leq 2.4068$$

$$0.0041 \leq \frac{A_h}{A_w} \leq 0.0046$$

$$0.5617 \leq \frac{R_c}{H_{m0}} \leq 2.5506 \tag{3.6}$$

where d_1 is the distance from the structure toe to center of drainage holes, A_h is the total area of drainage holes, and A_w is the total area of the vertical structure's seaward face. The equation had an *RMSE* of 0.0594. Equation 7 is for TSCC:

$$k_C = C_0\left[\left(\frac{d_w}{d_b}\right)^{5.3357} + \left(\frac{R_c}{H_{m0}}\right)^{-2.9027}\right], where\ \ C_0 = \begin{cases} 0.1518, & for\ cavity\ sideways \\ 0.1897, & for\ cavity\ upwards \end{cases};\ for:$$

$$0.6000 \leq \frac{d_w}{d_b} \leq 1.2000$$

$$0.5448 \leq \frac{R_c}{H_{m0}} \leq 1.9420 \tag{3.7}$$

where d_w is the crest height at the lengthwise midpoint, and d_b is the water depth over the crest at the lengthwise midpoint. The equation had a total *RMSE* of 0.3365 ($RMSE_{east}$ of 0.4150, $RMSE_{west}$ of 0.2200). For split-section adaptations, while r_i and b values were the same, different r_0 values distinguished the east and west sides. For TSCC, this accounted for differences in unit orientation; for TSGG, this accounted for geometrical and roughness differences. Equation 8 is for TSGG:

$$k_G = G_0\left[\left(\frac{h_t}{R_c}\right)^{-3.5116} + \left(\frac{L_c}{L_{m-1,0}}\right)^{2.7739} + \left(\frac{L_s}{L_{m-1,0}}\right)^{3.3244} + \left(\frac{R_c}{H_{m0}}\right)^{-4.4276}\right], where\ G_0 = \begin{cases} 0.0301 & for\ ECOncrete \\ 0.0279 & for\ Armourstone \end{cases}; for:$$

$$1.1371 \leq \frac{h_t}{R_c} \leq 2.7400$$

$$0.0554 \leq \frac{L_c}{L_{m-1,0}} \leq 0.1140$$

$$0.0979 \leq \frac{L_s}{L_{m-1,0}} \leq 0.2013$$

$$0.5448 \leq \frac{R_c}{H_{m0}} \leq 1.9420 \tag{3.8}$$

where h_t is the water depth at the structure toe, L_c is the length of the revetment crest's horizontal portion, L_s is the length of the revetment's sloping portion. The equation had a total *RMSE* of 0.2430 ($RMSE_{east}$ of 0.2352, $RMSE_{west}$ of 0.2515). Equation 9 is for TSJJ:

$$k_J = 0.0011\left[\left(\frac{d_1}{R_c}\right)^{7.3831} + \left(\frac{A_h}{A_w}\right)^{1.1732} + \left(\frac{R_s}{H_{m0}}\right)^{-7.4059} + \left(\frac{L_t}{L_{m-1,0}}\right)^{3.4160} + \left(\frac{L_a}{L_{m-1,0}}\right)^{2.6910} + \left(\frac{R_c}{H_{m0}}\right)^{-5.5067}\right]; for$$

$$1.2034 \leq \frac{d_1}{R_c} \leq 2.4068$$

$$0.0043 \leq \frac{A_h}{A_w} \leq 0.0046$$

$$0.4086 \leq \frac{R_s}{H_{m0}} \leq 1.1199$$

$$0.1594 \leq \frac{L_t}{L_{m-1,0}} \leq 0.1910$$

$$0.0807 \leq \frac{L_a}{L_{m-1,0}} \leq 0.0967$$

$$0.5448 \leq \frac{R_c}{H_{m0}} \leq 1.4932 \tag{3.9}$$

where L_t is the secondary wall's setback length, L_a is the armoured length of the drainage swale, and R_s is the secondary wall crest height. The equation had an *RMSE* of 0.3807. Equation 10 is for TSKK:

$$k_K = 0.0871\left[\left(\frac{R_s}{H_{m0}}\right)^{-3.2365} + \left(\frac{L_t}{H_{m0}}\right)^{-2.8904} + \left(\frac{R_c}{H_{m0}}\right)^{-2.5378}\right];\ for:$$

$$0.5448 \leq \frac{R_s}{H_{m0}} \leq 2.2113$$

$$0.0689 \leq \frac{L_t}{H_{m0}} \leq 0.1416$$

$$0.5448 \leq \frac{R_c}{H_{m0}} \leq 1.9838 \qquad (3.10)$$

with an *RMSE* of 0.2840. Equations 3.6 through 3.10 are further limited by $k \geq 0$ (i.e. the correction cannot be used to predict a negative overtopping value). *Fig. 7* shows the corrected experimental data alongside equations 2 and 3.

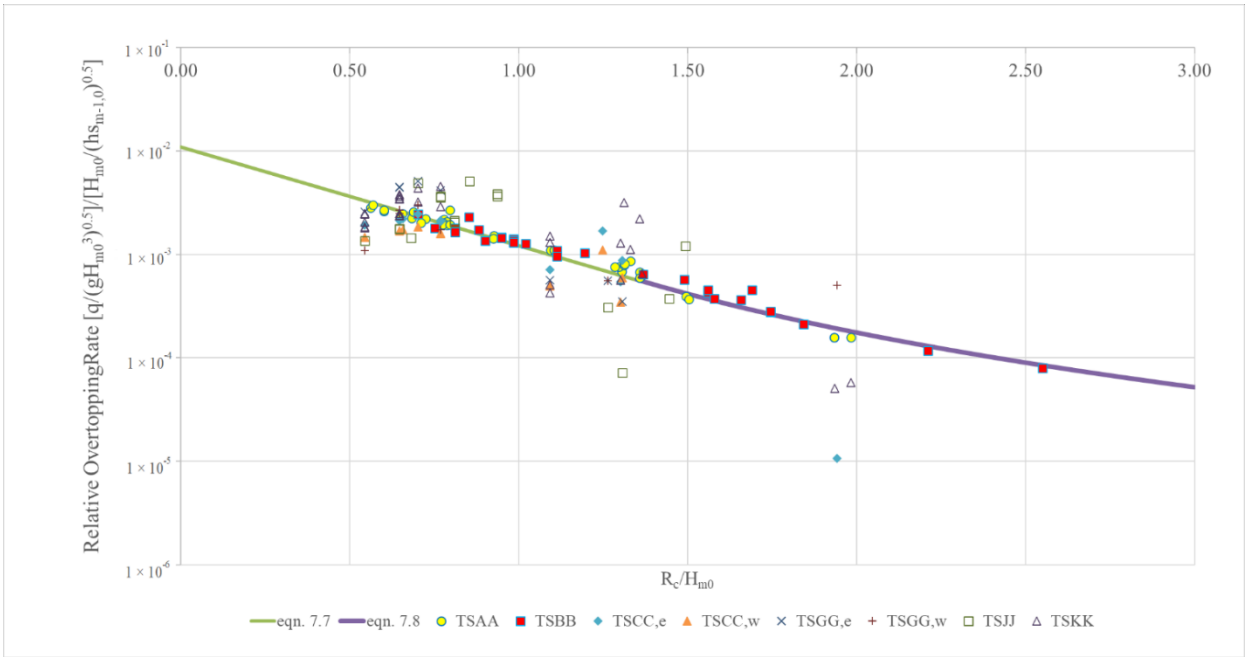

Fig. 3.7. k-factor corrected data for baseline vertical wall case (TSAA), vertical extension case (TSBB), eco-friendly breakwater case (TSCC), revetment case (TSGG), and secondary wall case (TSKK)

In *Fig. 7.*, the experimental data points were divided by their respective *k* values. For TSCC and TSGG, the east and west sides are separated. Some points are not presented because the OT was approximately zero.

3.5 Discussion

The results reveal the adaptations' performance in rising water levels. Referring to *Table 3.3*, every adaptation reduced OT compared to the baseline case. TSCC, TSJJ, and TSKK saw enhanced OT reduction at the 76.5 m water level compared to the 76.2 m water level while TSFF, TSBB, and TSGG saw approximately no change. In general, TSFF performed the best while the 0.5m extension of TSBB was the worst (still, however, reducing OT 36.8% compared to TSAA for the 76.5 m water level).

Vertical crest extensions drastically changed the performance of the structure. For TSBB, a 0.5 m extension reduced OT by 36.8% whereas a 1 m extension reduced OT by 60.0% at the 76.5 m water level (~63.0% improvement). For TSJJ, the east side had a 0.5 m crest extension in addition to the drainage swale, and reduced OT by 85.0% compared to 67.7% for the west side (~25.5% improvement). TSKK had two different secondary wall crest heights. The west wall's elevation was 78.5 m, causing an OT reduction of 47.7%, whereas the east side's 79.0 m crest height yielded an OT reduction of 75.5% (~58.2% improvement). Results show vertical extensions are an effective tool at the primary crest and at a setback. Dong et al. (2020) noted that all adaptations (mostly seaward) performed better at higher relative freeboard. Kisacik et al. (2022) noted similar results for their superstructures (mostly at the crest or landward). This study's findings agree – the highest reduction values in *Table 3.3* are observed at the lowest water levels (which tend to represent the highest relative freeboards). Also, Figs. S26 and S27 presents a general (if weak) decreasing trend with increasing relative freeboard.

Regarding relative performance to TSAA across all water levels, TSCC's, TSJJ's, and TSKK's performance reduced from 75.0 m to 76.2 m and then increased from the 76.2 m to the 76.5 m water level. However, TSGG saw approximately no change in performance across all three levels, while TSBB saw approximately no change in performance for the 1 m extension, but an increase in performance from the 75.0 m to the 76.2 m water levels, and a decrease from the 76.2 m to the 76.5 m for the 0.5 m extension.

Developing a prediction equation for TSFF was difficult because it yielded very low OT values. Practically, however, the section is worth considering where an abundance of large grain size material and seaward space is available. Potentially, waste material may also be considered as a less gray alternative (e.g. recycled concrete aggregate, rubber, etc.), but further investigation into the performance of specific materials would be required.

Regarding the prediction equations, the equations are based on small datasets and are valid for relatively narrow bounds. Therefore, it is recommended these equations be considered as tentative and further work be completed to confirm and refine the relationships. The *RMSE* values (TSAA/TSBB = 0.0594; TSCC = 0.3365 (0.4150 east, 0.2200 west); TSGG = 0.2430 (0.2352 east, 0.2515 west); TSJJ = 0.3807; TSKK = 0.2840), however, are comparable to Dong et al.'s (2020) four adaptations (reef breakwater = 0.524; diffraction pillars = 0.25; recurve wall = 0.5; vegetation = 0.26), which adds confidence to this study's equations. Moreover, to the authors' knowledge,

the study is novel by presenting an OT reduction coefficient, *k*, for drainage holes and drainage swales. The study also presents a *k* factor for a secondary wall case, effectively a stilling wave basin (SWB). The work of Kisacik et al. (2022) and its predecessor, Kisacik et al. (2019) extensively cover OT reduction of SWBs. However, only one of their geometries is similar to the geometry tested in this study (but was placed at the end of a more complex foreshore than this study). As well, Kisacik et al. (2022) and Kisacik et al. (2019) calculated their OT reduction factor as a function of relative freeboard, whereas equations in this study depend on the geometry of the wall. In any case, Kisacik et al. (2022) notes that because of the complex relationships surrounding the efficacy of SWBs, that physical model tests should be completed for new configurations. Therefore, at a minimum the current study hopes to contribute by providing physical modelling for another secondary wall.

3.5.1 Challenges and Limitations

It was difficult to determine the best way to assess the overtopping for dynamic conditions. Since the project aimed to be applicable to the real-world, the degree and rate of maintenance for perched beaches or rock slopes was pertinent, which is highly variable. In general, surfaces were re-finished after testing each water level. However, in the case of the drainage swale (TSJJ), no maintenance was provided.

Regarding the *k* for the TSAA and TSBB data, as noted in section 3.4.3 the discrepancy between the experimental data and the EurOtop equations was assumed to be a function of the drainage holes. However, it is difficult to confirm whether this is the case. Referring to *Figure 3.4*, the increasing scatter with increasing relative freeboard could have also resulted from the natural scattering of overtopping volumes. Because overtopping events were only measured at the tray locations, it is possible that a less-than-average volume of overtopping was captured by the trays for the tests with higher relative freeboard, produced for example by some bias in the flume which induced a non-uniform distribution of overtopping along the crest. Or, particularly for tests with very low overtopping rates, elements such as surface tension of water on the trays may have created underpredictions.

The reasons for scattering are difficult to explain. Consider the four left-most points on *Figure 3.5*. The tests had different relative freeboard levels, but the overtopping was approximately equal. Explanations for the discrepancy may be as simple as an uneven distribution of overtopping along the crest as mentioned above or may be derived through complex analysis of wave-structure interaction. Within the scope of this work, only acknowledgment of uncertainties (see section 3.4.1) may be possible.

Verification data was used for secondary analysis which potentially limited results, because the test-to-test variation of hydrodynamic parameters was not captured. Also, the verification wave heights were confounded to a minor degree by reflections – coefficients of reflection of 4-5% were measured.

The study was somewhat limited by the flume's east-to-west discrepancies, although assessing the two sides separately helped reduce those errors. Of course, when the geometry is continuous across the width of the flume, the two trays should produce the same result. Therefore, for design purposes, neither tray should be used individually as the conservative result. Instead, an approach similar to EurOtop (2018) should be used, which acknowledges natural scattering by increasing the design overtopping prediction as a function of the statistical spread of the overtopping measurements.

Also, a standard vertical wall without drainage holes was not tested. It is likely more practical to incorporate drainage holes on the vertical structure. However, additionally testing a smooth vertical wall would have aided comparisons to the EurOtop (2018) equations.

There are always limitations related to scaling; however, the current study was completed at a rather large, 1:15 scale. As well, OT error was possibly introduced because of the small collection width to crest width ratio, especially given the flume's east-to-west discrepancies. However, the trays were placed at the midpoints of the east and west sides, which ideally provided an average OT for each side. Subsequently, the trays were placed far away from both each other and the walls, so that those effects were minimized.

3.5.2 Future Work

Regarding future work, the analysis should incorporate economic considerations (e.g. cost of construction, materials, etc.). For example, while TSBB performed worse than TSFF, TSFF used more material and labor. Assuming the observation transfers to the prototype scale, then TSBB's worse functional performance might be overshadowed by its economic advantages. Future work should provide real-world cost estimates for each adaptation and incorporate them into a holistic economic assessment for various common situations (i.e., residential property, urban center). Formentin (2021) provides a methodology in the same vein and considers cost, overtopping reduction, wave load reduction (not considered as a part of this study), and environmental impact. However, Jonkman et al. (2013) presents cost estimate information for several coastal structures, noting that data varies even for the same region and defense structure type. But the authors do support assessing structures' cost with respect to its performance (Jonkman et al. 2013), supporting the work of Formentin (2021) and the current authors' opinions.

Li and Cox (2013) noted that after analyzing various case studies, step upgrading was more effective than designing for long term WLR projections. van Gent (2019) similarly notes that combining measures is likely the best option. Therefore, future work could make several step additions and determine cumulative overtopping effects. Possibly, composite reduction coefficients could be derived; this approach was considered by Kisacik et al. (2022).

Finally, Equations *3.6* to *3.10* could be modified so that the relative freeboard bounds matched those of Equations *3.2* and *3.3*, which was prevented in this study due to a lack of data. Future studies would further benefit from expanding the amount and range of wave conditions.

3.6 Conclusions

This study investigated how various water level rise adaptations (vertical extension, breakwater, perched beach, revetment, drainage swale, and secondary wall/stilling wave basin) reduced the mean overtopping (OT) compared to a traditional vertical seawall. The study tested each adaptation against three water levels, including a climate change (CC)-influenced 100-year flood level, to understand their performance under extreme water level and wave conditions. Generally, adaptations performed better at higher relative freeboard (R_c/H_{m0}), but individual performances differed significantly with respect to water level. Vertical extensions are expected to be a powerful and accessible tool to reduce OT. The determined prediction equations for select adaptations (drainage holes for baseline/vertical extension case, breakwater, revetment, drainage swale, and secondary wall/stilling wave basin), some of which are believed to be novel (drainage holes, drainage swale). The study used a Nature Based Solution (NBS), namely ECOncrete Coastalock amour units – an ecologically friendly armour unit, in three of the test series (breakwater, perched beach, and revetment). The units' use in this context is believed to be novel. The study has valuable practical applications for the Great Lakes (for which regional specific guidance is limited) but aims to provide universal guidance for retrofitting existing vertical structures for climate change-induced water level rise. The authors suggest that future work expands the number of test series and the breadth of investigated adaptations, and integrates cost and economic investment into a generalized efficacy assessment for a given adaptation and site-specific conditions.

4 Numerical Modelling of Climate Change-Adaptive Vertical Seawalls

Preprint of an article in preparation for submission entitled "Experimental and Numerical Modelling of Adaptive Vertical Coastal Structures"

4.1 Introduction

4.1.1 Background and Related Work

Climate change (CC) is predicted to augment coastal hazards. Mayo and Lin (2022) determined that due to sea level rise, the exceedance probability of the 100-year flood (HYF) level may increase up to 6.75 times for sites along the United States' northeast coast. Moreover, if climate change's impacts on tropical cyclone or storm climatology are considered, the value may be doubled. In coastal zone managers' attempts to mitigate climate change effects, coastal protection works may be useful, but only to a certain degree. Giardino et al. (2018) noted that a rock revetment reduced the expected annual damage for a small island nation by about 30 percent compared to a no-revetment case. However, they also determined the number of annually affected people will approximately double by 2100 if no additional adaptation measures are implemented. Clearly, coastal structures' reduced performance due to climate change may have significant consequences. Some authors argue that upgrading coastal structures will be necessary to mitigate climate change's influence (Formentin 2021).

Two previous physical modelling studies are the present study's foundation. Baker et al. (2023) conducted an experimental modelling study in the Large Wave-Current Flume (LWCF) at the National Research Council's Ocean, Coastal, and River Engineering research centre (NRC-OCRE). The study reviewed how adaptations to a conventional rock-armoured coastal revetment reduced wave overtopping when subjected to extreme hydrodynamic conditions, such as those induced by climate change. Kerr et al. (2025) was a direct follow-up to the work of Baker et al. (2023), and was conducted in the same testing facility, focussing on adaptations to a conventional vertical seawall. The present study investigates the numerical reproduction of select test cases completed by Kerr et al. (2025). Both studies intended to have practical application; to help engineers understand the impact of various retrofit designs on wave overtopping. However, physical modelling on its own is not sufficient. Kamphuis (2020) notes that physical and numerical modelling, along with prototype measurements, need to be integrated. To this effect, the present study integrates numerical modelling analysis with the previous experimental results.

Researchers over the past few years have used IH2VOF, a two-dimensional numerical model (Losada et al. 2007; Lara et al. 2011), to study wave overtopping. Pilechi et al. (2018) compared physical modelling results of free-surface elevations and wave overtopping on rubble mound structures to numerical model predictions. As part of their study, Oliveira et al. (2020) investigated

how wave overtopping (both total cumulative and mean discharge) compared between IH2VOF, XBeach, and empirical formulas, for a sloped seawall. Stagnitti et al. (2023) calibrated and validated an IH2VOF model using physical model data. They then used the model to extend a wave overtopping database for existing and upgraded breakwaters. Neves et al. (2021) compared wave overtopping for 2D physical model tests with three numerical models (including IH2VOF) on a smooth impermeable dike with promenade. Di Lauro et al. (2020) compared the average and cumulative overtopping discharges for a wave energy conversion breakwater structure to existing vertical wall overtopping prediction equations. Lastly, Dang et al. (2021) compared the wave overtopping prediction performance of existing empirical EurOtop (2018) equations, neural network predictions, and IH2VOF for a non-conventional stepped seawall.

4.1.2 Novelty and Scope of Work

The present study reproduces key results from Kerr et al.'s (2025) physical modelling program. To this effect, numerically investigated structures are a traditional vertical seawall, vertical seawall with crest extensions, and a stilling wave basin/secondary wall. The study compares significant wave heights and peak periods, and cumulative overtopping volumes.

Regarding this paper's structure, section 2 discusses the physical modelling program by Kerr et al. (2025); section 3 discusses the numerical modelling setup including the integration of physical modelling conditions, the results including both the sensitivity and primary analyses, and relevant discussion; Section 4 provides conclusions of the work.

To the authors' knowledge, the current study is a novel application of IH2VOF. Few studies have reviewed overtopping discharges at traditional vertical seawalls, especially in the context of a physical modelling program for retrofitted vertical structures. The study aims to provide engineers and designers with practical information about IH2VOF's performance, and to contribute to design aids for the retrofit of traditional coastal structures.

4.2 Experimental Modelling Program

Kerr et al. (2025) completed a physical modelling study in the 97m long, 2m wide, and 2.9m deep LWCF at NRC-OCRE, in Ottawa, Canada. The research reviewed, at a 1:15 Froude scale, how adaptations to a conventional vertical seawall reduced wave overtopping in the face of climate change and water level rise. Capacitance wave probes (WPs, five offshore and four nearshore) measured hydrodynamic conditions, and two overtopping collection systems measured wave overtopping cumulative volumes and discharges.

The experimental test setup is depicted in *Fig. 4.1*. At the left boundary (x = 0), the flume is outfitted with a wave machine equipped with active wave absorption (AWA), and capable of generating significant wave heights of up to 1.1 m high. At the right boundary, the flume has progressive porosity expanded-metal absorbers which feature reflection coefficients less than five percent. The flume is outfitted with a subfloor used for generating reversible currents (not employed for the present study). *Table 4.1* shows the test program, while *Table 4.2* presents the

investigated adaptations. *Fig. 4.1.*, *Table 4.1*, and *Table 4.2* are re-produced from Kerr et al. (2025):

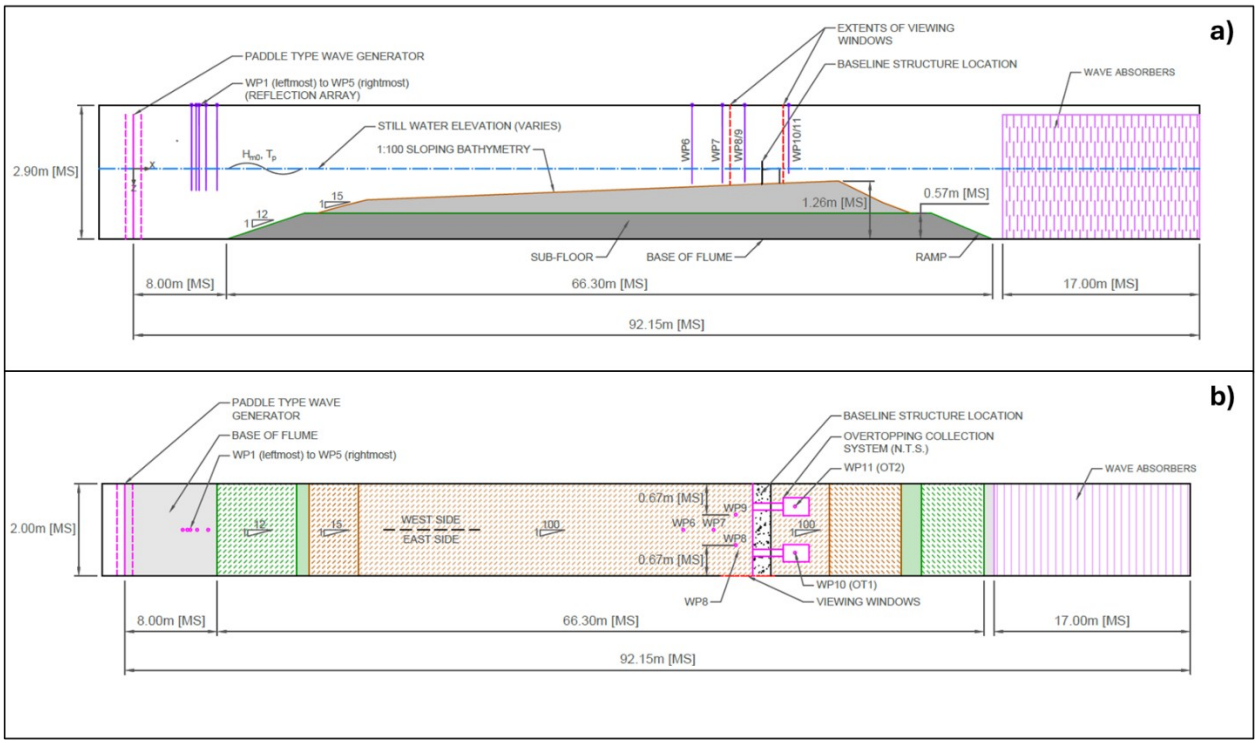

Fig. 4.1. Side and plan views of the experimental test setup in the LWCF, OCRE-NRC, Ottawa, Canada (not to scale)

Table 4.1. Experimental wave test matrix

Test no.	Ref. Name	Water Level at toe (m, MS)	Water Level at WM (m, MS)	Wave Height, H_{m0} (m, FS)	Wave Height, H_{m0} (m, MS)	Peak Period, T_p (s, FS)	Peak Period, T_p (s, MS)
1	M1			1.90	0.127	6.9	1.8
2	M2			2.57	0.171	8.1	2.1
3	M3	0.251	1.450	3.24	0.216	9.0	2.3
4	M4			3.91	0.261	9.7	2.5
5	M5			5.00	0.333	10.8	2.8
6	F1			1.90	0.127	6.9	1.8
7	F2			2.57	0.171	8.1	2.1
8	F3	0.331	1.530	3.24	0.216	9.0	2.3
9	F4			3.91	0.261	9.7	2.5
10	F5			5.00	0.333	10.8	2.8
11	C1			1.90	0.127	6.9	1.8
12	C2			2.57	0.171	8.1	2.1
13	C3	0.351	1.550	3.24	0.216	9.0	2.3
14	C4			3.91	0.261	9.7	2.5
15	C5			5.00	0.333	10.8	2.8

Note: FS = Full Scale; MS = Model Scale; WM = Wave Machine

Table 4.2. Experimental test series matrix

Test series ref. name	Description	Wave conditions tested
TSAA	Baseline vertical wall	M1-M5, F1-F5, C1-C5,
TSBB	Vertical extension	M1,M3,M5, F1,F3,F4, C1,C3-C5,
TSCC	Eco-friendly submerged breakwater	M1,M3,M5, F1,F3-F5, C1,C3,C5
TSDD	Perched beach	M1,M3-M5
TSEE	Modified perch beach	M1,M3,M4
TSFF	Cobble beach	M1,M3,M4, F1,F3,F4, C1,C3,C4
TSGG	Revetment	Same as TSFF
TSHH	Drainage swale	M1,M3
TSII	Modified drainage swale	M3,M4
TSJJ	Further modified drainage swale	M3,M4, F1,F3,F4, C1,C3,C4
TSKK	Secondary wall	Same as TSFF

Three representative water levels were tested. The first was a mean water level (MWL) at 75.0 m, the second a 100-year flood (HYF) level at 76.2 m, and the third an augmented 100-year flood level to include the effect of climate change-induced water level rise, at 76.5 m.

4.3 Numerical Modelling and Analysis

4.3.1 Model Characteristics

IH2VOF solves the two-dimensional Reynolds Averaged Navier-Stokes (RANS) equations (IHCantabria 2012). The algebraic nonlinear k-ε model relates the Reynolds stress tensor to the strain rate of the mean flow (IHCantabria 2012). A volume of fluid (VOF) method traces free surface movement (Lara et al. 2011). For flow in porous media, IH2VOF relies on the Volume-Averaged Reyolds Averaged Navier-Stokes equations (VARANS). The reader is directed to Lara et al. (2011) and Losada et al. (2007) for more detailed descriptions of the model. The computational domain is discretized using rectangular cells. Either uniform or non-uniform meshes are possible, allowing for increased resolution around areas of interest.

4.3.2 Model Parameters and Boundary Conditions

While previous authors accounted for the presence of reflections by completing a reflection analysis (De Finis et al. 2020), this study assumed reflections in the experimental data, used as numerical wave generation input, were minor (see section 2.0). This is a realistic assumption because the end-of-the-flume wave absorbing system and the wave maker's AWA feature significantly reduced wave reflection.

The experimental setup used two WPs at x = 52.83 m from the wave machine: WP8 and WP9 (*Fig. 4.1.*). However, since IH2VOF is a two-dimensional model only one WP could be used. Therefore, this study assumed that comparing the numerical wave conditions x = 52.83 m to the average of the experimental WP8 and WP9 data was sufficient. Henceforth, this location is referred to as WP8.

Regarding other parameters, the number of waves (~250) was consistent. The study employed the static paddle generation method, and a default smoothing time of 10s. Second order generation was initially considered but was not used because it was computationally intensive and IH2VOF had difficulty generating the static paddle. A default initial step of 0.005s was used. For overtopping analysis, a 0.1 s time interval was selected as the minimum overtopping event duration. The aspect ratio ($\Delta x/\Delta y$) in the highest resolution zone was maintained at approximately 1.65-1.66. Note that aspect ratios of $\Delta x/\Delta y < 2.5$ are preferrable to help avoid false breaking phenomena (IHCantabria, 2012). Referring to the literature, Dogan (2016) selected an aspect ratio of 4, Peters (2014) selected a ratio just over 1, and Oliveira et al. (2020) selected a ratio of 2.2. Therefore, the selected aspect ratio is considered adequate. The "activate turbulence" option was considered, whereby the k-epsilon turbulence model was applied using the default IH2VOF values. However, no difference was observed between either water level at the structure toe or total cumulative wave overtopping volume. Therefore, the turbulence model was not used for the analysis.

4.3.2.1 Replication of Physical Modelling Conditions

The experimental bathymetry geometry and hydrodynamic conditions were modeled in IH2VOF. The experimental flume's orientation was maintained in the numerical model (refer to *Fig. 4.1*): the left boundary was the wave machine (x = 0 m) and waves travelled rightward (positive x

direction) towards the right boundary. To replicate the experimental wave maker's AWA capabilities in IH2VOF, the left and right boundaries were given wave absorption (see section 2.0) capabilities. To this effect, the "left boundary absorption" and "right boundary absorption" options were selected for all tests. No sponge layer was used at either boundary. The upper boundary was set above the highest wave crest to eliminate its influence and better reflect the experimental modelling upper boundary of open atmosphere. A freshwater density of 1,000 kg/m^3 was used for both the experimental and numerical study.

Two different domain lengths were considered in the numerical sensitivity analysis. The "long" domain (LD) used the location of WP1 (closest wage gage to the wave generator) as the offshore boundary (x= 5.01 m from the wave generator, approximately 49.28 m from the vertical seawall). Alternatively, the "short" domain (SD) considered the location of WP6 as the offshore boundary (x= 48.3 m from the wave generator, approximately 5.99 m from the vertical seawall), which reduced computation times comparing to the long domain, but had limited length in front of the structure. Using the longest L via transitional water equations (Kamphuis 2020), the short domain had approximately 0.7L of distance before the structure, whereas IHCantabria (2012) recommended having a minimum distance of 1.2L to 1.5L. One author, however, noted that only 0.5L before the structure was required (Peters 2014).

In either case, the experimental time series measured at WP1 or WP6 was respectively used as the numerical wave input. To this effect, the "reconstruct wave series option" was used in IH2VOF to import the experimental time series, and as mentioned the "static paddle" was used as the paddle type. The experimental data was measured during the wave calibration phase, i.e. before any reflective structures were installed in the flume. Also, the other experimental wave probe locations were maintained in the numerical model.

Regarding the static paddle, the Dirichlet boundary condition used for the static paddle generation relies on component velocities. While it is an option to specify the initial horizontal and vertical velocities in the input file, this process was not completed because velocity measurements at the experimental wave probe locations were not taken. However, potentially this technique may increase the model's accuracy. Additionally, in this case the static paddle was a more reasonable choice than a dynamic paddle because the numerical wave boundary was placed at an experimental wave probe location which was fixed in space.

4.3.3 Sensitivity Analysis

4.3.3.1 Mesh Generation

In the literature, some authors use subzones (Dogan 2016; De Finis et al. 2020; Neves et al. 2021), while others opted for uniform meshes (Stagnitti et al. 2023; Peters 2014). This study implemented subzones to help reduce computation times while maintaining high fidelity wave propagation. The mesh geometries for the short and long domains are shown in *Fig. 4.2.*

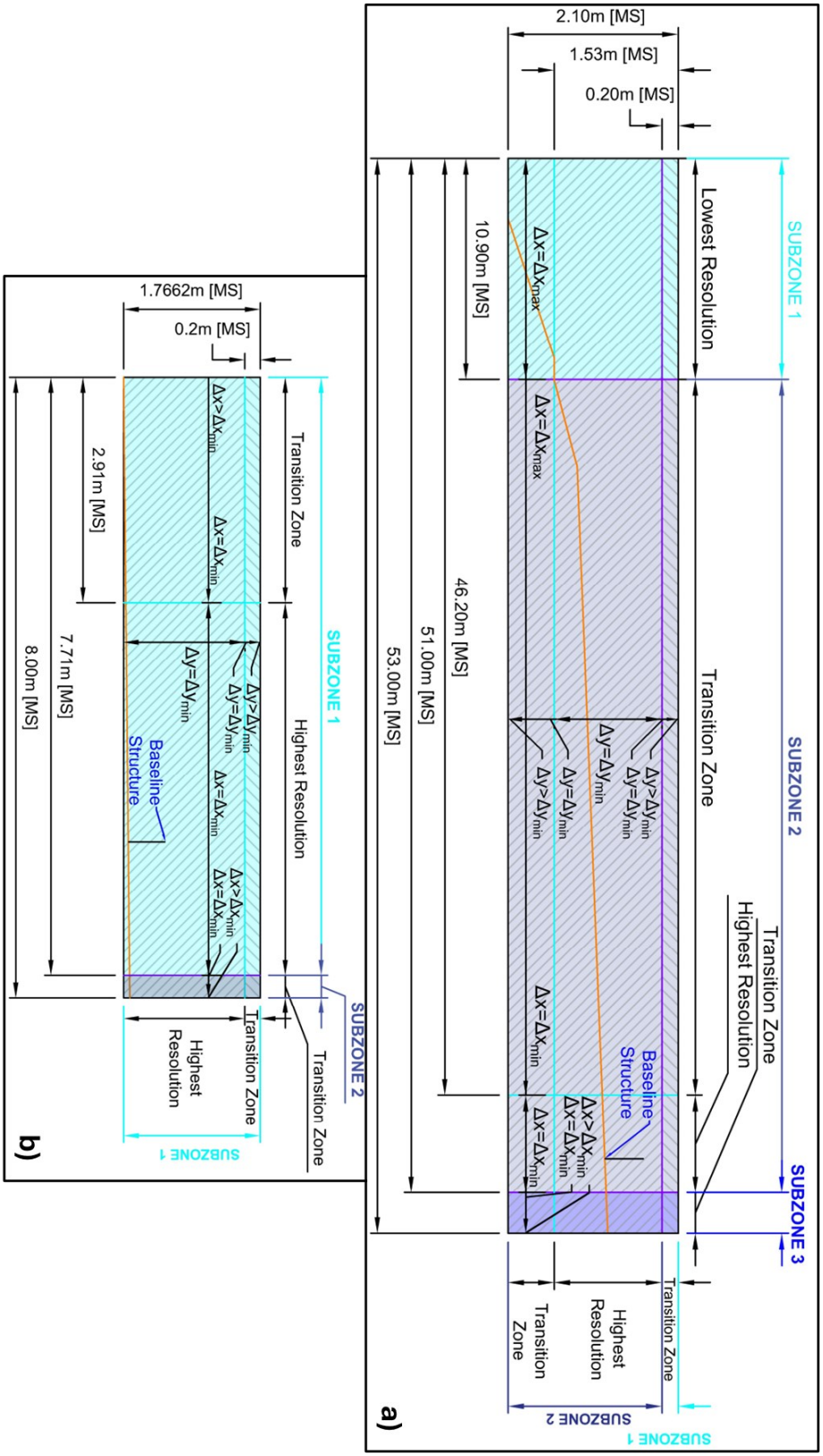

Fig. 4.2. Mesh resolution subzones for (a) long, and (b) short computational domains

Beginning with the long domain (*Fig. 4.2a*), in the *x*-direction, the lowest resolution section was selected to be from $x = 0$ to $x = 10.9$ m following wave breaking calculations (Kamphuis 2020). The maximum mesh resolution began at $x = 46.2$ m to encompass wave-structure interaction and the wave breaking area. Subzone 3 in the *x*-direction transitioned from the maximum resolution to a lower resolution. In the *y*-direction, the flume's height was truncated to 2.1 m, based on preliminary tests measuring runup for a critical wave case. Two subzones were used in the *y*-direction. The division between subzones 1 and 2 was at $y = 0.2$ m (IH2VOF has a positive *y*-direction pointed downward from the top of the mesh), such that the highest resolution encompassed the extents of all water/splash motion. The center line of subzone 2 was selected because the breaking analysis placed the majority of breaking waves above that vertical point on the bathymetry.

The short domain (*Fig. 4.2b*) truncated the long domain vertically from $y = 0$ m to $y = 1.76$ m (in IH2VOF coordinate system) and horizontally from $x = 43.29$ m to $x = 51.29$ m. Note, the short domain used for the wave sensitivity analysis was vertically too large – the 0.8 m trimmed from the long domain was not trimmed from the short domain. However, this only affected the simulation times which for that stage were compared separately between domains. For the overtopping sensitivity analysis, the height of the short domain was reduced to 1 m. To this effect, the maximum resolution zone height was reduced.

Regarding cell sizes, IHCantabria (2012) guidelines were utilized, entailing calculation of L and H. The limiting case noted in Peters (2014) is the lowest and shortest wave. In the experimental wave verification series, the lowest wave at WP8 was roughly 0.118m (MS). The corresponding L at a water level of 75.0m (FS) at WP8 is 2.798 m (MS, using transitional water equations (Kamphuis, 2020)).

4.3.3.2 Sensitivity Analysis for Waves

The sensitivity analysis was completed in two stages. Stage one used no seawall and focussed on wave propagation. The goal was to replicate the experimental wave calibration stage. One wave condition was tested for a series of numerical meshes, and for both domains. Significant wave heights, H_{m0}, and peak wave periods, T_p, were compared between the numerical and experimental results. *Table 4.3* shows the tested resolutions:

Table 4.3. Testing matrix for sensitivity analysis

Mesh	Cell Size criterion		Approximate Resolution (m)			x-direction lowest resolution limits	Number of cells	
	x-dir	y-dir	x-dir	y-dir	aspect		LD	SD
1	*L*/100	*H*/7	0.0280	0.0170	1.6438	*L*/100	233,085	29,744
2	*L*/120	*H*/8.5	0.0233	0.0140	1.6634	*L*/100	297,648	43,092
3	*L*/142	*H*/10	0.0197	0.0119	1.6537	*L*/100	374,842	59,388
4	*L*/170	*H*/12	0.0165	0.0099	1.6576	*L*/115	507,310	83,868
5	*L*/185	*H*/13	0.0151	0.0092	1.6502	*L*/125	593,769	100,466
6	*L*/200	*H*/14	0.0140	0.0085	1.6438	*L*/135		118,144
7	*L*/213	*H*/15	0.0131	0.0079	1.6537	*L*/145		131,068
8	*L*/227	*H*/16	0.0123	0.0074	1.6552	*L*/155		148,533

where "cell size criterion" refers to the cell size targets for the maximum resolution section. Regarding the "*x*-direction lowest resolution limits" column, the minimum resolutions were initially selected as $\Delta x = L_{min}/100$ and $\Delta y = H_{min}/7$ for all the test series, satisfying minimum cell size requirements. However, at higher resolutions the aspect ratio in the lowest resolution section (i.e. $\Delta x_{max}/\Delta y_{min}$) was too large, such that false breaking was possible. So, the minimum resolution was increased accordingly.

This stage used the M3 experimental case as input (*Table 4.1*). Additionally, 240 waves were run for each simulation. *Fig. 4.3*. presents the numerical WP locations for the long and short domains:

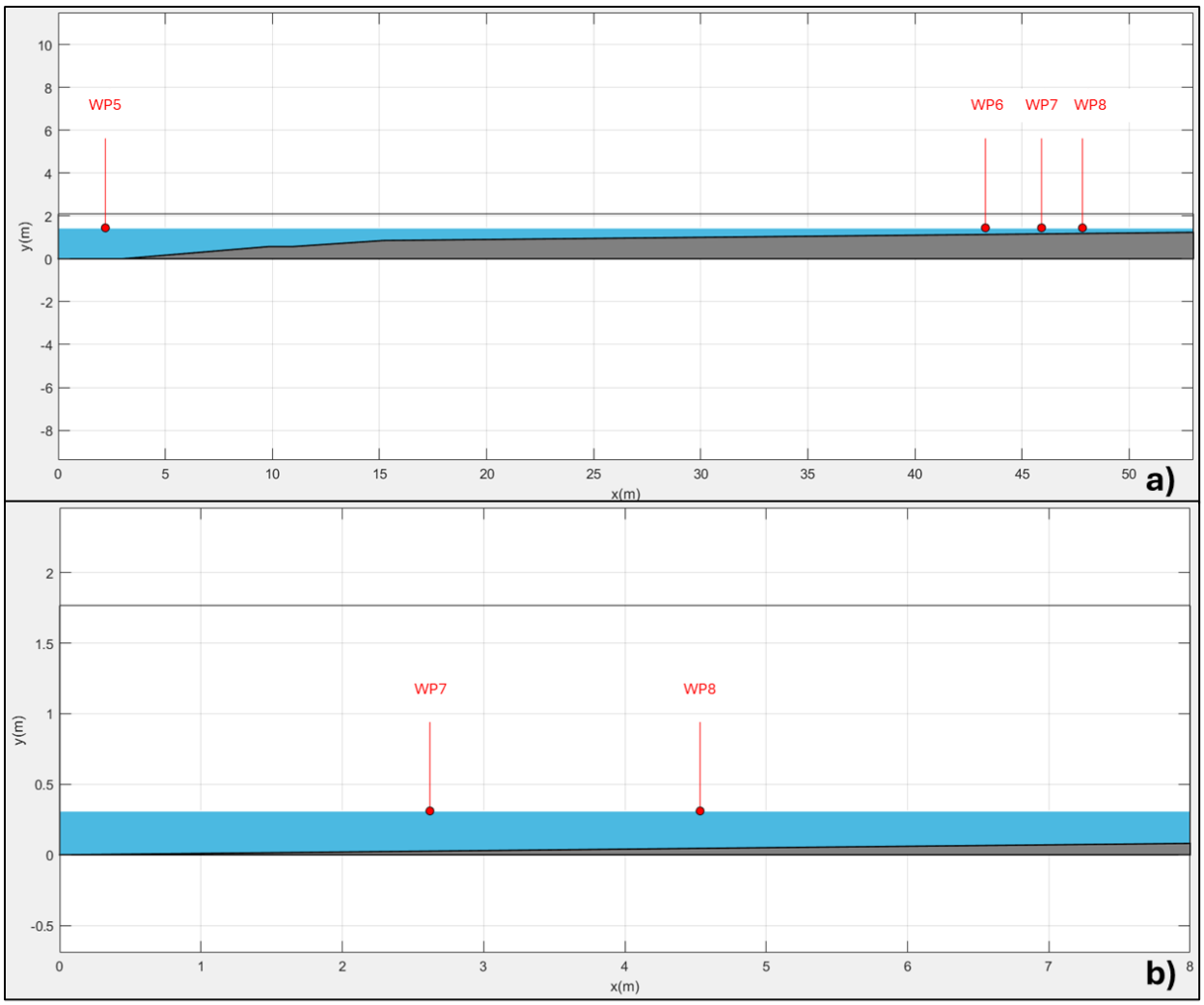

Fig. 4.3 Wave probe locations for wave sensitivity analysis, for (a) long and (b) short domains

NRC's GEDAP™ software (Miles 1990) was used for post-processing the experimental and numerical results using standard time- and frequency-domain algorithms. *Table 4.4* and *Table 4.5* show the experimental data, and the percent errors between the experimental and numerical data for both H_{m0} and T_p.

Table 4.4. Wave sensitivity analysis H_{m0} percent errors between numerical and experimental data

Mesh #	WP7 measured H_{m0} (m)	Percent Error (%)		WP8 measured H_{m0} (m)	Percent Error (%)	
		SD	LD		SD	LD
1	2.677	3.8	-9.5	2.597	-2.2	-10.5
2		3.9	-7.5		-2.8	-8.2
3		3.6	-6.7		-3.8	-7.5
4		3.3	-7.2		-5.6	-8.7
5		2.9	-6.8		-6.9	-8.0
6		1.7			-7.5	
7		2.8			-6.0	
8		1.8			-8.5	

Table 4.5. Wave sensitivity analysis T_p percent errors between numerical and experimental data

Mesh #	WP7 measured T_p (s)	Percent Error (%)		WP8 measured T_p (s)	Percent Error (%)	
		SD	LD		SD	LD
1	9.937	-8.7	-1.7	9.153	-16.8	13.5
2		-6.2	-1.6		-15.5	6.8
3		-6.0	-1.7		-15.2	6.7
4		-5.8	-1.7		2.2	6.7
5		-5.7	-1.7		10.2	6.7
6		-5.6			2.2	
7		-5.5			2.1	
8		-5.5			42.7	

In general, the wave heights in the numerical model were underpredicted (i.e. percent error less than 0) near the structure toe. It is assumed that the model overestimates wave breaking relative to the experimental conditions. Comparatively, the short domain had slightly better performance. Although, the most refined short domain mesh (mesh #8) did not necessarily perform any better than the first seven.

The long domain, however, better re-produced wave periods. Long domain predictions were consistent at both WP7 and WP8, with errors generally less than 7 percent (less mesh 1), whereas

the short domain predictions near the structure toe had high scatter. *Fig. 4.4* compares the key numerical and experimental time series for the short and long domains:

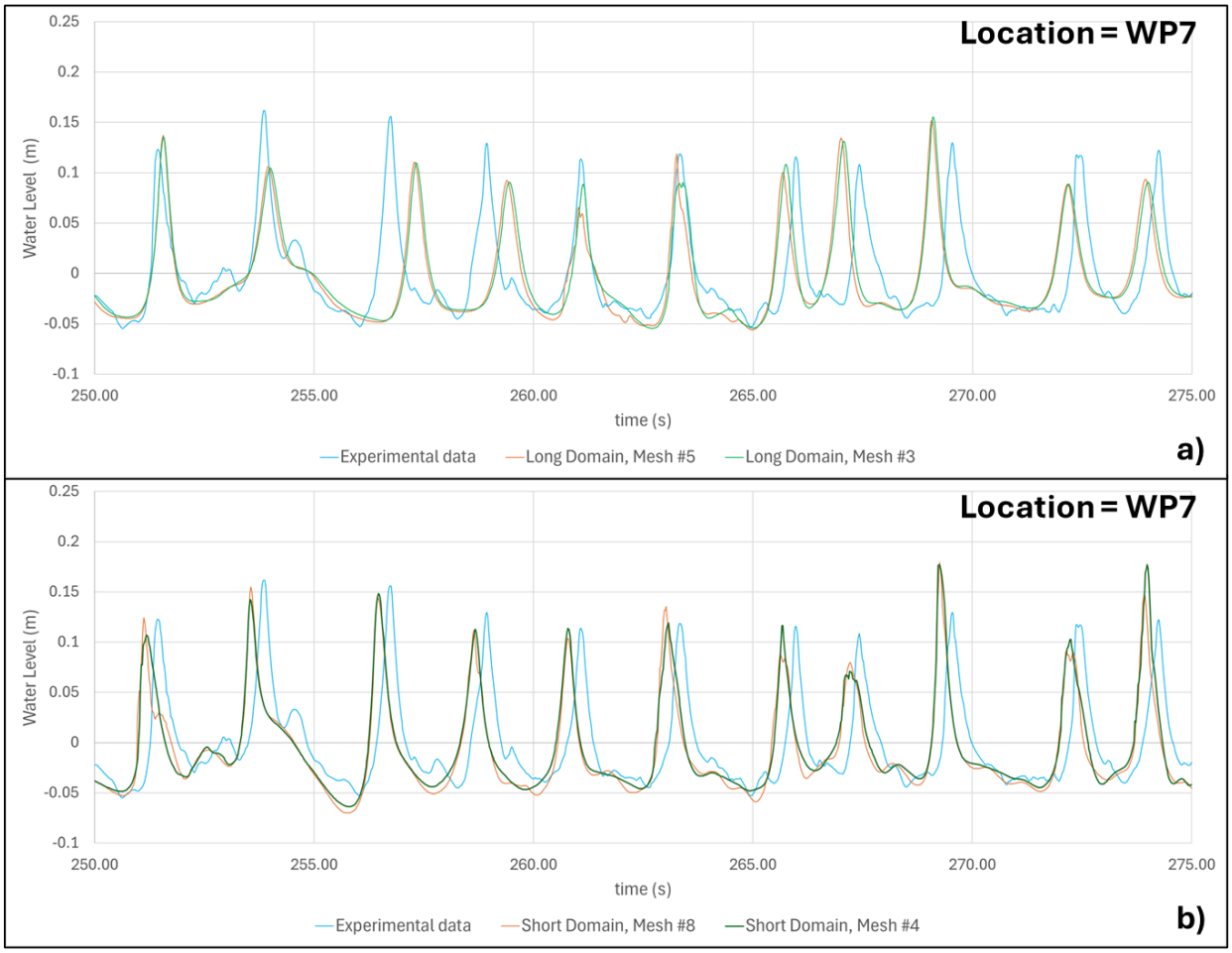

Fig. 4.4. Experimental vs. Numerical time series (75.0m w/L, 3.2m wave height; MS).

The results for both the finest mesh and a slightly less refined mesh are provided. In both cases, the finest mesh showed no significant improvement over the less refined mesh, entailing the less refined meshes will reduce computational effort while preserving simulation accuracy. Note that time synchronization between the experimental and numerical time series was accounted for in *Fig. 4.4*, and in all analyses. The experimental and numerical data were time-synchronized by lagging the numerical time series to account for the experimental wave propagation time from the generator to WP1/WP6. Therefore, in *Fig. 4.4* the experimental and numerical wave crests should theoretically match exactly on both axes.

Thus, following the sensitivity analysis for waves, the best long domain mesh was mesh # 3, and the best short domain mesh was mesh #4.

It should be noted that this portion of the sensitivity analysis could also have been completed with the vertical wall installed in the flume. To briefly compare the results, for the mesh #3 long domain

test (see *Table 4.6*), the wave heights at all four probes were compared to the corresponding experimental wave heights. IH2VOF underpredicted the experimental heights by ~14%, which is still a comparable result to the no-structure case considering that the waves were impacted significantly by wave-structure interaction.

4.3.3.3 Sensitivity Analysis for Overtopping

The second stage of the sensitivity analysis compared numerical and experimental cumulative overtopping volumes. The baseline structure (as shown in *Fig 4.6d*) was added to several long and short domain numerical meshes from *Table 4.3* to determine which domain and mesh could best reproduce overtopping. The IH2VOF overtopping measurement point was located at the landward edge of the wall, akin to the experimental tests.

Overtopping was measured differently in the experimental and numerical test series. Experimentally, overtopping was measured using collection trays and reservoirs (shown in *Fig. 4.6 (a)*, *(b)*, and *(c)*). A WP in each of the reservoirs measured the water elevation at 50 Hz. Based on the reservoir dimensions, each elevation time series was converted to a cumulative volume. In the numerical model, a digital WP measured the instantaneous overtopping, which was then integrated to form the cumulative overtopping volume (IHCantabria 2012).

Three tests were simulated for both domain lengths. *Table 4.6* shows the results of the six tests, including the percent errors relative to the experimental reference:

Table 4.6. Secondary sensitivity analysis results (MS)

Mesh	**Cell size criterion**		**Simulation times (min.)**		**IH-2VOF cumulative OT (m^3/m)**		**Reference experimental cumulative OT (m^3/m)**	**Percent Error (%)**	
	x-dir.	y-dir.	LD	SD	LD	SD		LD	SD
2	*L*/120	*H*/8.5	456	35	0.1947	0.6219	0.2704	-28.0	130.0
3	*L*/142	*H*/10	706	53	0.2455	0.7348		-9.2	171.8
4	*L*/170	*H*/12	1443		0.2530			-6.4	
6	*L*/200	*H*/14		141		0.9923			267.0

Moreover, the time series for each of these six tests were plotted together with the experimental data, displayed in *Fig. 4.5*. The experimental data was smoothed using GEDAP to remove unnatural oscillations; the procedure used a cubic spline curve fitting approach:

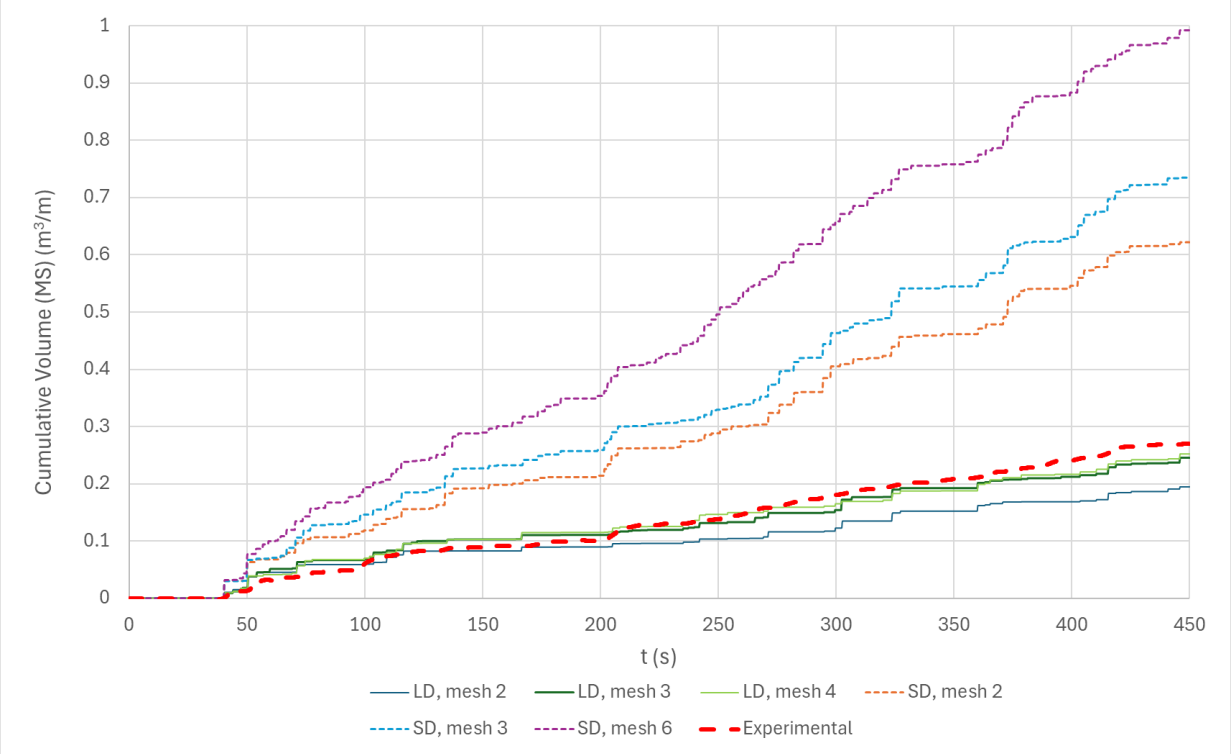

Fig. 4.5. Overtopping sensitivity analysis comparison

Assessing the results from *Table 4.6* and *Fig. 4.5*, the short domain meshes diverged from the experimental data, whereas the long domain meshes converged upon the experimental measurements. Although mesh #4 with the longer domain showed a slight improvement over mesh #3 (~3%), it took 12 hours longer to simulate. Further, the finest long domain mesh (mesh #5) was also investigated, but the model encountered stability issues. Therefore, all future simulations used mesh #3 with the longer domain.

4.3.4 Main Investigation Results and Discussion

Four distinct cross sections across three experimental test series, pictured in *Fig. 4.6.* (TSAA, TSBB, and TSKK, see *Table 4.2*), were replicated in the numerical model.

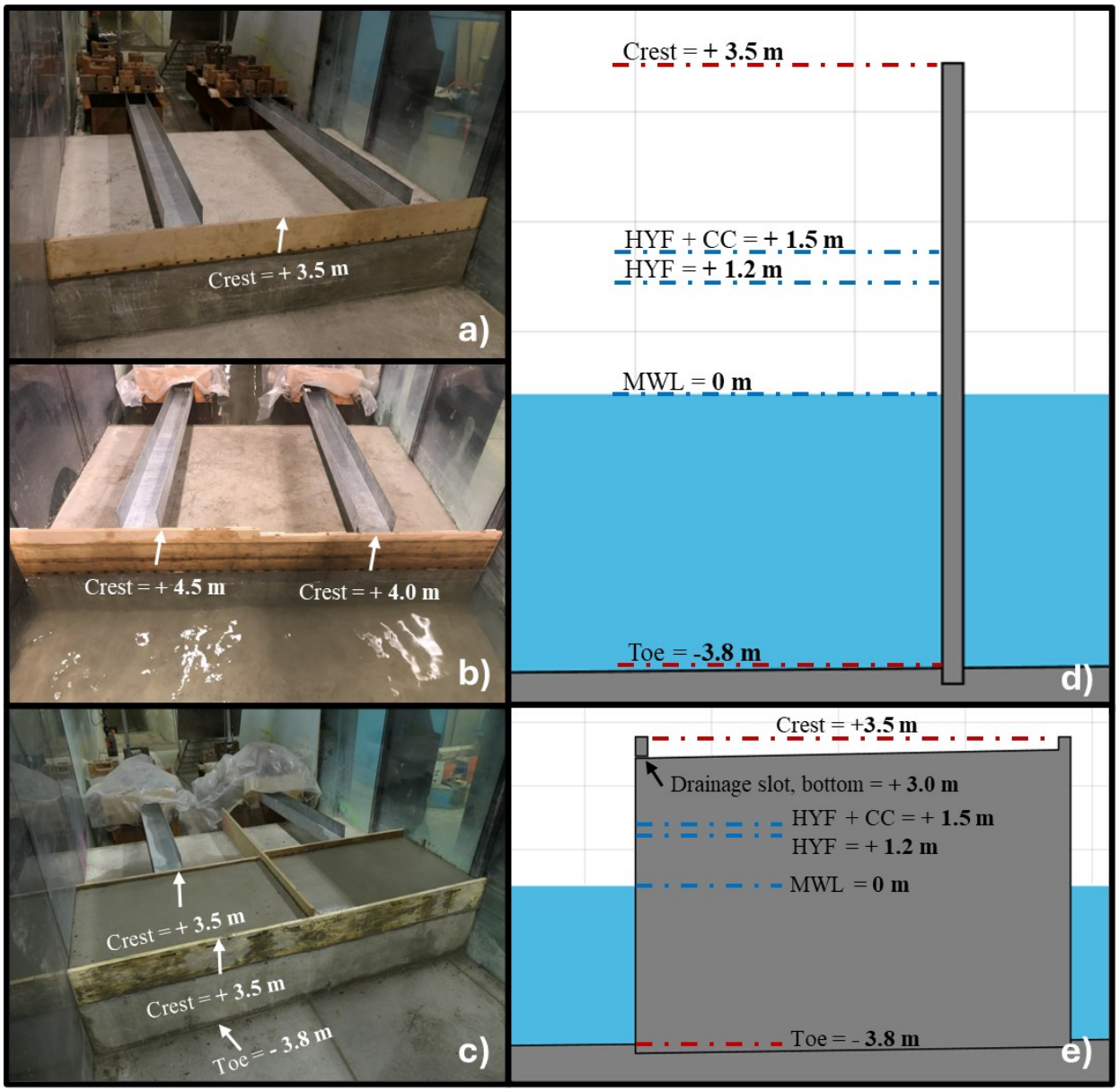

Fig. 4.6. (a) TSAA (baseline vertical seawall), (b) TSBB (vertical crest extensions), (c) TSKK (left side of figure; secondary wall/stilling wave basin with zero-extension secondary wall), (d) IH2VOF representation of TSAA, and (e) IH2VOF representation of TSKK.

Noting *Fig. 4.6(b)* and *(c)*, the TSBB and TSKK geometries were split sections. In TSBB, the west (left) side had a 1 m full-scale (FS) extension over TSAA, while the east (right) side had a 0.5 m FS extension. In TSKK, the west (left) side had a secondary wall height equal to the primary crest height (both equal to the TSAA crest height), while the east (right) side secondary wall crest was 0.5 m higher than the primary crest. Only the west (left) side of the flume for TSKK was modelled in IH2VOF.

Shown on *Fig. 4.6.*, the experimental vertical seawalls featured a landward platform to accommodate testing of various landward adaptations. For cases only involving the seawall itself (TSAA & TSBB), overtopping flows were collected directly behind the vertical wall meaning the landward platform should not have affected results. In the numerical model, for simplicity the seawall was represented by a vertical barrier of the same thickness as in the experiments.

For TSKK, rectangular drainage slots on the front of the wall drained water from the stilling basin (as shown in *Fig. 4.2c*). These drainage slots were incorporated into the numerical model by introducing a gap (as shown in *Fig. 4.6e*) in the 2D cross-section. The height of the gap was equivalent to the total area of the drainage holes across the width of the flume. For TSAA and TSBB, the drainage holes on *Fig. 4.6(a)* and *(b)* were not represented in the model. Note that in IH2VOF, all structures were otherwise placed at the same location, and with the same dimensions as they were constructed in the experimental model.

This study focussed on the structures outlined in *Fig. 4.6* because they were relatively simple vertical wall structures without porous elements. Subsequently, the number of variables requiring calibration was limited which allowed for an easier assessment of the model's ability to replicate overtopping at a vertical structure, an apparent knowledge gap in the literature.

4.3.4.1 Primary Test Series

The primary test series compared experimental and numerical cumulative overtopping volumes using the selected mesh (LD mesh #3), for several wave conditions and structures. *Table 4.7* outlines the test matrix for the primary analysis while *Table 4.8* presents the primary analysis' results, including the percent errors relative to the experimental data.

Table 4.7. Primary analysis test matrix

Test ID	Sea state*	W/L at WP1 (m)	Target FS H_{m0} (m)	Target FS T_p (s)	MS Length of Signal (s)	Appx. no. Waves
TSAA_1	M1	1.445	1.90	6.9	325	236
TSAA_2	M2		2.57	8.1	400	247
TSAA_3	M3		3.24	9.0	450	240
TSAA_4	M4		3.91	9.7		235
TSAA_5	F3	1.525	3.24	9.0		250
TSAA_6	C3	1.545				243
TSBB_low_1	M3	1.445				240
TSBB_low_2	C3	1.545				243
TSBB_high_1	M3	1.445				240
TSKK_1	M3					
***Referencing experimental test cases in Table 4.1**						

Table 4.8. Primary analysis results

Test ID	Sea state	FS cumulative overtopping (m^3/m)		Percent error (%)
		numerical	experimental	
TSAA_1	M1	0.004	2.338	**-99.8**
TSAA_2	M2	5.5	25.0	**-78.1**
TSAA_3	M3	55.2	60.8	**-9.2**
TSAA_4	M4	75.1	83.0	**-9.5**
TSAA_5	F3	183.2	294.6	**-37.8**
TSAA_6	C3	269.5	349.2	**-22.8**
TSBB_low_1	M3	33.5	37.1	**-9.6**
TSBB_low_2	C3	176.1	250.1	**-29.6**
TSBB_high_1	M3	13.8	24.3	**-43.3**
TSKK_1	M3	14.9	19.3	**-22.7**

The numerical results underpredict the experimental data for all cases. In only two cases, however, the difference is in the order of one magnitude or more. Also, the numerical results are likely still overpredicted comparatively because the numerical model used a smooth vertical wall, while the experimental structure had drainage holes on the face of the wall which further dissipated wave energy (*Fig. 4.6.*).

4.3.4.2 Correction Analysis

To address the consistent under-prediction of overtopping, the wave input time series was augmented based on the wave sensitivity analysis (refer to *Table 4.4*). The numerical wave height prediction at WP8 was approximately 7.5 % low at the toe of the structure for case M3, so the input time series was accordingly multiplied by 7.5 % and used to re-run simulations for that sea state. One test was performed for all four of the geometries (TSAA, $TSBB_{low}$, $TSBB_{high}$, TSKK), and the results are presented in *Table 4.9*.

Table 4.9. Correction test series results

Test ID	Sea state	Approximate no. waves	FS cumulative overtopping (m^3/m)		Percent error (%)
			numerical	experimental	
corr_TSAA	M3	240	61.9	60.8	**1.8**
corr_TSBB_low		240	14.5	15.0	**-2.9**
corr_TSBB_high		155	38.9	37.1	**4.9**
corr_TSKK		240	18.0	19.3	**-6.5**

The errors significantly decreased between the analysis and correction tests. In fact, all remaining errors fell below 7 % and were distributed above and below zero, which indicates the underpredicted wave heights were at least partially responsible for the underpredicted overtopping. Also, the manual correction proved effective for three cases of a standard vertical seawall, and for a stilling wave basin case. For practical use, when using the model for design users may also consider a correction to their input data to account for any systematic discrepancies in the model. Future work should confirm whether this is applicable to other cases. *Fig. 4.7* shows the cumulative overtopping time series for a primary test, TSKK_1, its associated correction case, corr_TSKK, and the experimental data:

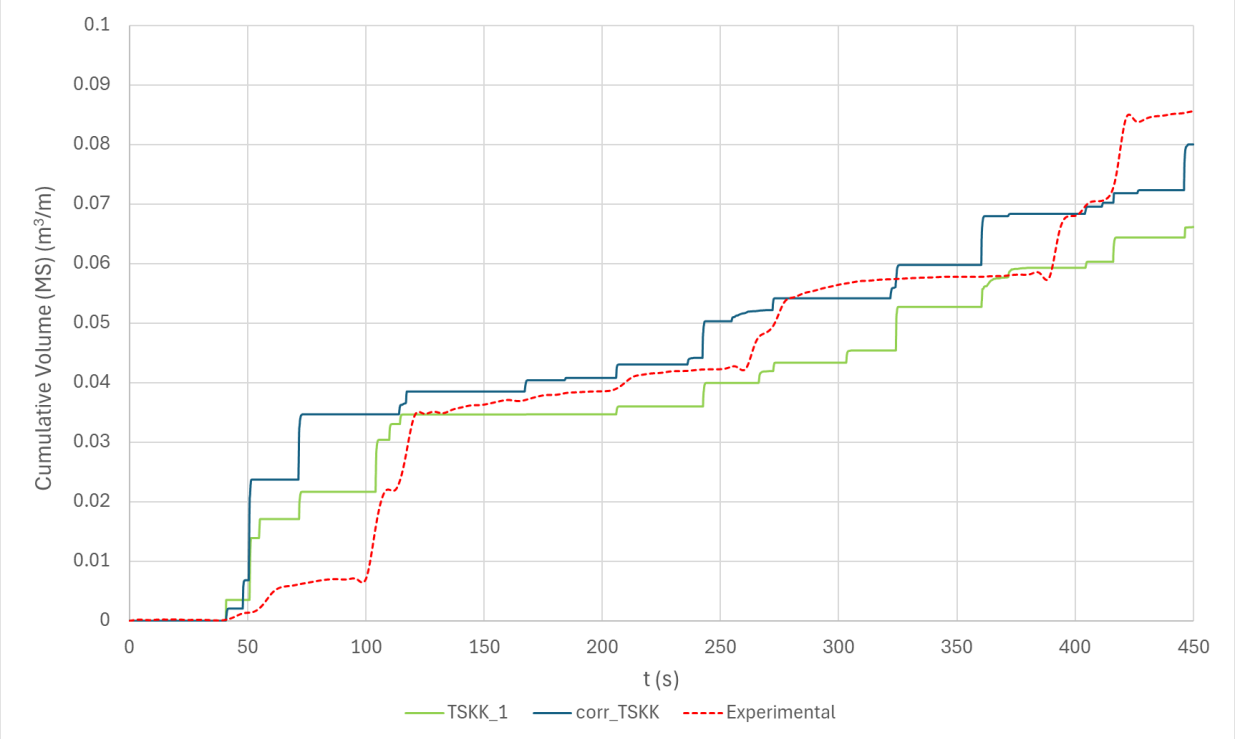

Fig. 4.7. Cumulative overtopping comparison between TSKK_1, corr_TSKK, and the associated experimental data

While the final cumulative values were reasonable, *Fig. 4.7.* reveals discrepancies between specific overtopping events. For example, the experimental series features a significant overtopping event between 100 s and ~125 s. While both numerical series predict a similar event, the original series predicts this between 45 s and 75 s, and the corrected series occurring between 45 s and 115 s. Additionally, the third large event in the experimental series, occurring between 390 s and 425 s, is missed by both numerical simulations.

4.3.4.3 Comparison to EurOtop (2018) Data

Experimentally measured and numerically simulated overtopping rates were compared against standard overtopping prediction equations. EurOtop (2018) equations 7.7 and 7.8 (equations *4.1* and *4.2* below) predict overtopping rates for vertical wall structures:

$$\frac{q}{\sqrt{gH_{m0}{}^3}} = 0.011\left(\frac{H_{m0}}{h \cdot s_{m-1,0}}\right)^{0.5} \exp\left(-2.2\frac{R_c}{H_{m0}}\right), \qquad 0 < \frac{R_c}{H_{m0}} < 1.35 \tag{4.1}$$

$$\frac{q}{\sqrt{gH_{m0}{}^3}} = 0.0014\left(\frac{H_{m0}}{h \cdot s_{m-1,0}}\right)^{0.5} \left(\frac{R_c}{H_{m0}}\right)^{-3}, \qquad \frac{R_c}{H_{m0}} \geq 1.35 \tag{4.2}$$

Where q is the mean overtopping discharge per unit width, g is the gravitational acceleration, H_{m0} is the significant wave height, R_c is the crest freeboard, h is the depth at the structure toe, and s_{m-}

$_{1,0}$ is the wave steepness. For this analysis, only results with vertical walls (TSAA and TSBB) were included. A plot showing the numerical results, equations *4.1* and *4.2*, and the experimental data is shown below in *Fig. 4.8*:

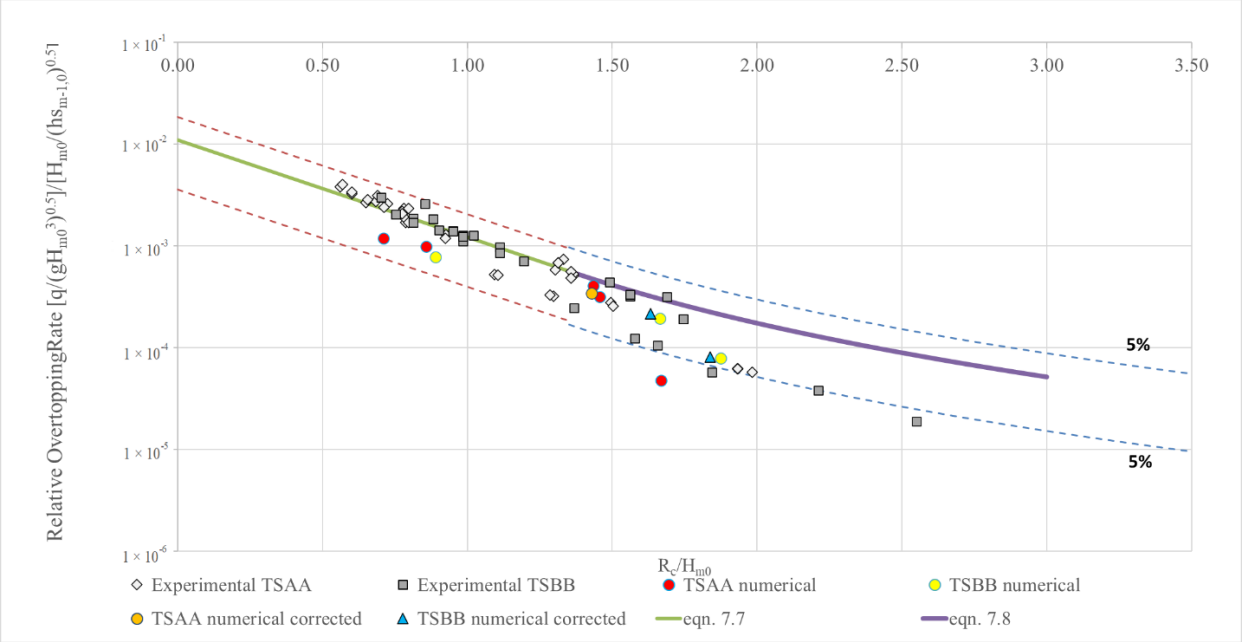

Fig. 4.8. Comparison of the experimental results, numerical results, and predictions from the EurOtop (2018) equations

where the figure includes the 5 % confidence bounds. The white and grey points are experimental data from Kerr et al. (2025). Comparing numerical data to EurOtop predictions conveys the model's ability to replicate the overtopping mechanism because the plot is based on dimensionless ratios which account for numerical wave height discrepancies (like those in *Table 4.4*). Hence, the correction test series results were plotted alongside the main test series data, and no significant increase in model performance was observed.

In *Fig. 4.8.*, for a given value of relative freeboard (R_c/H_{m0}), the numerical data always underpredicted the wave overtopping compared to EurOtop equations. However, the performance of the numerical model at replicating overtopping is still reasonable. The numerical data falls within the bounds of the experimental data, and only two of the twelve points fell outside of the EurOtop 5% bounds.

Quantitatively, the root mean squared error (*RMSE*) was calculated separately between the prediction equations and the experimental data, and between the prediction equations and the numerical data, using the relative overtopping rate as the variable:

$$RMSE = \sqrt{\frac{1}{n}\sum_{i=1}^{n}\left(\log\left(\frac{q}{\sqrt{gH_{m0}^3}}\right)_1 - \log\left(\frac{q}{\sqrt{gH_{m0}^3}}\right)_2\right)^2} \tag{4.3}$$

where $(q/(gH_{m0}^3)^{0.5})_1$ is either the numerical or experimental relative overtopping prediction, and $(q/(gH_{m0}^3)^{0.5})_2$ is the prediction from equation *4.1* or *4.2*, depending on relative freeboard. Taking the *log* of the relative overtopping is consistent with other analysis (Salauddin and Pearson 2019; Dong et al. 2020; Dong et al. 2024). When outliers in the numerical data were omitted (based on above $Q3 + 1.5IQR$), the experimental ($RMSE_{exp} = 0.2050$) and numerical ($RMSE_{num} = 0.2256$) *RMSE* values were comparable (note, $RMSE_{num} = 0.9495$ if no outliers were removed). In a different form and still using relative overtopping rate as the main parameter, the numerical data exhibited an average absolute percent error of 40.4 % compared to the EurOtop predictions (when outliers were omitted, the value reduced to 30.0 %), compared to an experimental value of 22.0 %.

4.3.4.4 Challenges and Limitations, and Future Work

While the model performed generally satisfactorily, it did struggle to replicate cases with more frequent wave breaking (i.e. higher wave heights). In the analysis series, the model exhibited difficulties with M5 and F3 for $TSBB_{low}$, and with the M4 case for TSKK. The model also struggled with higher resolutions – mesh 5 (~593 000 cells) in the overtopping sensitivity analysis could not be completed (but mesh 4 with ~507 000 cells was successful). Possibly, the demanding conditions were responsible – a very long numerical flume, high-breaking conditions, and a fine grid resolution.

The numerical study was also limited by the available experimental time series data. As mentioned, for the numerical model, only offshore or nearshore generation were viable, resulting in either a very long or a very short numerical domain. Having an additional WP near the start of the 1:100 slope (refer to *Fig. 4.1*) would have simplified the extent of the numerical bathymetry, reduced computational efforts, and reduced the domain size compared to the longer domain that was utilized.

Finally, the study was limited, possibly significantly, by the mesh's discretization around the structure. A follow-up simulation was conducted which adjusted the mesh very slightly, so that the front face of the vertical wall perfectly aligned to the intersection between two columns of cells. The top face of the wall was also similarly aligned to the intersection. The length of the wall parallel to wave propagation was also increased. All other conditions remained the same. The total cumulative wave overtopping was found to be reduced by approximately 25 percent in the "aligned" test, compared to the original test used in the analysis. This finding may indicate systematic errors within the analysis related to the structure not being properly represented by the original mesh.

The authors suggest future work focussed on practicality. This study's foundation was two physical modelling programs which aimed to address climate-change driven augmented coastal hazards by contributing to design guidance of retrofitted structures. This study used numerical models to propagate that aim; to build knowledge regarding numerical models' value as retrofit design aids. While this study showed that replication of experimental results may be achieved through manual calibration of input wave conditions, future research should continue to investigate the practical applications of the model. For example, using the model to investigate other

adaptation cases (e.g. Stagnitti et al. (2023)), and validating the results through physical model tests.

4.4 Conclusions and Recommendations

This study investigated the performance of IH2VOF, a two-dimensional RANS numerical model, at replicating results of experimental tests of overtopping of coastal structures which were experimentally investigated in the Large Wave-Current Flume at NRC-OCRE, Ottawa, Canada. The experimental work investigated how adaptations to a traditional vertical seawall reduced wave overtopping when subjected to augmented wave conditions. This study numerically replicated four of the experimental structures (baseline vertical seawall, vertical seawall with lower and higher crest extensions, and stilling wave basin/secondary wall). A sensitivity analysis showed that using a longer mesh for the numerical flume replicated better the cumulative wave overtopping volumes. Primary results revealed that the numerical model tended to underpredict significant wave heights compared to experimental results, as well as slightly underpredict cumulative wave overtopping compared to accepted design equations. However, the numerical results exhibited acceptable accuracy when simulating the experimental data and both the experimental and numerical results were compared to currently existing design equations. It is recommended that numerical models be used as a design tool for the retrofit of traditional vertical coastal structures. More integrated physical and numerical studies may help develop a design database in this regard, as in Stagnitti et al. (2023).

5 Discussion

5.1 Limitations

Regarding the physical model, omitting stability considerations presents a limitation. In the experimental study, the baseline structure among other adaptations (crest extensions, stilling wave basin) was completely rigid. Also, measurement of wave forces and pressures were not undertaken. Dynamic structural responses were neglected. For example, a mobile bed was not considered – the bed was immobile for all tests; neither material degradation nor durability were investigated, which in the field may impact a vertical wall's ability to harbour structural additions or withstand construction. Therefore, wave interaction with the structure is uncertain, as is whether any data was collected for wave trains which induced structural instabilities. This possibly limits the results' applicability, because real designs must consider structural stability in addition to overtopping considerations.

A baseline vertical wall with a smooth face was not tested, limiting results in two ways. First, the experimental data post-processing often referenced EurOtop data. However, since EurOtop equations are developed for a smooth vertical wall (see *Fig. 2.6.*), discerning between the non-smooth face effects, and natural bias or error within the LWCF or overtopping measurement systems is impossible. Albeit the non-smooth face on the baseline and crest-extended structures likely had a small effect, because the raw data was still well-aligned to the EurOtop equations. But, its true magnitude was not determined. Secondly, the quality of comparison between the numerical model and the experimental data was affected. Because the numerical model used a smooth face, it biased those results higher – the drainage holes would dissipate incoming energy to some (speculatively minor) degree. Note, it was still reasonable to represent the numerical wall with a smooth face: the data could be more accurately compared to EurOtop data, and the effect was assumed to be minor – it was uncertain whether translating the perforations into two dimensions would be any more accurate than representing the numerical baseline structure with a smooth face. Two numerical tests with the perforations were completed. The initial tests revealed that the perforations reduced overtopping between 30 and 40 percent on average, with higher error correlating to higher relative freeboard. However, tests' accuracy is uncertain because they were unvalidated by physical results.

As described in Section *3.0* several adaptations featured two different structures, split halfway across the flume's width. The split sections investigated more parameters for a given test, saving time. Consequently, increased efficiency was offset by greater measurement uncertainty. For example, a separate k factor was created for each geometry, including distinguishing leading constants for the split sections (i.e. TSCC, TSGG). For example, if only one unit orientation was used for the TSCC breakwater, a more refined equation may have been possible. Also, more tests

would have been available for east to west uncertainty analysis (see Section 3.0). Albeit this may be a trade-off rather than a pure limitation.

In the experimental study, probes were placed in two general locations: offshore, and nearshore – those locations were suitable for the experimental study because wave overtopping analysis required knowledge of offshore and nearshore conditions. However, for the numerical modelling, the experimental probe locations proved to be a limitation. First, a prolonged sensitivity analysis resulted because two domain lengths were compared. Moreover, neither domain appeared to be ideal – the short domain lacked significant accuracy at reproducing wave overtopping, and the long domain required many more cells and computational effort to obtain required mesh resolutions. As mentioned in Section *4.0*, the complex domain speculatively caused the intermittent model instability. Having a wave probe in the experimental model at the start of the flume's 1:100 bathymetry, for example, would have reduced the computational effort, allowed for finer resolutions, and likely resulted in more stable performance of the numerical model.

5.2 Applications

Integrating physical and numerical modelling is a crucial aspect of successful coastal management (Kamphuis 2020). Moreover, an integrated solution may involve a joint database of physical and numerical data or validated numerical models capable of its own database development – see Stagnitti et al. (2023). This study's limitations may have allowed only a modest contribution in this regard. However, it still adds to the knowledge base regarding retrofit design options – studies which reviewed vertical wall adaptations are limited except for parapets or crest extensions. Adaptations at the crest, and seaward and landward of the crest were tested, acknowledging that design restrictions may limit construction either seaward or landward of the wall (or in the case of a crest extension, both).

The study used ECOncrete Coastalock armour units, a novel eco-friendly armour unit, in several structures (most prominently in TSCC and TSGG). Some results from this study were used in the creation of a design guideline document for Coastalock units – a clear practical application.

6 Conclusions and Recommendations

6.1 Conclusions

This study used physical and numerical modelling to investigate adaptations to a traditional vertical seawall under changing water levels and wave conditions. A comprehensive physical modelling program investigated how several adaptations to a traditional vertical seawall reduced wave overtopping under three water levels (including a representative climate change level) and five significant wave heights. The numerical modelling replicated key experimental cases using IH2VOF, a state-of-the-art two-dimensional numerical model, to assess its performance. Key conclusions from the works are as follows:

- Experimental tests showed that vertical wall extensions are key for reducing wave overtopping in harsh wave conditions, whether installed at the crest as in TSBB (36.8% and 60.0% overtopping reductions compared to the original crest height, see Section 3.5) or TSJJ (25.5% comparative reduction), or at a setback as in TSKK (58.2% comparative reduction).
- Existing wave overtopping prediction equations for vertical walls were modified for five of the test series (TSAA and TSSBB, TSCC, TSGG, TSJJ, and TSKK) to account for their retrofits. The method used to develop the equations (see Section 3.4.3) showed good performance. The average RMSE between this study's equation and EurOtop (2018) equations for all five test series (0.261) was very comparable to the average RMSE for a study of similar scope (0.384) (Dong et al. 2020).
- For this study, IH2VOF underpredicted nearshore significant wave heights by ~10.3% and underpredicted wave overtopping by ~36.2%, when compared to the corresponding experimental data. However, the experimental and numerical data performed similarly when both were compared separately to EurOtop (2018) predictions, producing RMSE values of 0.2050 and 0.2256, respectively (when numerical outliers were negated; see section 4.3.4.3). Despite some limitations, this study showed IH2VOF's potential to be used as a design aid for vertical wall retrofit design. For another type of structure (see Section 2.3.2.2), Stagnitti et al. (2023) used a calibrated and validated IH2VOF model to develop prediction equations, providing further established evidence of the model's promise as a retrofit design aid.

6.2 Recommendations for Future Work

Based on the results and analysis of this study, the following future work is recommended:

- Incorporate hydraulic stability assessments into future tests regarding adapting structures, including for additional structures and test conditions. This would lead to a more

comprehensive understanding about the performance of retrofitted structures, and more rigorous design guidelines.

- Include prototype (real structures) or large-scale measurements where possible to further validate experimental and numerical measurements. Although EurOtop (2018) does not specify any significant scale effects for vertical structures, prototype measurements further confirm the notion.
- More test programs should investigate unique solutions to retrofitted structures. There is limited knowledge regarding vertical structure adaptations. For engineering use, a wide range of adaptation options for many scenarios should be available. Test programs should also investigate alternate bed slopes, in addition to different wave conditions, including investigating the effects of wave obliquity. Experimental tests were conducted in a two-dimensional flume, tests in three-dimensional basins are recommended. The study did not directly consider combined wave loading scenarios. However, the tests that combined the highest wave heights and water levels may be representative of longer return period combined wave loading cases. Albeit site- or region-specific combined wave loading scenarios not represented by this study should be considered in future works.
- Integrate cost and economic investment into a generalized assessment for site specific conditions. As discussed in Section 3.0, hydraulic performance is only one portion of design. While one adaptation may reduce the wave overtopping more than another adaptation, economic or construction considerations may guide the final recommendation. Future work should assess adaptation options both hydraulically and economically.
- Further develop joint databases of physical and numerical data for design purposes -- numerical models or equations are more accessible for engineers than physical models. Studies should integrate physical and numerical data to produce design tools for specific retrofits.

7 References

Ahrens, J. P. 1989. "Dynamic Revetments". *Coastal Engineering 1990*. 1837-1850.

Albert, D.A. 2007. "Natural community abstract for sand and gravel beach." Michigan Natural Features Inventory, Lansing, MI.

Aminti, P., and L. Franco. 1988. "Wave overtopping on rubble mound breakwaters." In Proc., 28th International Coastal Engineering Conference, American Society of Civil Engineers, Vol 1, 770-781.

Atria Engineering Inc. 1997. "Wave Uprush and Overtopping: Methodologies and Applications – Great Lakes-St. Lawrence River System".

Baker, S., E. Murphy, A. Cornett, and P. Knox. 2022. "Experimental study of wave attenuation across an artificial salt marsh." *Frontiers in Built Environment*, 8. https://doi.org/10.3389/fbuil.2022.893664.

Baker, S., P. Knox, M. Provan, and E. Murphy. 2023. "Retrofitting rock-armoured revetments to combat wave overtopping amidst rising sea levels." *Unpublished*.

Bayle, P. M., G. M. Kaminsky, C. E. Blenkinsopp, H. M. Weiner, and D. Cottrell. 2021. "Behaviour and performance of a dynamic cobble berm revetment during a spring tidal cycle in North Cove, Washington State, USA." *Coastal Engineering*, 167: 103898. https://doi.org/10.1016/j.coastaleng.2021.103898.

Berrio, Y., G. Rivillas-Ospina, G. Ruiz-Martínez, A. Arango-Manrique, C. Ricaurte, E. Mendoza, R. Silva, D. Casas, M. Bolívar, and K. Díaz. 2023. "Energy conversion and beach protection: Numerical assessment of a dual-purpose WEC farm." *Renewable Energy*, 219: 119555. https://doi.org/10.1016/j.renene.2023.119555.

Bradbury, A.P., and N.W. Allsop. 1988. "Hydraulic Effects of Breakwater Crown Walls. In Proc., Breakwaters '88 Conference, Institution of Civil Engineers, London, UK, 385-396.

Carus, J., M. Paul, and B. Schröder. 2016. "Vegetation as self-adaptive coastal protection: Reduction of current velocity and morphologic plasticity of a brackish marsh pioneer." *Ecology and Evolution*, 6 (6), 1579–1589. https://doi.org/10.1002/ece3.1904.

Cecioni, C., Y. Pepi, and L. Franco. 2024. "New 2D laboratory experiments on wave overtopping at vertical walls under impulsive and non-impulsive conditions." *Coastal Engineering*. 197: 104689. https://doi.org/10.1016/j.coastaleng.2024.104689.

Chapman, M. G., and A. J. Underwood. 2011. "Evaluation of ecological engineering of 'armoured' shorelines to improve their value as habitat." *Journal of Experimental Marine Biology and Ecology*, 400 (1–2): 302–313. https://doi.org/10.1016/j.jembe.2011.02.025.

City of Toronto. 2018. “Road Engineering Design Guidelines. 2.0 Lane Widths.” Toronto, ON.

Cooper, J. A. G., and J. Pile. 2013. “The adaptation-resistance spectrum: A classification of contemporary adaptation approaches to climate-related coastal change.” *Ocean & Coastal Management*, 94: 90–98. https://doi.org/10.1016/j.ocecoaman.2013.09.006.

Dang, B. L., V. Q. Dang, M. A. Wahab, and H. Nguyen-Xuan. 2021. “Numerical modelling investigation of wave overtopping on stepped-type seawall structures”. *In Proc., International Conference on Computational Methods (ICCM)*. https://sci-en-tech.com/ICCM2021/PDFs/4724-15247-1-PB.pdf

De Finis, S., A. Romano, and G. Bellotti. 2020. “Numerical and laboratory analysis of post-overtopping wave impacts on a storm wall for a dike-promenade structure.” *Coastal Engineering*, 155: 103598. https://doi.org/10.1016/j.coastaleng.2019.103598.

Di Lauro, E., M. Maza, J. L. Lara, I. J. Losada, P. Contestabile, and D. Vicinanza. 2020. “Advantages of an innovative vertical breakwater with an overtopping wave energy converter.” *Coastal Engineering*, 159: 103713. https://doi.org/10.1016/j.coastaleng.2020.103713.

Dogan, G. G. 2016. “Study of rubble mound and caisson type breakwaters by experimental and numerical modelling under extreme waves”. M.S Thesis. Middle East Technical University.

Dong, S., M. Salauddin, S. Abolfathi, and J. M. Pearson. 2024. “Improved prediction of wave overtopping rates at vertical seawalls with recurve retrofitting.” *Ocean Engineering*, 302: 117647. https://doi.org/10.1016/j.oceaneng.2024.117647.

Dong, S., S. Abolfathi, M. Salauddin, Z. H. Tan, and J. M. Pearson. 2020. “Enhancing climate resilience of vertical seawall with retrofitting - A physical modelling study.” *Applied Ocean Research*, 103: 102331. https://doi.org/10.1016/j.apor.2020.102331.

Falkenrich, P., J. Wilson, I. Nistor, N. Goseberg, A. Cornett, and A. Mohammadian. 2021. “Nature-Based coastal protection by large woody debris as compared to seawalls: A Physical model study of beach morphology and wave Reflection.” *Water*, 13 (15): 2020. https://doi.org/10.3390/w13152020.

Formentin, S. M. 2021. “Key performance indicators for the upgrade of existing coastal defense structures.” *Journal of Marine Science and Engineering*, 9 (9):994, 1-30. https://doi.org/10.3390/jmse9090994.

Foss, O., C. E. Blenkinsopp, P. M. Bayle, K. Martins, S. Schimmels, and L. P. Almeida. 2023. “Comparison of dynamic cobble berm revetments with differing gravel characteristics.” *Coastal Engineering*, 183: 104312. https://doi.org/10.1016/j.coastaleng.2023.104312.

Foti, E., R. E. Musumeci, and M. Stagnitti. 2020. “Coastal defence techniques and climate change: a review.” *Rendiconti Lincei. Scienze Fisiche E Naturali*, 31 (1), 123–138. https://doi.org/10.1007/s12210-020-00877-y.

Franco, C., and L. Franco. 1999. “Overtopping Formulas for Caisson Breakwaters with Nonbreaking 3D Waves.” *Journal of Waterway Port Coastal and Ocean Engineering*, 125 (2): 98–108. https://doi.org/10.1061/(asce)0733-950x(1999)125:2(98.

Garner, A. J., Mann, M. E., Emanuel, K. A., Kopp, R. E., Lin, N., Alley, R. B., Horton, B. P., DeConto, R. M., Donnelly, J. P., and Pollard, D. 2017. “Impact of climate change on New York City’s coastal flood hazard: Increasing flood heights from the preindustrial to 2300 CE.” *Proceedings of the National Academy of Sciences*, *114*(45), 11861–11866. https://doi.org/10.1073/pnas.1703568114

Giardino, A., K. Nederhoff, and M. Vousdoukas. 2018. “Coastal hazard risk assessment for small islands: assessing the impact of climate change and disaster reduction measures on Ebeye (Marshall Islands).” *Regional Environmental Change*, 18 (8): 2237–2248. https://doi.org/10.1007/s10113-018-1353-3.

Gittman, R. K., F. J. Fodrie, A. M. Popowich, D. A. Keller, J. F. Bruno, C. A. Currin, C. H. Peterson, and M. F. Piehler. 2015. “Engineering away our natural defenses: an analysis of shoreline hardening in the US.” *Frontiers in Ecology and the Environment*, 13 (6): 301–307. https://doi.org/10.1890/150065.

IHCantabria. 2026. “IH2VOF.” Accessed March 31, 2026. https://ih2vof.ihcantabria.com/model.

IHCantabria. 2012. *IH2VOF course.* Cantabria, Spain.

Jebakumar, J. P. P., G. Nandhagopal, B. RajanBabu, S. Ragumaran, A. S. Kiran, and V. Ravichandran. 2022. “Ecological appraisal of geotextiles in coastal erosion protection engineering.” *Journal of Coastal Research*, 38 (2), 345-354 https://doi.org/10.2112/jcoastres-d-21-00067.1.

Johannessen, J., MacLennan, A., Blue, A., Waggoner, J., Williams, S., Gerstel, W., Barnard, R., Carman, R., and Shipman, H. 2014. “Marine Shoreline Design Guidelines.” Olympia, WA: Washington Department of Fish and Wildlife.

Jonker, R. G., A. AlYousif, B. Hofland, A. Antonini, A. Zoon, and G. Smith. 2024. “OpenFOAM design sensitivity analysis on a homogeneous low-crested structure with concrete elements seaward of a vertical seawall to reduce overtopping.” *Ocean Engineering*, 300: 117423. https://doi.org/10.1016/j.oceaneng.2024.117423.

Jonkman, S. N., M. M. Hillen, R. J. Nicholls, W. Kanning, and M. Van Ledden. 2013. “Costs of Adapting Coastal defences to Sea-Level rise— New estimates and their implications.” *Journal of Coastal Research*, 290: 1212–1226. https://doi.org/10.2112/jcoastres-d-12-00230.1.

Kamphis, J. W. 2000. *Introduction to Coastal Engineering and Management*. Singapore: World Scientific.

Kamphuis, J. W. 2020. *Introduction to Coastal Engineering and management*. Singapore: World Scientific.

Kennedy, D. M., and J. L. D. Woods. 2012. "The influence of coarse woody debris on gravel beach geomorphology." *Geomorphology*, 159–160, 106–115. https://doi.org/10.1016/j.geomorph.2012.03.009.

Kerr, S., Nistor, I., Baker, S. "Adapting Vertical Coastal Structures to Sea Level Rise." [In submission].

Kerr, S., Baker, S., Nistor, I. "Experimental and Numerical Modelling of Adaptive Vertical Coastal Structures." [In submission]

Kerr, S., Baker, S., Nistor, I. (2025). "Experimental and Numerical Modeling of Climate Change-Adaptive Coastal Structures, Phase II: Vertical Seawalls." Oral Presentation. Coastal Zone Canada, Charlottetown, PEI.

Kisacik, D., G. O. Tarakcioglu, and C. Baykal. 2019. "Stilling wave basins for overtopping reduction at an urban vertical seawall – The Kordon seawall at Izmir." *Ocean Engineering*, 185, 82–99. https://doi.org/10.1016/j.oceaneng.2019.05.033.

Kisacik, D., G. O. Tarakcioglu, and L. Cappietti. 2022. "Adaptation measures for seawalls to withstand sea-level rise." *Ocean Engineering*, 250: 110958. https://doi.org/10.1016/j.oceaneng.2022.110958.

Kortenhaus, A., Pearson, J., Bruce, T., Allsop, N.W.H. and van der Meer, J.W. 2003. "Influence of parapets and recurves on wave overtopping and wave loading of complex vertical walls". Coastal Structures 2003, 369-381. Portland: ASCE. https://doi.org/10.1061/40733(147)31

Lara, J. L., A. Ruju, and I. J. Losada. 2011. "Reynolds averaged Navier–Stokes modelling of long waves induced by a transient wave group on a beach." *Proceedings of the Royal Society a Mathematical Physical and Engineering Sciences*, 467 (2129): 1215–1242. https://doi.org/10.1098/rspa.2010.0331.

Li, B., D. E. Reeve, and C. A. Fleming. 2005. "Design for enhanced marine habitats in coastal structures." *Proceedings of the Institution of Civil Engineers - Maritime Engineering*, 158 (3), 115–122. https://doi.org/10.1680/maen.2005.158.3.115.

Li, C., and R. Cox. 2013. "Stability of Hanbars for upgrading of breakwaters with sea level rise." Coasts and Ports 2013: 21st Australasian Coastal and Ocean Engineering Conference and the 14th Australasian Port and Harbour Conference, 477-482. Sydney, NSW.

Loke, L. H. L., and P. A. Todd. 2015. "Structural complexity and component type increase intertidal biodiversity independently of area." *Ecology*, 97 (2), 383–393. https://doi.org/10.1890/15-0257.1.

Losada, I. J., J. L. Lara, R. Guanche, and J. M. Gonzalez-Ondina. 2007. "Numerical analysis of wave overtopping of rubble mound breakwaters." *Coastal Engineering*, 55 (1): 47–62. https://doi.org/10.1016/j.coastaleng.2007.06.003.

Lv, J., M. Wang, X. Hu, Z. Cao, and H. Ba. 2021b. “Experimental study on the durability and microstructure of marine concrete covered with barnacles.” *Construction and Building Materials*, 317: 125900. https://doi.org/10.1016/j.conbuildmat.2021.125900.

Lv, J., Z. Cao, and X. Hu. 2021a. “Effect of biological coating (Crassostrea gigas) on marine concrete: Enhanced durability and mechanisms.” *Construction and Building Materials*, 285: 122914. https://doi.org/10.1016/j.conbuildmat.2021.122914.

Marin-Diaz, B., D. Van Der Wal, L. Kaptein, P. Martinez-Garcia, C. H. Lashley, K. De Jong, J. W. Nieuwenhuis, L. L. Govers, H. Olff, and T. J. Bouma. 2023. “Using salt marshes for coastal protection: Effective but hard to get where needed most.” *Journal of Applied Ecology*, 60 (7): 1286–1301. https://doi.org/10.1111/1365-2664.14413.

Mayo, T. L., and N. Lin. 2022. “Climate change impacts to the coastal flood hazard in the northeastern United States.” *Weather and Climate Extremes*, 36: 100453. https://doi.org/10.1016/j.wace.2022.100453.

Miles, M.D. 1990. “The GEDAP Data Analysis Software Package.” National Research Council Canada, Ottawa.

Ministry of Natural Resources. 2001. “Technical Guide For Great Lakes - St. Lawrence River Shorelines”. Peterborough, ON.

Moreno, L., V. Negro, L. Garrote, J. J. Muñoz-Pérez, J. S. López, and M. D. Esteban. 2020. “An engineering method for the preliminary functional design of perched beaches: Design Guidelines.” *Journal of Coastal Research*, 95 (SI): 283-288. https://doi.org/10.2112/si95-055.1.

Natanzi, A. S., B. J. Thompson, P. R. Brooks, T. P. Crowe, and C. McNally. 2020. “Influence of concrete properties on the initial biological colonisation of marine artificial structures.” *Ecological Engineering*, 159: 106104. https://doi.org/10.1016/j.ecoleng.2020.106104.

Neves, M. G., E. Didier, M. Brito, and M. Clavero. 2021. “Numerical and Physical Modelling of Wave Overtopping on a Smooth Impermeable Dike with Promenade under Strong Incident Waves.” *Journal of Marine Science and Engineering*, 9 (8): 865. https://doi.org/10.3390/jmse9080865.

Odériz, I., N. Knöchelmann, R. Silva, R. A. Feagin, M. L. Martínez, and E. Mendoza. 2020. “Reinforcement of vegetated and unvegetated dunes by a rocky core: A viable alternative for dissipating waves and providing protection?” *Coastal Engineering*, 158: 103675. https://doi.org/10.1016/j.coastaleng.2020.103675.

Oliveira, J. N. C., F. S. B. F. Oliveira, M. G. Neves, M. Clavero, and A. A. Trigo-Teixeira. 2020. “Modeling Wave Overtopping on a Seawall with XBeach, IH2VOF, and Mase Formulas.” *Water*, 12 (9): 2526. https://doi.org/10.3390/w12092526.

Pearson, J., Bruce, T., Allsop, W., Kortenhaus, A., & Van der Meer. 2005. “Effectiveness of recurve walls in reducing wave overtopping on seawalls and breakwaters". In Proc., 29th

International Conference of Coastal Engineering, 4404-4416. Lisbon: ICCE. https://doi.org/10.1142/9789812701916_0355.

Pearson, J., Bruce, T., W. Allsop, and X. Gironella. 2003. "Violent Wave Overtopping – Measurements At Large And Small Scale." In Proc., 28th International Conference on Coastal Engineering, 2227-2238. Cardiff, Wales. https://doi.org/10.1142/9789812791306_0187.

Pedersen, J. 1996. "Experimental study of wave forces and wave overtopping on breakwater crown walls." Series paper 12. Aalborg University, Denmark.

Pedersen, J., and H. F. Hurcharth. "Wave forces on crown walls". In proc., 23rd International Coastal Engineering Conference, American Society of Civil Engineers, Vol 2, 1489-1502.

Perkol-Finkel, S., T. Hadary, A. Rella, R. Shirazi, and I. Sella. 2017. "Seascape architecture – incorporating ecological considerations in design of coastal and marine infrastructure." *Ecological Engineering*, 120, 645–654. https://doi.org/10.1016/j.ecoleng.2017.06.051.4

Peters, R. B. M. 2014. "Report additional thesis: Evaluation of the IH2VOF model for modelling of hydraulic properties near breakwater toes". Master of Hydraulic Engineering thesis. Delft University of Technology.

Pilechi, A., S. Baker, and A. Cornett. 2018. "Evaluation of a numerical wave modelling tool for studying the overtopping of rubblemound breakwaters". *In Proc., International conference on the application of physical modelling in coastal and port engineering and science (Coastlab18),* Santander, Spain. https://publications-cnrc.canada.ca/eng/view/ft/?id=94ba2dba-798a-49ad-adae-8da16d881b9c

PlaNYC. 2013. "*A Stronger, More Resilient New York"*. New York, NY.

Rambabu, N., and V. K. Srineash. 2022. "A review on methodologies to upgrade the coastal structures to enhance the coastal resilience." *OCEANS 2022 - Chennai*, 1–9. https://doi.org/10.1109/oceanschennai45887.2022.9775524.

Rosenberg, Y. 2023. "Achieving Biodiversity Uplift on Marine Infrastructure". Brooklyn, NY: ECOncrete.

Rupasinghe, M., R. S. Nicolas, B. S. Lanham, and R. L. Morris. 2023. "Sustainable oyster shell incorporated artificial reef concrete for living shorelines." *Construction and Building Materials*, 410: 134217. https://doi.org/10.1016/j.conbuildmat.2023.134217.

Salauddin, M., and J. M. Pearson. 2019. "Laboratory investigation of overtopping at a sloping structure with permeable shingle foreshore." *Ocean Engineering*, 197: 106866. https://doi.org/10.1016/j.oceaneng.2019.106866.

Sayar, S. D., I. Nistor, S. Baker, J. Gutiérrez, and Y. Rosenberg. 2024. "Hydraulic Performance of Low-Crested and Emergent Breakwaters with Ecologically Designed Armor Units." *J.*

Waterway, Port, Coastal, Ocean Eng., 151 (2) : 04024027. https://doi.org/10.1061/jwped5.wweng-2158.

Schoonees, T., A. G. Mancheño, B. Scheres, T. J. Bouma, R. Silva, T. Schlurmann, and H. Schüttrumpf. 2019. "Hard structures for coastal protection, towards greener designs." *Estuaries and Coasts*, 42 (7), 1709–1729. https://doi.org/10.1007/s12237-019-00551-z.

Sella, I., T. Hadary, A. J. Rella, B. Riegl, D. Swack, and S. Perkol-Finkel. 2021. "Design, production, and validation of the biological and structural performance of an ecologically engineered concrete block mattress: A Nature-Inclusive Design for shoreline and offshore construction." *Integrated Environmental Assessment and Management*, 18 (1), 148–162. https://doi.org/10.1002/ieam.4523.

Sinay, L., and R. W. Carter. 2020. "Climate change adaptation options for coastal communities and local governments." *Climate*, 8 (1): 7. https://doi.org/10.3390/cli8010007.

Shaughnessy, E. J., I. Katz, and J. Schaffer. 2005. *Introduction to fluid mechanics*. New York, United States of America: Oxford University Press, Inc.

Smiley, K. T., I. Noy, M. F. Wehner, D. Frame, C. C. Sampson, and O. E. J. Wing. 2022. "Social inequalities in climate change-attributed impacts of Hurricane Harvey." *Nature Communications*, 13 (1): 3418. https://doi.org/10.1038/s41467-022-31056-2.

Soernesen, P., J. Jensen, and P. Klagenberg. 2011. "How To Decide When To Adapt Coastal Protection To Climate Change." In Proc., *Coastal Engineering Proceedings*, 1(32): 5. Shanghai, China. https://doi.org/10.9753/icce.v32.management.5.

Stagnitti, M., J. L. Lara, R. E. Musumeci, and E. Foti. 2023. "Numerical modeling of wave overtopping of damaged and upgraded rubble-mound breakwaters." *Ocean Engineering*, 280: 114798. https://doi.org/10.1016/j.oceaneng.2023.114798.

Stantec Consulting Ltd., Zuzek Inc., and SJL Engineering. 2022. "*Municipality of Lakeshore Shoreline Management Plan Final Report*."

Strauss, B. H., P. M. Orton, K. Bittermann, M. K. Buchanan, D. M. Gilford, R. E. Kopp, S. Kulp, C. Massey, H. De Moel, and S. Vinogradov. 2021. "Economic damages from Hurricane Sandy attributable to sea level rise caused by anthropogenic climate change." *Nature Communications*, 12 (1): 2720. https://doi.org/10.1038/s41467-021-22838-1.

Suedel, B. C., J. Calabria, M. V. Bilskie, J. E. Byers, K. Broich, S. K. McKay, A. S. Tritinger, C. B. Woodson, and E. Dolatowski. 2022. "Engineering coastal structures to centrally embrace biodiversity." *Journal of Environmental Management*, 323: 116138. https://doi.org/10.1016/j.jenvman.2022.116138.

Sweet, W.V., B.D. Hamlington, R.E. Kopp, C.P. Weaver, P.L. Barnard, D. Bekaert, W. Brooks, M. Craghan, G. Dusek, T. Frederikse, G. Garner, A.S. Genz, J.P. Krasting, E. Larour, D. Marcy, J.J. Marra, J. Obeysekera, M. Osler, M. Pendleton, D. Roman, L. Schmied, W.

Veatch, K.D. White, and C. Zuzak. 2022. “Global and Regional Sea Level Rise Scenarios for the United States: Updated Mean Projections and Extreme Water Level Probabilities Along U.S. Coastlines.” NOAA Technical Report NOS 01. National Oceanic and Atmospheric Administration, National Ocean Service, Silver Spring, MD, 111 pp. https://oceanservice.noaa.gov/hazards/sealevelrise/noaa-nostechrpt01-global-regional-SLR-scenarios-US.pdf

Takahashi, S. “Design of vertical breakwaters”. Port and Airport Research Institute, Japan.

Toft, J. D., K. L. Accola, S. D. Roches, J. N. Kobelt, H. S. Faulkner, J. R. Morgan, B. S. Perla, M. Metler, and M. N. Dethier. 2023. “Coastal landforms and fetch influence shoreline restoration effectiveness.” *Frontiers in Marine Science*, 10: 1199749. https://doi.org/10.3389/fmars.2023.1199749.

Tuozzo, S., A. Di Leo, M. C. Ciccaglione, F. Dentale, L. C. Lopez, M. Calabrese, and M. Buccino. 2025. “Vertical seawalls protected by rubble mound structures: prediction tools and physical insight.” In Proc., 38th International Conference of Coastal Engineering. Rome, Italy. https://doi.org/10.9753/icce.v38.papers.57

United States Army Corps of Engineers. 1995. “Design of Coastal Revetments, Seawalls, and Bulkheads” Washington, D.C.

United States Army Corps of Engineers. 2002. “Coastal Engineering Manual”. Washington, D.C.

US EPA. 2005. “State of the Great Lakes. What is the State of the Great Lakes Alvars and Cobble Beaches?”. Accessed March 26, 2025. https://publications.gc.ca/collections/Collection/En161-3-15-2005E.pdf

USGS. 2003. Accessed March 26, 2025. https://pubs.usgs.gov/of/2006/1195/htmldocs/images/chart.pdf

Van Den Bos, J., H. J. Verhagen, M. Zijlema, and B. Mellink. 2014. “Towards a practical application of numerical models to predict wave-structure interaction: an initial validation.” *In Proc., Coastal Engineering Proceedings*, Seoul, Korea: 1 (34): 50. https://doi.org/10.9753/icce.v34.structures.50.

Van Der Meer, J. W. 1988. “Rock slopes and gravel beaches under wave attack.” Doctoral Thesis. Delft University of Technology.

Van der Meer, J.W., N.W.H. Allsop, T. Bruce, J. De Rouck, A. Kortenhaus, T. Pullen, H. Schüttrumpf, P. Troch, and B. Zanuttigh. 2018. “Manual on wave overtopping of sea defences and related structures. An overtopping manual largely based on European research, but for worldwide application.” www.overtopping-manual.com.

Van Der Meulen, F., S. IJff, and R. Van Zetten. 2022. “Nature-based solutions for coastal adaptation management, concepts and scope, an overview.” *Nordic Journal of Botany*, 2023 (1). https://doi.org/10.1111/njb.03290.

van Gent, M. R. A. 2019. “Climate Adaptation of Coastal Structures”. In Proc., Proceedings of the 9th Short Course/Conference on Applied Coastal Research , 37-44. Bari, Italy.

Wang, Y., C. Jiang, B. Deng, F. Yuan, and Y. Ma. 2025. “Numerical investigation of solitary waves interaction with a vertical wall on a reef flat under the influence of wind.” *Ocean Engineering*, 340: 122221. https://doi.org/10.1016/j.oceaneng.2025.122221.

Ward, D. L., and J. P. Ahrens. 1992. “Overtopping rates for Seawalls.” US Army Corps of Engineers, Mississippi, U.S.A. https://apps.dtic.mil/sti/tr/pdf/ADA250876.pdf

Weaver, R. J., and A. L. Stehno. 2024. “Mangroves as coastal protection for restoring Low-Energy waterfront property.” *Journal of Marine Science and Engineering*, 12 (3): 470. https://doi.org/10.3390/jmse12030470.

Wilson, J. 2020. “The efficacy and design of coastal protection using large woody debris.” M.A.Sc. Thesis. University of Ottawa.

Yuanita, N., A. Kurniawan, I. M. Nurmansyah, and F. M. Rizaldi. 2021. “A physical model simulation of combination of a geo-bag dike and mangrove vegetation as a natural coastal protection system for the Indonesian shoreline.” *Applied Ocean Research*, 108: 102516. https://doi.org/10.1016/j.apor.2020.102516.

Appendix A: Chapter 3 Supplemental Materials

This appendix is the supplemental materials section for Chapter 3. The section was directly re-produced here.

A.1 TSBB to TSKK Photographs

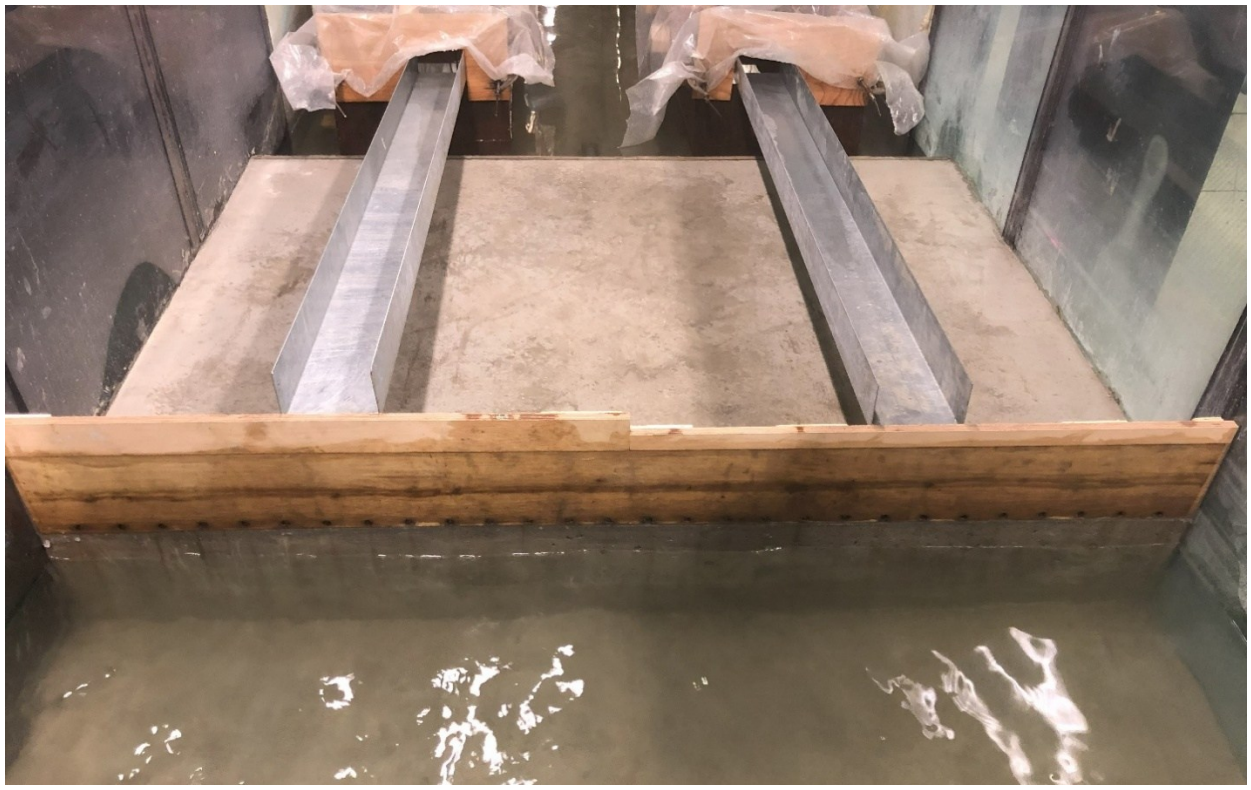

Fig. A1. Vertical extension case (TSBB)

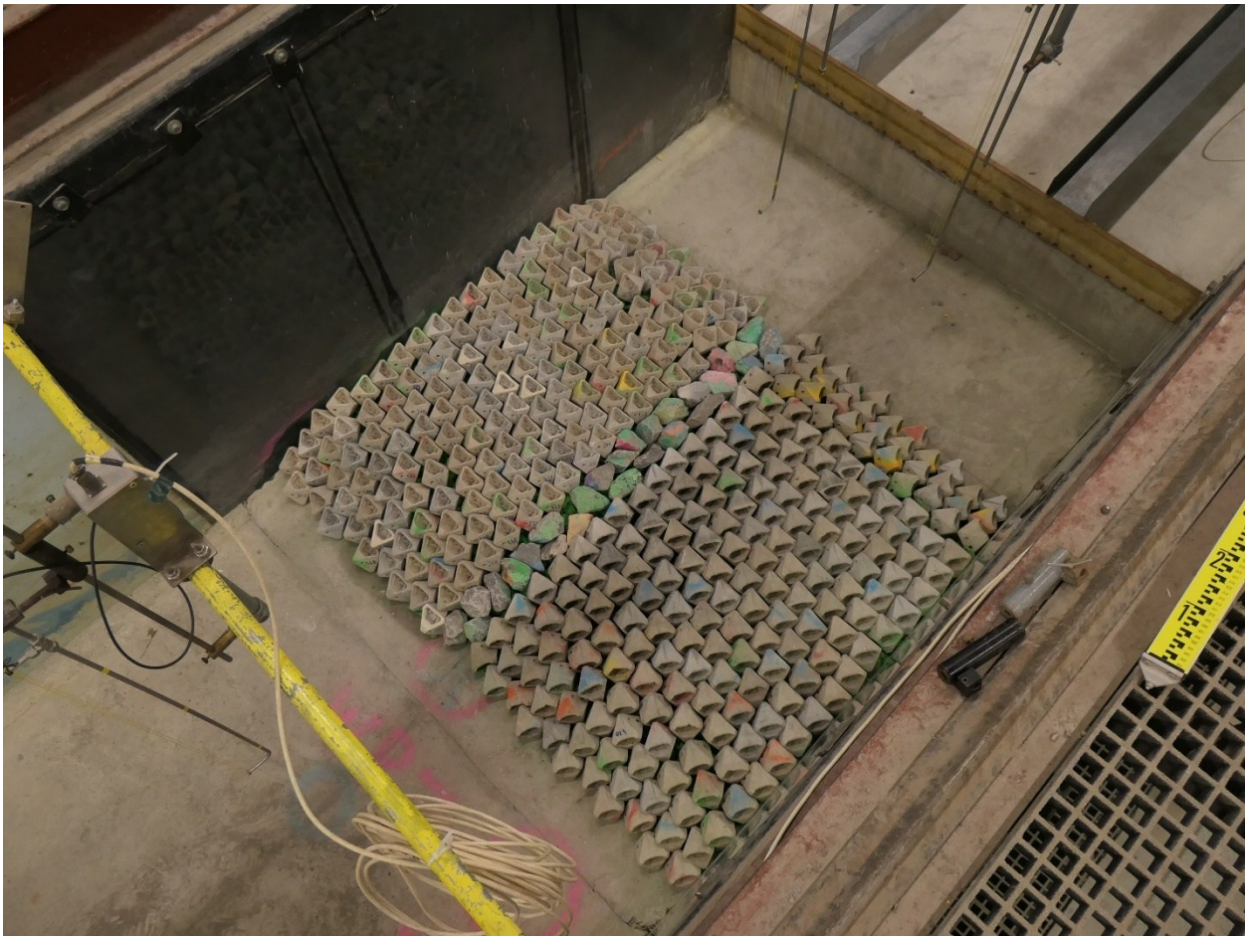

Fig. A2. Eco-friendly submerged breakwater case (TSCC) view no.1

Fig. A3. Eco-friendly submerged breakwater case (TSCC) view no.2

Fig. A4. Perched beach case (TSDD)

Fig. A5. Modified perched beach case (TSEE)

Fig. A6. Cobble beach case (TSFF)

Fig. A7. Revetment case (TSGG)

Fig. A8. Drainage swale case (TSHH)

Fig. A9. Modified drainage swale case (TSII)

Fig. A10. Further modified drainage swale case (TSJJ)

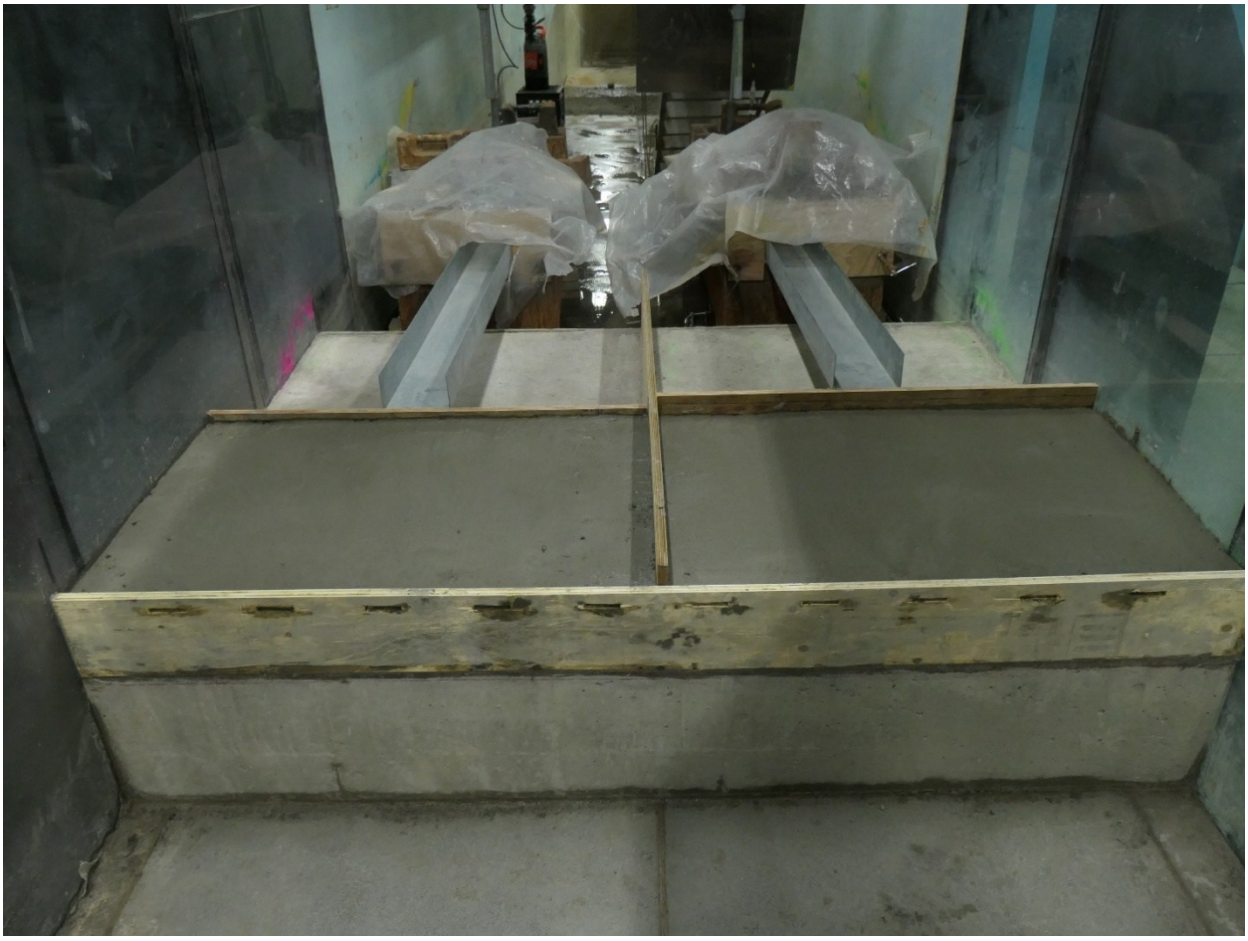

Fig. A11. Secondary wall case (TSKK)

A.2 Wave Probe Locations

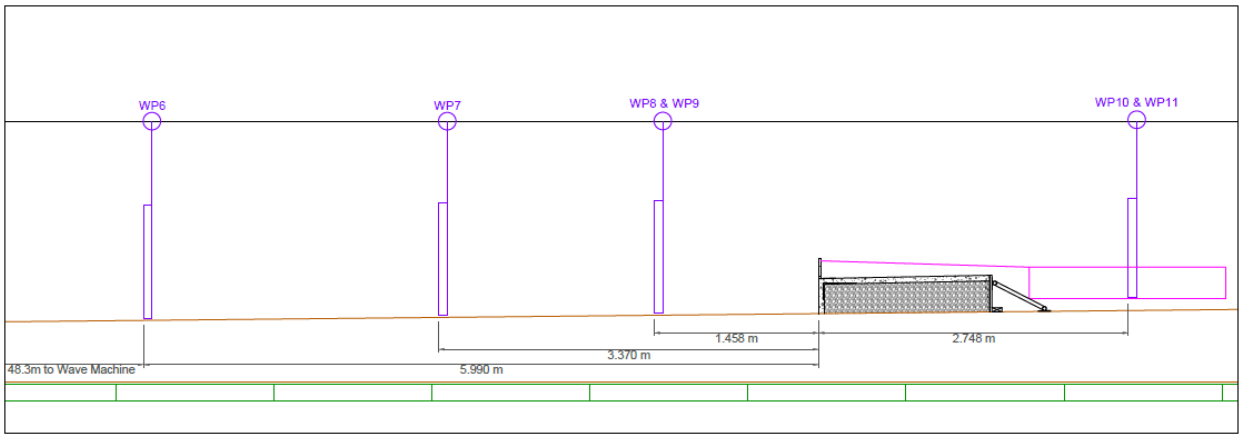

Fig. A12. Baseline vertical wall case (TSAA), vertical extension case (TSBB), drainage swale cases (TSHH, TSII, TSJJ), and Secondary wall (TSKK) wave probe locations

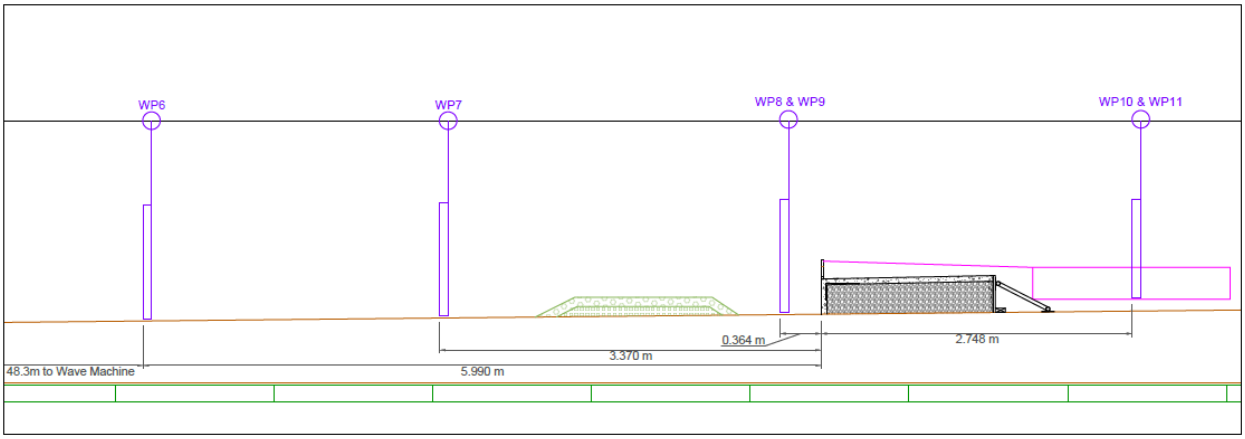

Fig. A13. Eco-friendly submerged breakwater case (TSCC) wave probe locations

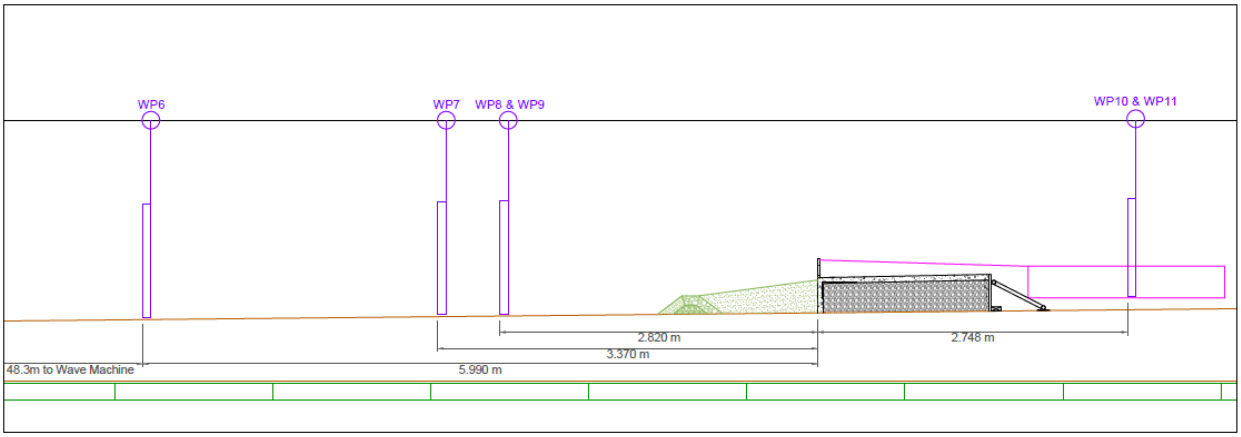

Fig. A14. Perched beach cases (TSDD, TSEE) wave probe locations

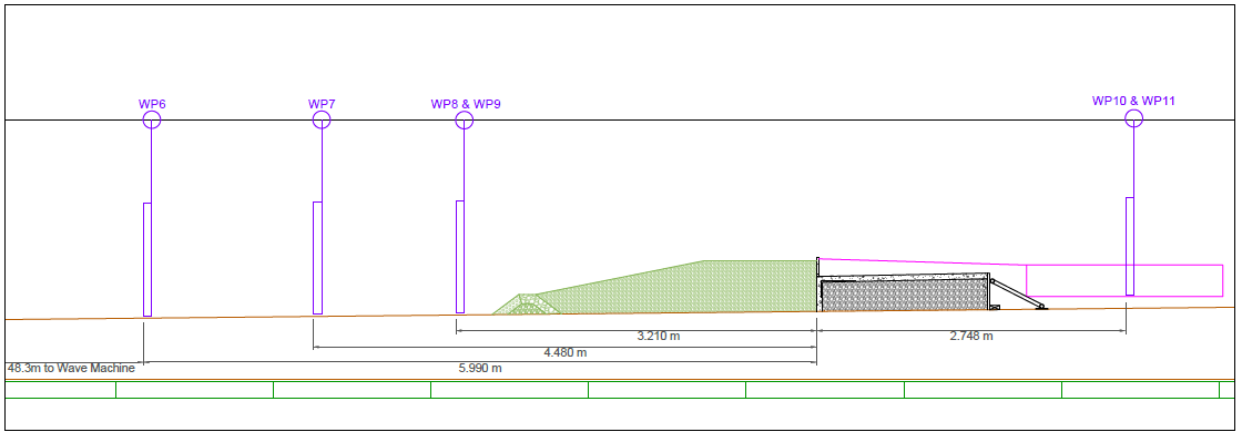

Fig. A15. Cobble beach case (TSFF) wave probe locations

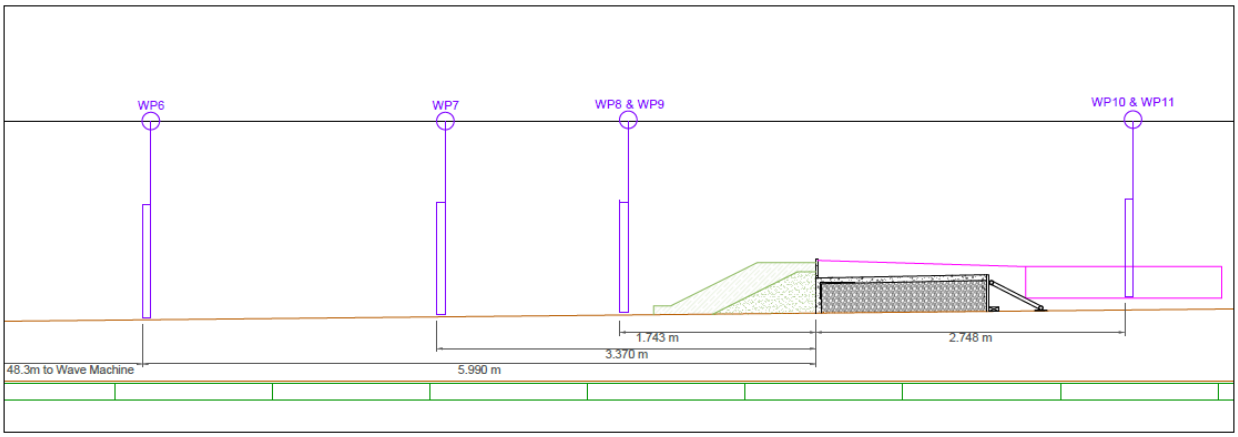

Fig. A16. Revetment case (TSGG) wave probe locations

A.3 TSAA to TSKK Front Profile Drawings

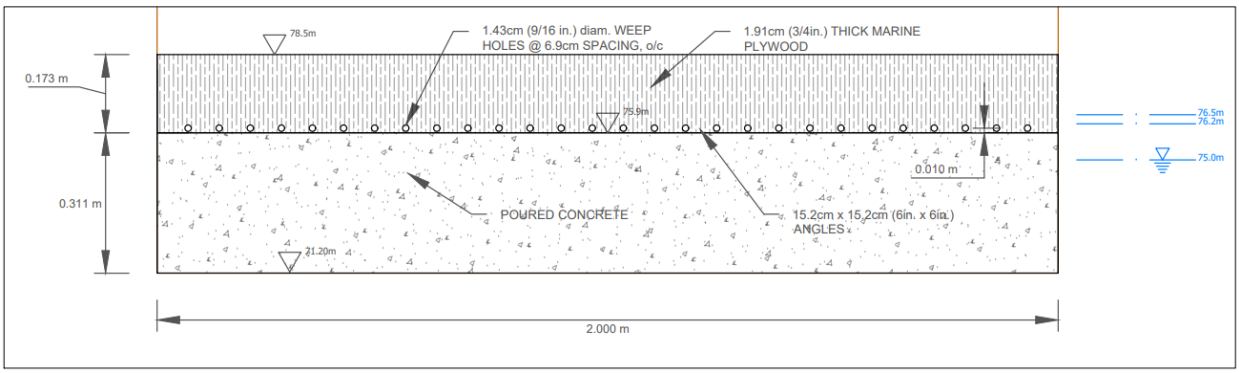

Fig. A17. Baseline vertical wall case (TSAA) front profile sketch

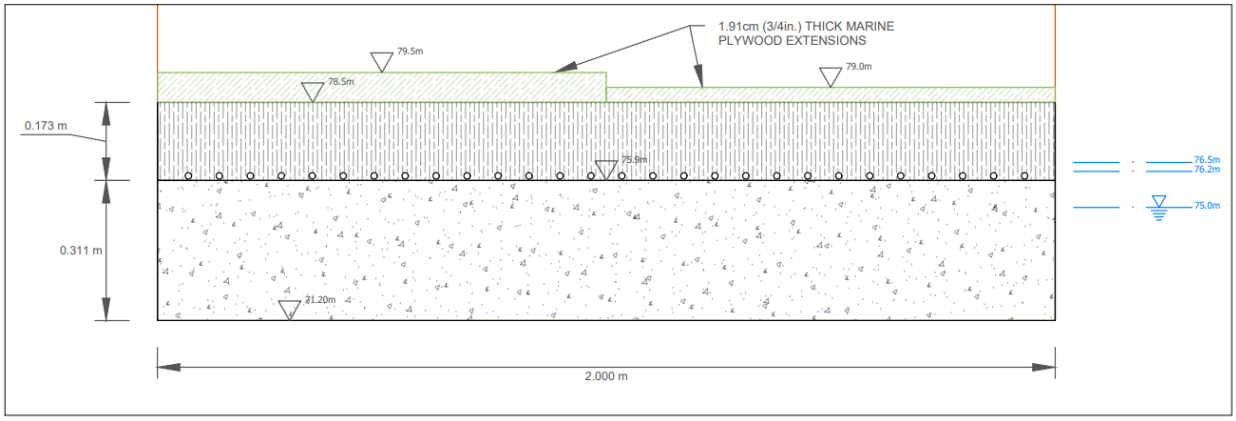

Fig A18. Vertical extension case (TSBB) front profile sketch

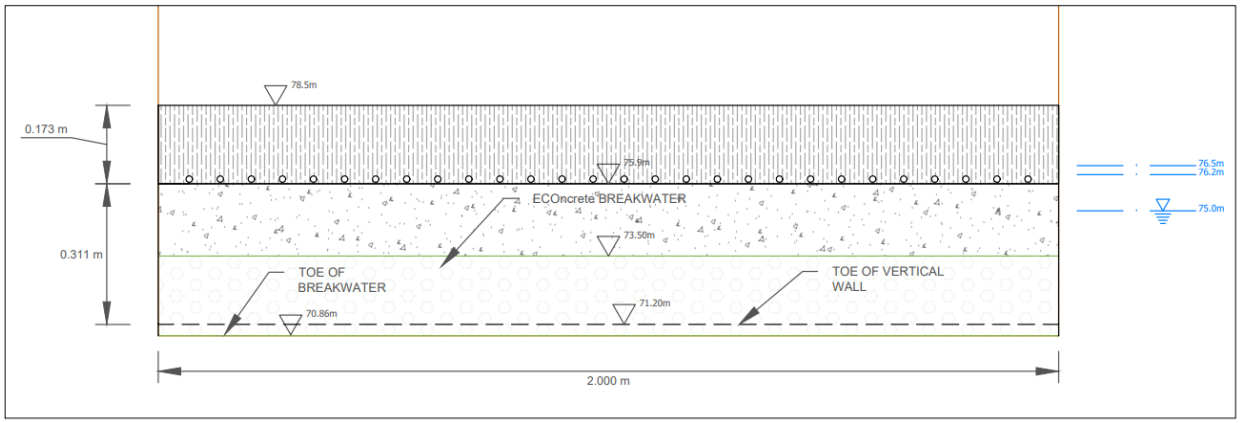

Fig A19. Eco-friendly submerged breakwater case (TSCC) front profile sketch

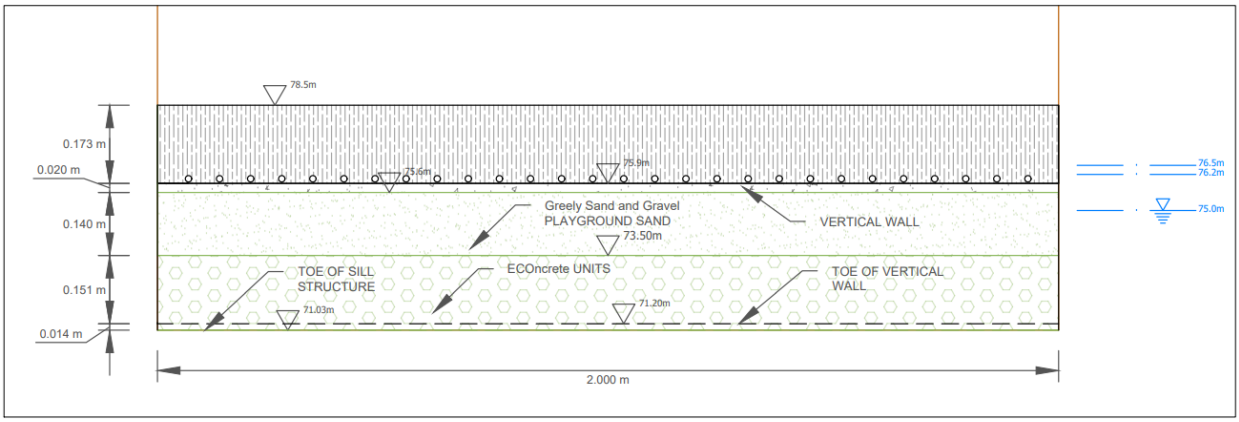

Fig. A20. Perched beach case (TSDD) front profile drawing

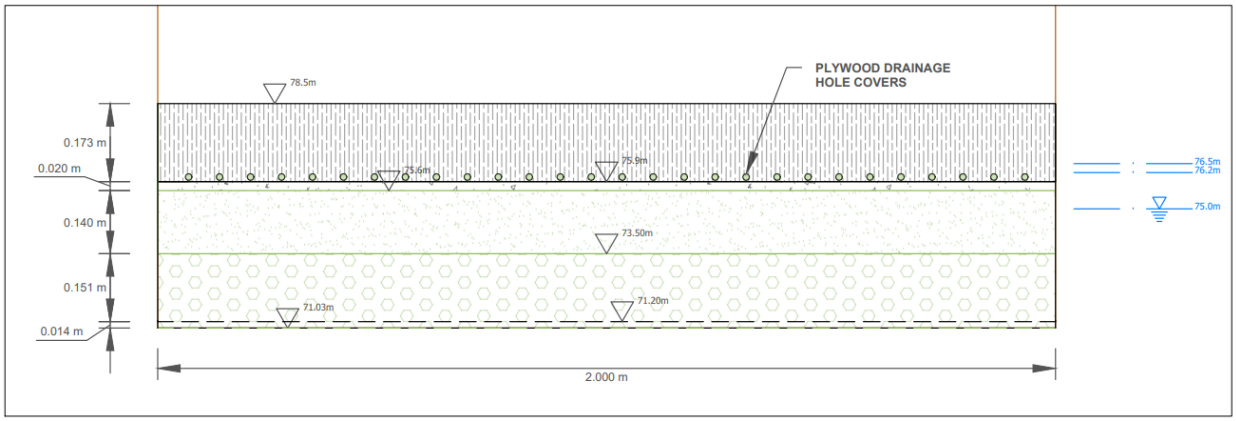

Fig. A21. Modified perched beach case (TSEE) front profile drawing

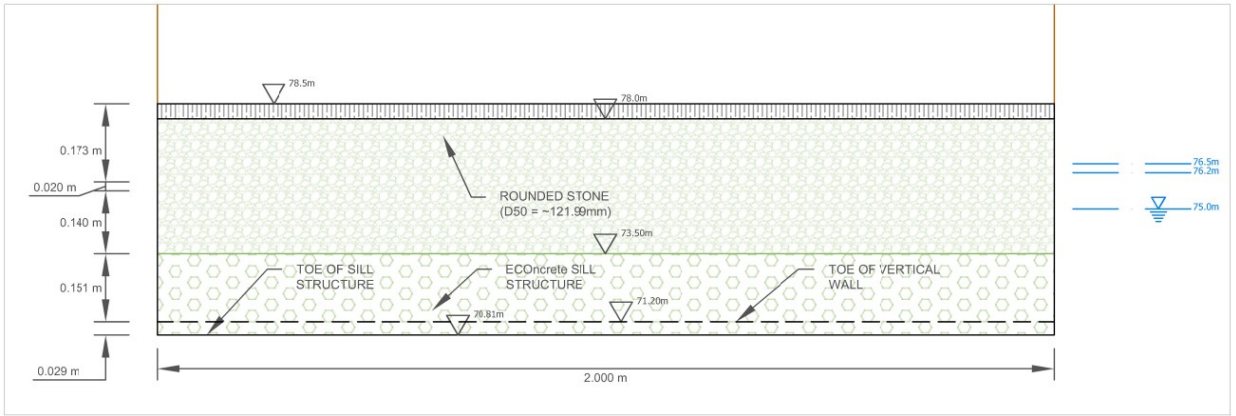

Fig. A22. Cobble beach case (TSFF) front profile sketch

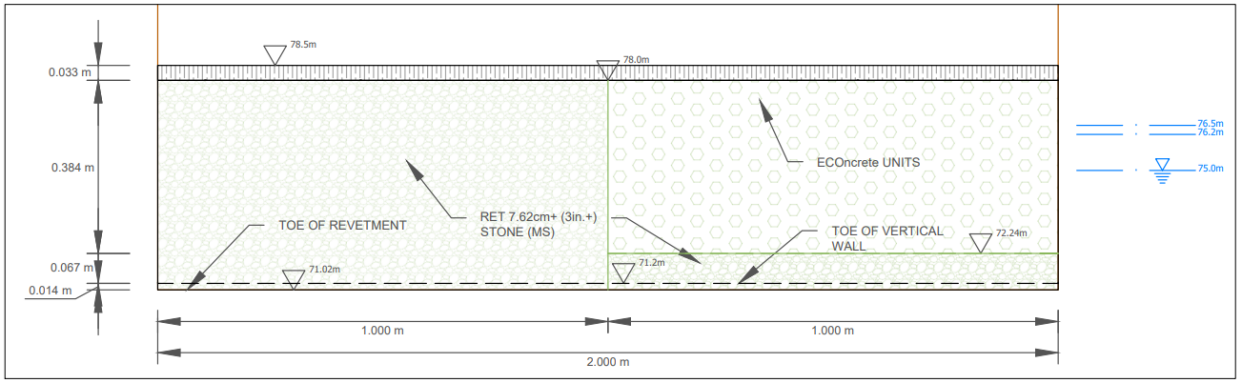

Fig A23. Revetment case (TSGG) front profile sketch

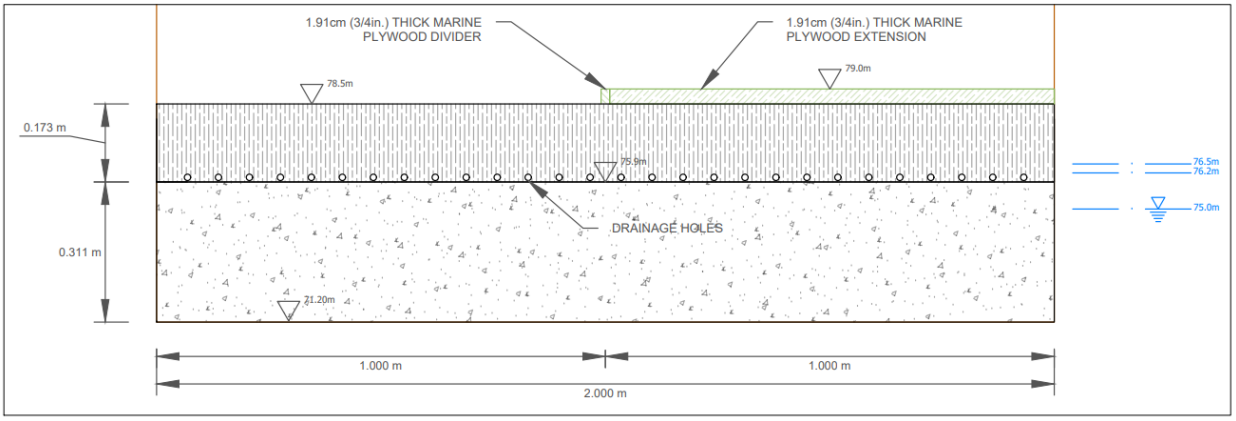

Fig A24. Drainage swale cases (TSHH, TSII, TSJJ) front profile sketch

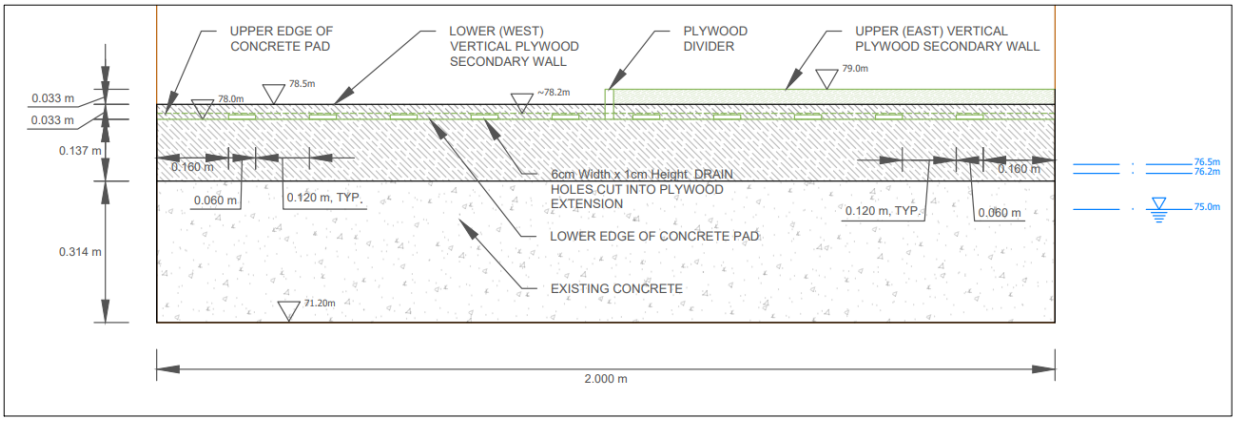

Fig A25. Secondary wall (TSKK) front profile sketch

A.4 Additional Plots

It is also pertinent to investigate how each adaptation reduces OT relative to the baseline case. Fig. 19 and Fig. 20 below show the percent differences between the OT of a given test and the OT for the associated TSAA test. Note that there is a practical lower limit of -100%, entailing the absolute overtopping for that test was negligible (~0).

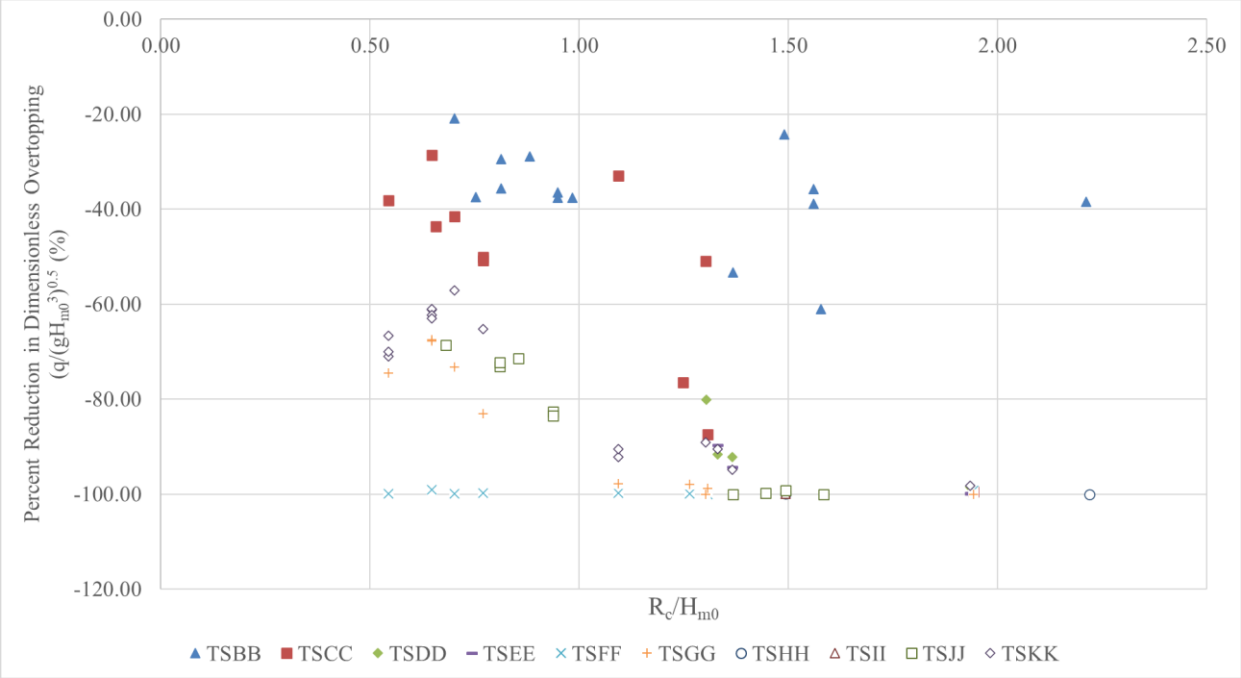

Fig A26. Percent differences to TSAA for a given test, east OT tray

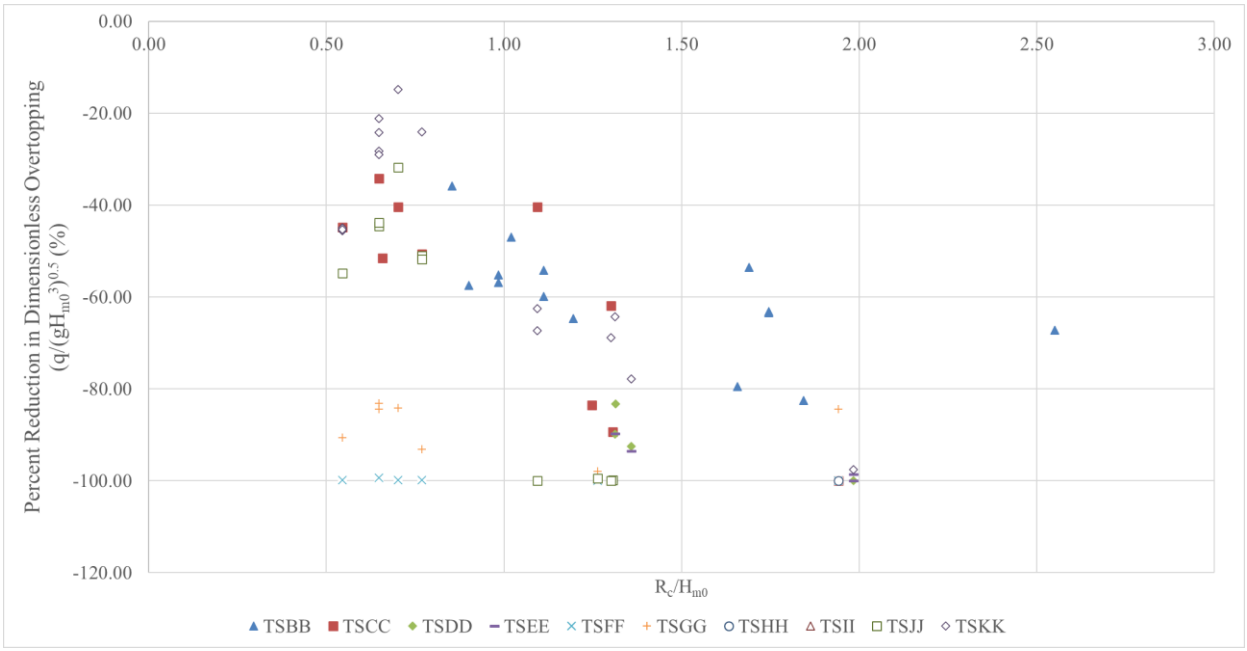

Fig. A27. Percent differences to TSAA for a given test, west OT tray